NASA / CR-2002-211749

The Steady Flow Resistance of Perforated Sheet Materials in High Speed Grazing Flows

Asif A. Syed, Jia Yu, H. W. Kwan, and E. Chien
GE Aircraft Engines, Cincinnati, Ohio

July 2002

The NASA STI Program Office ... in Profile

Since its founding, NASA has been dedicated to the advancement of aeronautics and space science. The NASA Scientific and Technical Information (STI) Program Office plays a key part in helping NASA maintain this important role.

The NASA STI Program Office is operated by Langley Research Center, the lead center for NASA's scientific and technical information. The NASA STI Program Office provides access to the NASA STI Database, the largest collection of aeronautical and space science STI in the world. The Program Office is also NASA's institutional mechanism for disseminating the results of its research and development activities. These results are published by NASA in the NASA STI Report Series, which includes the following report types:

- TECHNICAL PUBLICATION. Reports of completed research or a major significant phase of research that present the results of NASA programs and include extensive data or theoretical analysis. Includes compilations of significant scientific and technical data and information deemed to be of continuing reference value. NASA counterpart of peer-reviewed formal professional papers, but having less stringent limitations on manuscript length and extent of graphic presentations.

- TECHNICAL MEMORANDUM. Scientific and technical findings that are preliminary or of specialized interest, e.g., quick release reports, working papers, and bibliographies that contain minimal annotation. Does not contain extensive analysis.

- CONTRACTOR REPORT. Scientific and technical findings by NASA-sponsored contractors and grantees.

- CONFERENCE PUBLICATION. Collected papers from scientific and technical conferences, symposia, seminars, or other meetings sponsored or co-sponsored by NASA.

- SPECIAL PUBLICATION. Scientific, technical, or historical information from NASA programs, projects, and missions, often concerned with subjects having substantial public interest.

- TECHNICAL TRANSLATION. English-language translations of foreign scientific and technical material pertinent to NASA's mission.

Specialized services that complement the STI Program Office's diverse offerings include creating custom thesauri, building customized databases, organizing and publishing research results ... even providing videos.

For more information about the NASA STI Program Office, see the following:

- Access the NASA STI Program Home Page at ***http://www.sti.nasa.gov***

- E-mail your question via the Internet to help@sti.nasa.gov

- Fax your question to the NASA STI Help Desk at (301) 621-0134

- Phone the NASA STI Help Desk at (301) 621-0390

- Write to:
  NASA STI Help Desk
  NASA Center for AeroSpace Information
  7121 Standard Drive
  Hanover, MD 21076-1320

NASA / CR-2002-211749

The Steady Flow Resistance of Perforated Sheet Materials in High Speed Grazing Flows

Asif A. Syed, Jia Yu, H. W. Kwan, and E. Chien
GE Aircraft Engines, Cincinnati, Ohio

National Aeronautics and
Space Administration

Langley Research Center
Hampton, Virginia 23681-2199

Prepared for Langley Research Center
under Contract NAS3-98004, Tasks 3 and 13

July 2002

Available from:

NASA Center for AeroSpace Information (CASI)
7121 Standard Drive
Hanover, MD 21076-1320
(301) 621-0390

National Technical Information Service (NTIS)
5285 Port Royal Road
Springfield, VA 22161-2171
(703) 605-6000

Summary

This report presents the results of a research program to determine the effects of high speed grazing air flow on the Acoustic Resistance of perforated sheet materials used in the construction of acoustically absorptive liners used in the nacelles of commercial aircraft engines. A limited amount of testing was also conducted on liner samples with so-called linear "wiremesh" type face sheets.

Steady or DC Flow Resistance of porous sheet materials is known to be a major component of the Acoustic Resistance of sound suppression [1] liners used in the fan inlet, fan exhaust and core exhaust ducts of turbo fan engines. Therefore, tests were conducted to measure the DC Flow Resistance characteristics of a set of perforated face sheets in a flow duct apparatus. A set of six liner-samples with linear "wiremesh" type face sheets were investigated in the same way. These tests were performed at grazing flow velocities up to Mach 0.8. (Altogether six samples of linear "wiremesh" type face sheets were also tested.)

The acoustic liner samples were fabricated to cover typical variations in the perforated face sheet parameters, such as the hole-diameter, the porosity and the sheet thickness. In addition, an attempt was made to include the variations due to different manufacturing processes that may have some impact on the DC Flow Resistance. Thus a set of liner samples were fabricated with perforated face sheets representing the following materials and manufacturing processes.

- Aluminum sheets with punched holes
- Glass-fiber Epoxy composite sheet with hole produced by pin-mandrels (GEAE & Boeing)
- Graphite Epoxy composite sheet with holes produced by a mechanical drilling process (used by B. F. Goodrich)
- Graphite Epoxy composite sheet produced by a "Pin-less Process" and finished with an erosion resistant coating (Middle River Aircraft Systems)
- A special liner sample with a laser drilled thin plastic sheet (polyurethane film - PU) bonded on a high porosity perforated sheet to create face sheet holes with very small diameters.

All test samples were constructed by using the sheet reticulation of the adhesive to bond the face sheet to a 3/8-inch cell size honeycomb core.

The samples with the linear "wiremesh" type face sheets were cut out from existing panels used in previous research under Task Order 25 [1].

The tests conducted under this contract show that the DC flow resistance data from perforated sheets correlate strongly with the grazing flow Mach Number and the Porosity of the face sheet. The data also show correlation against the ratio of the boundary layer displacement thickness to hole-diameter.

The data from the composite sheets produced by the pin-mandrel tools and the drilling processes correlate like the data obtained from punched Aluminum sheets.

The data from the face sheet sample produced by the Pin-less Process and Erosion Coating showed significantly lower increase in resistance due to grazing flow than a punched Aluminum face sheet of the same porosity.

The increase in resistance with grazing flow for punched Aluminum sheets, as measured under this program, is in good agreement with previous published results [2, 3] up to Mach 0.4. However, above Mach 0.4, the increase in resistance with flow velocity is significantly larger than expected.

Finally, the tests demonstrated that there is a significant increase in the resistance of linear "wiremesh" type face sheet materials with increasing Mach number. Thie effect should be included in any design considerations.

Conclusions

- A new correlation for the Resistance of acoustic liners, made with perforated face sheets, has been obtained. This correlation is based on data at grazing flow speeds up to Mach 0.8.
- The increase in resistance with grazing flow Mach number is bigger than predicted by previous correlations proposed by Rice and Heidelberg. This difference is more significant at grazing flow speeds above Mach 0.5.
- Non-linearity characteristics decrease with grazing flow Mach number. Effectively, liners with perforated face sheets become linear (insensitive to acoustic particle velocity) under engine operating conditions.
- Grazing flow effects on the Resistance of laser drilled (micro-porous) face sheets (sample #13), are much bigger than predicted by Heidelberg-Rice correlation at all grazing flow speeds.
- DynaRohr type liners with wiremesh-on-perforate face sheets, do show significant increase in Resistance with increasing grazing flow Mach number. This effect should be included in design considerations.

Recommendations

The following work is recommended for future research sponsored by NASA.

1.0 Conduct tests to measure the mass Reactance of face sheet materials under grazing flow conditions. These tests should be conducted with the In-Situ method for Impedance measurement.

2.0 Evaluate and develop new liner concepts that can provide substantial increase in noise suppression over conventional single layer liners.

CONTENTS

Summary i
Conclusions ii
Recommendations ii

1.0 Introduction 1
2.0 Testing and Analysis 2
2.1 Test Panels and Samples 2
2.2 Tests Conducted at the B.F. Goodrich (BFG) Plant 3
2.2.1 DC Flow Resistance Tests 3
2.2.2 Impedance Tube Measurements 5
2.2.3 Flow Duct Insertion Loss Data 5
2.3 DC Flow Resistance Measurements in the Flow Duct Apparatus at GE 7
2.3.1 Flow Resistance Data without Grazing Flow {M=0.0} 7
2.3.2 Flow Resistance Data with Grazing Flow 9
2.3.3 Boundary Layer Measurements 11
2.3.4 Normalization of Test Data 11
2.3.5 Test Data 12
3.0 Correlation of Test Data 13
3.1 Correlation for the metallic perforated face sheets 15
3.2 Correlation for the perforated face sheets made from composite materials 16
3.3 The Non-linearity Issue - Sensitivity to the Normalized Flow Velocity through the Face Sheet 17
3.4 The Effects of the Boundary Layer Displacement Thickness, δ^* 17
3.5 Comparison with the correlation by Rice and Heidelberg 18
3.6 Grazing Flow Effects for Liners with Linear Face Sheets.. 18
4.0 Discussion, Conclusions and Recommendations 19

Nomenclature 22
References 23
Tables 1 through 3 ..... 24 to 28
Figures 1 through 44 ..... 29 to 82

Appendix I – B. F. Goodrich Semi-empirical Acoustic Impedance Model A-1
Appendix II -- Procedure for Computing and Normalizing DC Flow Resistance Data B-1

1.0 Introduction

The work reported herein was started in 1998, with GE Aircraft Engines (GEAE) as the principal contractor and B.F. Goodrich (BFG) as a major subcontractor. This work aimed at improvement in the following areas of acoustic treatment design technology.

a. The modeling of the impedance of acoustic liners with perforated face sheets. More specifically, a better understanding of the effects of grazing flow on the resistance and mass reactance of face sheet materials was required.
b. Evaluation of advanced suppression prediction codes, developed under NASA contracts, versus measured engine data. Development of new codes implementing recent advances.

Of the above, the effort on the evaluation and development of codes was terminated due to a substantial reduction in the funding available for this contract.

The test plan proposed by GEAE included the following three different methods for the measurement or eduction of the acoustic impedance of single-degree-of-freedom (single layer) acoustic liners.

(i) **Steady flow resistance measurement in grazing flow:** This method does not involve any acoustic data requiring accurate frequency domain information of magnitude and phase. Instead, steady pressure and temperature measurements are required to determine the steady flow resistance under given grazing flow conditions. Therefore the measurement technique is simpler and less risky. However, this method can not provide any data on the effects of grazing flow on the mass reactance of the face sheet.

(ii) **Impedance measurement by the "In-situ" method [3]:** This method requires the measurement of acoustic signals at the face sheet and the back wall of a cavity. The complex ratio of these signals at a given frequency, together with the cavity depth and the speed of sound, are used to compute the acoustic Impedance of the single layer liner. The real part of the complex impedance is the acoustic resistance and the imaginary part represents the acoustic reactance. Syed conducted an analysis of the measurement uncertainties in this method. This analysis showed that the errors in the reactance data due to errors in measured magnitude and phase of the complex ratio (mentioned above) might be acceptable. Moreover, it was argued that taking the average values of data from up to eight different cavities could minimize this error. Some preliminary test data were presented[4] at the "Orifice Impedance Model Workshop," in February 1998 in Chula Vista, California.

(iii) Impedance eduction from insertion loss data. This method requires the measurement of the acoustic insertion loss in the flow duct facility at the BF Goodrich plant at Chula Vista in California. J. Yu described the method [5] at the Orifice Impedance Model Workshop held at Chula Vista in February 1998. It involves the determination of the acoustic modal coefficients or amplitudes from an insertion loss test with a liner of known acoustic impedance. These modal coefficients are then used to compute the insertion loss spectrum for a liner of unknown impedance. In these computations, first the acoustic reactance of the liner is assumed to be known and the resistance is varied until a close agreement with the measured insertion loss spectrum is achieved. This process is then repeated with the mass reactance also. In this way, values of the acoustic resistance and mass reactance of the test panel can be educed.

The work planned by GE to perform acoustic impedance measurements by the In-situ Method was also deleted due to reduced funding.

This report contains the details of the work done by GE Aircraft Engines and by BF Goodrich.

2.0 Testing and Analysis

2.1 Test Panels and Samples

The sandwich construction of a test panel is schematically shown in the sketch below

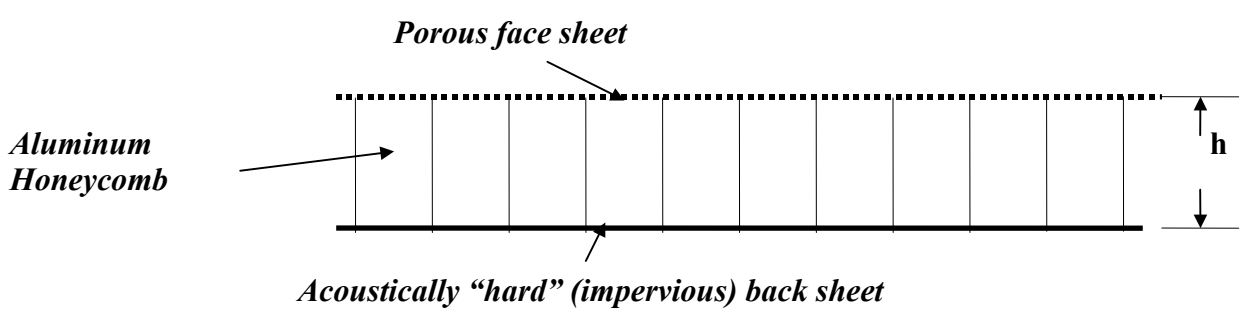

h is the depth of the honeycomb core. The focus of this test program was on perforated face sheets only. The face sheets were made from metallic and composite materials. The perforations were produced by different manufacturing processes that are currently used in the production of acoustic liners for aircraft engine nacelles. These processes included

- Punching for Aluminum face sheets
- Drilling (BFG, Graphite-Epoxy composite)
- Forming by pin-mandrels (GEAE & Boeing - Graphite- and Fiberglas-Epoxy composites)
- the "Pin-less" process (MRAS – Graphite and Fiberglas-Epoxy)

The sheet reticulation process was used for the bonding of the face sheet to the honeycomb core.

Table 1 shows the nominal parametric details of the acoustic panels that were tested in flow duct apparatuses at GE, BFG and NASA LaRC.

Two additional panels with linear wiremesh-on-perforate face sheets were also fabricated for insertion loss testing in the flow duct at BF Goodrich (BFG) plant in Chula Vista, California. The objective for testing these panels will be discussed later in this report.

For each liner design (Table 1), two acoustic treatment panels were fabricated. The first panel, shown in Figure 1, is 5.5 inch wide and 24 inches long, designed for testing in the GE and BFG Flow Ducts. The second panel, shown in Figure 2, is 2 inch wide and 15.852 inches long. It was designed for testing in the flow duct at NASA LaRC. Thus, two sets of 15 treatment panels were be fabricated; one set for GEAE & BFG and the second set for NASA LaRC.

Corresponding to each test panel, a set of test samples, for DC flow resistance and normal incidence Impedance tube measurements, was also fabricated. These samples were used by GE to conduct DC flow tests in grazing flow conditions.

A sample with "Wiremesh-on-Perforate" type linear face sheet was also tested. The test results created enough interest to require the testing of additional samples. Consequently, five more samples with wiremesh type linear face sheets were tested under Task order 13, sub-task 2G. These are described in section 3.6.

2.2 Tests Conducted at the B. F. Goodrich Plant

2.2.1 DC Flow Resistance Tests

BF Goodrich (BFG) measured the DC Flow Resistance of the perforated face sheet materials, for samples 1 through 12, before and after bonding to the honeycomb core. The data from these tests are summarized in Table 2. Note that the porosity values in Table 2 were computed from the DC-flow data using the process described below.

A sample of the acoustic treatment panel, without the impervious back sheet is tested in a DC Flow apparatus. These DC flow resistance data are used to obtain, by linear regression, a correlation of the form

$$\mathbf{R_0 = a_0 + b_0\, U_0} \qquad \ldots\ldots\ldots\ldots \qquad (1)$$

where R_0 is the flow resistance (cgs Rayl), U_0 is the flow velocity (cm/s) through the test sample and a_0 and b_0 are constants to be determined by the linear

regression process. The suffix "0" denotes that the flow resistance data are normalized to reference values of temperature and pressure (530°R & 14.7 psia) at the sample.

For Perforated sheet materials with square edged holes, the effective values of porosity σ, hole diameter d, and face sheet thickness t, are related as follows [1, 5]:

$$\mathbf{C_d = 0.80695 \sqrt{\{\sigma^{0.1} / \exp(-0.5072\ t/d)\}}} \qquad \ldots\ldots\ldots\ldots \qquad (2)$$

$$\mathbf{b_0 = \{\rho_0/(2\ C_d^2)\}\ \{(1-\sigma^2)/\ \sigma^2\}} \qquad \ldots\ldots\ldots\ldots \qquad (3)$$

$$\mathbf{d = \sqrt{[(4\ s_1 s_2\ \sigma)/\pi]}} \qquad \ldots\ldots\ldots\ldots \qquad (4)$$

$\mathbf{s_1}$ and $\mathbf{s_2}$ (***assumed to be known***) are the values of the hole spacing as illustrated below.

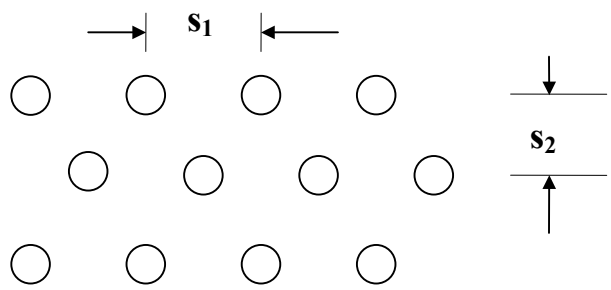

The thickness, t, of the face sheet is also assumed to be known (from measurements). The following iterative process is used to compute the values of σ and d.

1. Assume $\mathbf{C_d} = 0.76$, and $\mathbf{t/d} = 0.3$ (say)
2. Compute σ from equation (3) and d from equation (4). Compute new value of (t/d) .
3. Compute new value of C_d from equation (2)
4. Repeat step 2. Compare new value of σ with its previous value. If the difference is insignificant, then stop the iteration. Otherwise repeat steps and 3 and 2.

   This iterative process is illustrated in the diagram below.

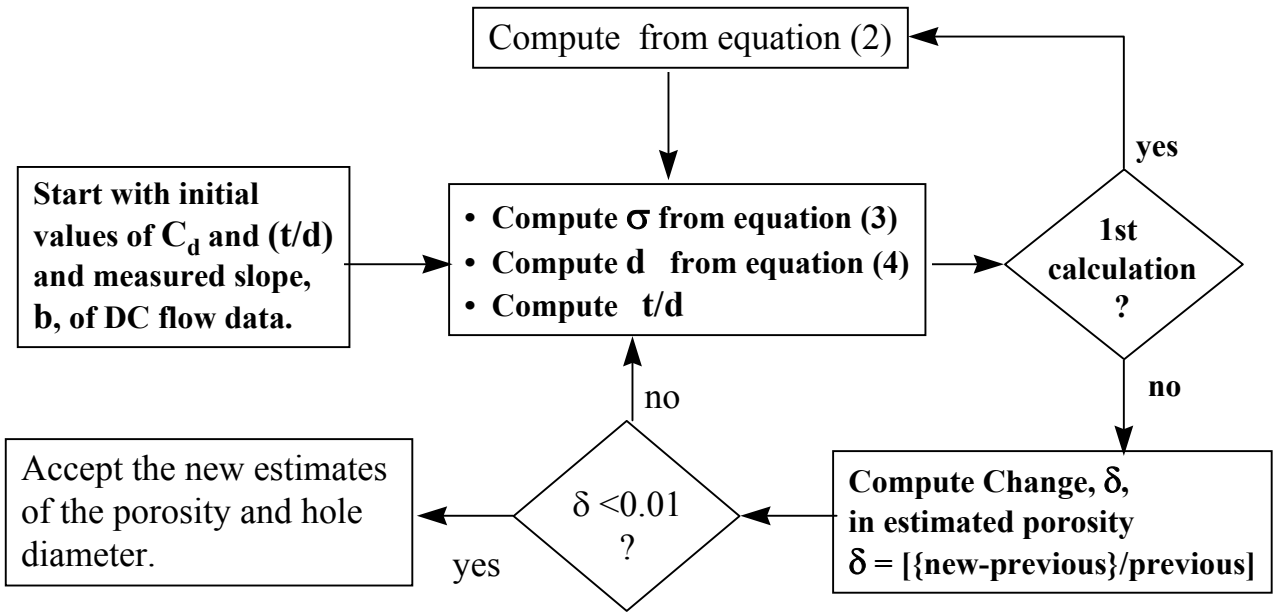

2.2.2 Impedance Tube Measurements

A sample from each of the 12 treatment panels was tested in the impedance tube apparatus. The test apparatus is described in Appendix I. The test data and the corresponding predicted impedance data are contained in the Excel file ***NM-Imp-data.xls*** of reference [6].

2.2.3 Flow Duct Insertion Loss Data

The flow duct apparatus used in the Insertion Loss measurements is schematically illustrated in Figure 3. In the flow duct apparatus at BFG, the acoustic excitation is in the upstream reverberation chamber. Over the frequency range of interest, the acoustic fields inside the two reverberation chambers are considered to be diffused. Therefore, the acoustic power in a reverberation chamber can be deduced from one measurement in it. The principal acoustic measurements made for a given test condition (test panel, flow Mach number) are the sound pressure level (SPL dB) spectra in the upstream and the downstream reverberation chambers. The acoustic insertion loss is defined as follows

$$\mathbf{IL\ dB}\ (f) = \mathbf{SPL_U}\ (f) - \mathbf{SPL_D}\ (f) \qquad \ldots\ldots \qquad (5)$$

where f is the acoustic frequency, suffixes U and D represent acoustic data from the upstream and the downstream chambers respectively.

The acoustic power suppression due to a treatment panel in the test section is obtained as follows

$$\Delta\mathbf{PWL\ dB(f)} = [\mathbf{IL\ dB}\ (f)]_{\mathbf{LINER}} - [\mathbf{IL\ dB}\ (f)]_{\mathbf{HW}} \ldots\ldots\ldots \qquad (6)$$

where

$[\text{IL dB}(f)]_{\text{LINER}}$ is the insertion loss with the acoustic liner in the test section, and

$[\text{IL dB}(f)]_{\text{HW}}$ is the insertion loss with hard walls in the test section.

This measurement technique has been developed and routinely used by BFG to compare the acoustic performance of liners with small design changes.

Jia Yu of BFG described the proposed use of this measurement, for the eduction of liner impedance under grazing flow conditions, in a recent workshop [5]. It involves the use of 2D modal propagation theory in a flow duct with one-side-lined. In order to use this method, a knowledge of the coefficients of acoustic modes propagating in the duct, upstream of the lined test section, is required. Since linear liners, with wiremesh-type face sheets, are minimally affected by the grazing flow conditions, the impedance of the two linear panels discussed in section 3.1 will be estimated with good accuracy. For this purpose these two treatment panels, with known acoustic impedance characteristics, are tested first in the flow duct at the required grazing flow conditions. From the known impedance value $Z(f)$, a set of modal coefficients is determined by minimizing the difference between the predicted and the measured values of $\Delta PWL(f)$. These modal coefficient data are saved, to be used later.

In order to educe the acoustic impedance of a treatment panel with a perforated sheet, it will be tested at flow conditions for which the modal coefficient data have been previously established by the method described above. Using the modal coefficient data, 2D modal analysis theory and an estimate of the impedance $Z(f)$, $\Delta PWL(f)$ will be calculated. By iterating on the impedance value, the difference between the measured and the calculated values of $\Delta PWL(f)$ will be minimized. The value of acoustic impedance that corresponds to the minimum difference between the measured and calculated $\Delta PWL(f)$ values represents the best estimate of the impedance of the liner at frequency f. The process is repeated over the frequency range for which $\Delta PWL(f)$ data have been measured.

A similar methodology was employed at Rolls Royce [7] in the mid 1970's. In that work, however, the assumption of equal modal energies was used to compute the acoustic power suppression.

Flow duct insertion loss data for treatment panels 1 through 13, for three panels with DynaRohr face sheets, and three composite panels #14, #15A and 15B from GEAE were tested by BFG. The data from these tests are contained in the file ***data.xls*** of reference [6]. These insertion loss data were acquired at air flow speeds of Mach 0.0, 0.1, 0.3, 0.5 and 0.7.

Note that BFG did not complete the eduction of acoustic impedance from the measured insertion loss data because of funding cuts. Instead, they compared predicted suppressions with measured insertion loss data using the

Rice-Heidelberg[2] correlation for impedance prediction. Dr. Kwan presented these data during the review held at NASA LaRC.[11]

2.3 DC Flow Resistance Measurements in the Flow Duct Apparatus at GE

These tests were performed in the **Acoustic Laboratory** at GEAE, in Evendale, Ohio.

A new flow duct apparatus was designed, fabricated and set up in the Acoustic Laboratory. The flow duct apparatus is schematically shown in Figure 4a. Note that the apparatus is designed to measure flow resistance in the following two modes.

- **Pull Mode** – in this mode, air is sucked into the test sample from the flow duct using a vacuum pump.
- **Push Mode** – in this mode, air is blown through the test sample into the flow duct using pressurized air.

The details of the installation of the acoustic treatment sample in the flow duct and the description of the data acquisition are shown in Figures 4b and 4c respectively. Figure 5 is a photograph of the flow duct showing some components of the DC Flow apparatus and its rectangular cross section. Note that this duct was designed to test panels of the size that are tested in the duct at BFG used for Insertion Loss testing.

All treatment samples of Table 1 were tested. In addition, the following two samples were also tested.

- a perforated Aluminum sheet sample, called the "GEAE's Standard Perforate"
- a sample with a wiremesh-on-perforate "DynaRohr" type face sheet.

The DC flow tests were carried out at grazing flow Mach numbers from 0 to 0.7 in steps of 0.1. These values were set at the inlet to the duct where the boundary layer thickness is negligible. However, at the test location, due to boundary layer growth, the free stream Mach numbers had higher values. Thus DC flow test data were taken at grazing flow speeds approaching Mach 0.8.

2.3.1 Flow Resistance Data without Grazing Flow {M =0.0}

It is generally well known that the steady (DC) flow resistance of perforated sheet materials is different when the direction of flow through the test sample is reversed. This is because the shape and the edges of the holes may be different on the two sides of the perforated sheet material as a result of the techniques and processes employed in manufacturing. For this reason DC flow resistance is measured in the Pull and Push modes described above. Figure 6 shows a plot of typical DC flow resistance data. Also shown are straight-line fits through the data from the push and the pull modes of testing. The values of the porosity from the slopes of these lines are computed by the following simple formula.

$$\mathbf{b_0 = \rho_0/(2\, C_d^2 \sigma^2)} \qquad \ldots\ldots\ldots \qquad (7)$$

Instead of following the procedure proposed by BFG (see section 2.2.1, above), a constant value of 0.76 was used for the discharge coefficient. The rationale for this is explained below.

GEAE and MRAS found that equation (2) in section 2.2.1 does not accurately determine the discharge coefficient in terms of the geometrical parameters of the perforated sheet materials. In order to establish a more accurate correlation, GEAE conducted DC flow measurements on a set of 19 perforated sheet samples covering a wide range of porosities and hole diameters. The data from these tests are summarized in Figure 7. The measured discharge coefficient data are plotted against the measured porosity determined from geometrical data. There is a lot of scatter in the values of $\mathbf{C_d}$. A polynomial fit through the data is also shown. Figure 8 shows the results of a statistical analysis of this set of data. It can be seen that the curve is relatively flat for porosity values between 5% and 15%. Therefore, a constant value, 0.76, for the discharge coefficient, was selected for calculating the porosity. Using this value for $\mathbf{C_d}$, in equation (7), the porosity is given by

$$\boldsymbol{\sigma = \sqrt{\{0.001039/b\}}} \qquad \ldots\ldots\ldots \qquad (8)$$

Equation (8) was used to compute the effective porosity (open area ratio) of the face sheet materials from DC flow data measured without grazing flow.

<u>Repeatability of Data without Grazing Flow (M=0.0)</u>

Repeated measurements of the flow resistance data for treatment samples #3 and #4 were obtained over several days to establish the repeatability of DC flow testing in the flow duct apparatus. First these measurements were made without grazing flow because the variation in these tests is considered to be due to the following:

- Unsteady response of the instrumentation and the data acquisition system
- Unsteadiness in the flow through the test sample.

Figure 9 shows data measured with the test sample #3. Five sets of data, obtained on five different days are plotted. Clearly, data from repeated tests on the same sample do not agree perfectly. However, this is expected of any measurement system. Therefore, we have to establish the variance of such measurements, using statistical methods. For this purpose, the DC flow data measured with the test sample #4 were used. Figure 10 shows statistical distribution plots for two parameters. The first parameter is the resistance, R100, corresponding to the flow velocity of 100 cm/s through the face sheet. The second parameter is the POA (per cent open area). Note, the POA is computed from the slope, b, only. R100 is computed the measured intercept and the slope. The data presented in Figure 10 are based on the intercept, a, and the slope, b that are the mean values from the "push" and the "pull" modes of air flow, as shown below.

$$\mathbf{a = \{a_{pull} + a_{push}\}/2} \qquad\qquad \mathbf{b = \{b_{pull} + b_{push}\}/2}$$

The statistical plots and data in Figure 10 are based on 18 different repeated tests. It is shown that the flow resistance, R100 is measured at 7.97±0.24 cgs Rayl (±3% of the mean value). Also, the POA is measured at 12.04% ±0.29%. Note that the POA determined from geometrical data is within the range 11.4% to 12.7% due to the uncertainties in the measured values of the hole diameter and the hole spacing.

2.3.2 Flow Resistance Data with Grazing Flow.

The procedure used in the reduction and analysis of DC flow data is described and discussed first. Figures 11a and 11b illustrate the steps that are used in the process. Figure 11a shows a plot of the measured pressure drop across the test sample, against the velocity of the airflow through the porous face sheet. Note that the airflow is measured by the laminar element flow meter, which is not affected by the grazing flow over the test sample. The measured data are labeled "UNCORRECTED." Note that the plot has a finite pressure drop across the test sample when the velocity of the airflow through it is zero. If the uncorrected data were used in computing DC flow resistance, then we would get very large values of resistance ($\pm \infty$) as the airflow velocity approaches zero. This absurd result is due to a *bias error* in the measured pressure drop across the test sample. Shifting the plot so that it passes through zero eliminates this bias error. The plot labeled "CORRECTED" shows this. The continuous plot of DC flow resistance in Figure 11b is obtained by using the corrected pressure drop data in Figure 11a.

Using the procedure described above, the DC flow resistance data measured at different grazing flow Mach numbers can be reduced. An example of such data is shown in the plots of Figure 12. It can be seen that of grazing flow has a big impact on the DC flow resistance of the test sample. Under zero grazing flow, the mean particle velocity of the airflow through the face sheet primarily affected the resistance of the test sample. Under grazing flow conditions, the free stream Mach number of the grazing flow is the principal parameter of interest. The non-linearity (sensitivity to particle velocity normal to the face sheet) of the perforated test sample is of very little interest under grazing flow conditions that are typically experienced in engine nacelles.

<u>DC flow Resistance at Root-Mean-Squared (*rms*) Values of Particle Velocity</u>

In acoustic applications, the air particle velocity normal to the porous face sheet of a liner is periodic. That is, air particles move through the liner surface in push and pull modes. It is normal in acoustics to refer to root-mean-square (***rms***) values of acoustic velocities and acoustic pressures. Therefore, it is more useful to express flow resistance data in terms of ***rms*** values. The following procedure was used to accomplish this.

Figure 13a is a plot of typical flow resistance data obtained under grazing flow conditions. A 3rd order polynomial fit through the data is then obtained. Figure

13b shows a plot of flow velocity through the test sample during one cycle. This distribution of flow velocities corresponds to a specific ***rms*** value. The polynomial from Figure 13a is used to compute the flow resistance values corresponding to the flow velocities of Figure 13b. From these data, plotted in Figure 13c, a ***rms*** value of the flow resistance is computed. In this way, a set of ***rms*** values of flow resistance corresponding to a set of ***rms*** values of particle velocity through the test sample are obtained. Figure 13d shows a typical plot of ***rms*** flow resistance data against ***rms*** flow velocities.

Observe that the slope of the plot in Figure 13d is relatively small, compared to the slope under zero grazing flow. This implies that the porous face sheet material tends to become "linear" as a result of grazing flow.

It should be noted that the measured DC flow resistance data correspond to flow velocities in the range -150 (cm/s) $\leq U_0 \leq 250$ (cm/s). Therefore, ***rms*** Resistance data corresponding to rms flow velocities that are greater than 150 (cm/s), require extrapolation. Hence, the accuracy of such data may be questioned.

A polynomial fit through the data of Figure 13d can be used to obtain the following set of data:

- $R_0(0, M)$ the value of flow resistance at ***rms*** flow velocity of 0 (cm/s)
- $R_0(20, M)$ the value of flow resistance at ***rms*** flow velocity of 20 (cm/s)
- $R_0(100, M)$ the value of flow resistance at ***rms*** flow velocity of 100 (cm/s)
- $R_0(150, M)$ the value of flow resistance at ***rms*** flow velocity of 150 (cm/s)
- $NLF(150{:}20, M) = \{R_0(150, M) / R_0(20, M)\}$

where M is the Mach number of the grazing flow and R is the ***rms*** flow resistance (cgs Rayl). The suffix 0 indicates that the data are corrected to "reference" temperature and pressure conditions at the surface of the treatment sample. GEAE uses 70°F and 29.92 inches of Hg., respectively, for reference temperature and pressure values. The rationale for correcting DC flow Resistance data to reference conditions of temperature and pressure is discussed in Appendix II.

As pointed out above, the slope of the ***rms*** Resistance versus ***rms*** flow velocity plot, under grazing flow conditions, is relatively small and the curve may be approximated to a straight line for ***rms*** flow velocities less than 150 cm/s. Thus a knowledge of the intercept, $R_0(0)$, and the nonlinearity factor, NLF(150:20), is sufficient to estimate the Acoustic Resistance under the grazing flow Mach number that corresponds to the engine operating conditions of interest.

Finally, the Resistance data, $R(U_0, M)$, were normalized by the characteristic impedance, $(\rho_0 c_0)$, of air at the reference temperature and pressure. These data were then analyzed and correlated in terms of the design parameters of the face sheet material and the grazing flow conditions.

2.3.3 Boundary Layer Measurements

Boundary Layer flow velocity profile measurements were made over the test sample at two Mach numbers only. This was done to minimize test time in order to minimize the cost of testing which included the cost of the high-pressure air supply (labor of the operators of the 401-compressor system). Also, towards the end of the testing, the boundary layer probe system broke down. Therefore it was not possible to acquire data for every test sample. This was not considered a serious problem for the reasons stated below.

Note that the flow duct upstream of the small test sample is unchanged throughout the test program. The flow velocity profiles measured over the test sample were due to boundary layer development upstream of the test sample. Therefore, the test sample itself was not expected to affect the boundary layer profiles measured over it. This is exactly what was observed from the test data. Hence, the data acquired is representative of the flow profiles for all test samples.

Figure 14 shows typical velocity profiles measured at Mach 0.3 (approximately). Also shown are the values of the displacement and the momentum thickness (δ^*, θ). Note that as expected, the airflow through the test sample did not have much effect on the boundary layer profile and thickness data.

2.3.4 Normalization of Test Data

As mentioned in section 2.3.2, all flow resistance data were normalized to reference temperature (T_0 =70°F) and pressure (P_0 = 14.7 psia) conditions at the surface of the liner test sample. To compute the flow resistance at any other temperature and pressure values, use the following procedure.

The normalized data presented in this report is given by

$$\mathbf{R_0\,(U_0\,,\,M) = a_0(M) + b_0(M)\,U_0} \qquad \ldots\ldots\ldots\ldots \qquad (9)$$

Where

M Mach number of grazing air flow over the liner surface
R Flow Resistance (cgs Rayl)
U Flow particle velocity normal to the liner surface (cm/s)
a The Intercept - value of resistance, R, corresponding to U=0
b The slope – the rate of increase of resistance, R, with velocity U

The suffix "0" represents the reference conditions of temperature (**T_0**) and pressure (**P_0**). The values of **a_0** and **b_0** depend on the geometric parameters of the perforated face sheet.

The flow resistance at any temperature, **T**, and pressure, **P**, can be computed from

$$\mathbf{R(U,\,M) = a(M) + b(M)\,U} \qquad \ldots\ldots\ldots\ldots\ldots \qquad (10)$$

where

$$\mathbf{a(M) = a_0(M)\ (\mu/\mu_0) \approx a_0(M)\ (T/T_0)^{0.75}} \quad \ldots\ldots\ldots\ldots\ldots \quad (11)$$

$$\mathbf{b(M) = b_0(M)\ (\rho_0/\rho) = b_0(M)\ (P_0/P)\ (T/T_0)} \ldots\ldots\ldots\ldots \quad (12)$$

2.3.5 Test Data

The normalized DC flow data for the liner samples (#1 through #15), tested under grazing flow conditions, are presented in Figures 15 through 28.

Figure 15 shows tabulated data showing the face sheet parameters and the measured DC flow data for a set of grazing-flow Mach number values. Note that for each value of grazing flow Mach number, the DC flow resistance data consists of the following

$\mathbf{R_0}$	the "Intercept" -- value of flow resistance corresponding to zero particle velocity.
NLF	Non-linearity Factor $\mathbf{NLF_{150/20}}$ – ratio of resistance values flow velocities of 150 (cm/s) and 20 (cm/s). That is, $NLF_{150/20}$ = R(150)/R(20).
$\mathbf{R_0}$*	$\mathbf{R_0/(\rho_0 c_0)}$, non-dimensional resistance; ρ_0 is the density of air and $\mathbf{c_0}$ is the speed of sound.
oar.$\mathbf{R_0}$*	$\mathbf{R_0}$* multiplied by the open area ratio, **oar**.

The slope $\mathbf{b_0}$, can be calculated as follows

$$\mathbf{b_0 = R_0\ \{(NLF-1)/(150-20\ NLF)\}} \quad \ldots\ldots\ldots\ldots \quad (13)$$

Using $\mathbf{R_0}$ for $\mathbf{a_0}$, and $\mathbf{b_0}$ from equation (13), the flow resistance at any particle velocity, $\mathbf{U_0}$, can be computed from equation (10).

<u>Repeatability of test data under grazing flow conditions</u>

Because of the considerable cost of conducting tests under grazing flow conditions, it was not possible to conduct very extensive testing to obtain repeatability data. However a limited amount of repeat testing was done on sample number 3. In addition, two different samples from liner #14 were tested and two samples from two different panels, #15-1 and #15-2 (from MRAS) were tested.

The data from sample #3 is shown in Figures 17a through 17c. In Figure 17c, data from the two tests are plotted for comparison. The repeatability is very good up to grazing flow Mach number values of 0.6. Maximum variation in test data is observed at Mach 0.8.

The data from the two different samples from liner #14 are compared in Figure 27c. There is very good agreement between the two sets of measurements up to Mach 0.7. Again, maximum variation is observed at Mach 0.8.

The data from the two test panels, #15-1 and #15-2, produced by MRAS, are compared in Figure 28c. Again, there is very good agreement between the two sets of measurements up to Mach 0.6. At higher grazing flow speeds, the variation increases with Mach number. However, in this case, the data variation at Mach 0.8 is much smaller than observed for liners #3 and #14.

Flow Resistance Data for a liner sample with Linear "wiremesh-on-perforate" face sheet.

The measured data, in non-dimensional form, is plotted against grazing flow Mach number, in Figure 29. Also plotted is the predicted values using the approximate relation, $\Delta R^* = 0.5$ M, based on earlier work by Syed.[10]

Note that the increase in resistance is quite modest at Mach number values up to 0.4. At higher grazing flow speeds, the resistance increases much more rapidly with increasing values of grazing flow Mach number.

3.0 Correlation of Test Data

The parameters of interest in the DC flow measurement, in high speed grazing flows, are tabulated below.

Symbol	Description
t	Thickness of the porous face sheet sample.
d	Diameter of the holes, if perforated face sheet
σ	Porosity or open area ratio (OAR)of the porous face sheet. This is a non-dimensional parameter.
T	Static temperature of the air
ρ	Density of the air
μ	Coefficient of viscosity of the airflow through the test sample
c	Speed of sound at temperature, **T**
u	Velocity of air flowing through the test sample
V	Free stream velocity of the grazing flow (parallel to the duct wall)
δ^*	Boundary layer displacement thickness

In the analysis of sound propagation in acoustically lined ducts, the acoustic resistance of the liner is normalized by the characteristic impedance, ρc, of air. Similarly, the DC flow

resistance should be normalized as $\left\{\frac{\Delta P}{\rho c u}\right\}$. Other non-dimensional groupings of the above parameters are:

$$\left\{\frac{t}{d}\right\} \;;\; \left\{\frac{u}{c}\right\} \;;\; \left\{\frac{V}{c}\right\} \;;\; \left\{\frac{\rho c d}{\mu}\right\} \;;\; \left\{\frac{\delta^*}{d}\right\} \;;\; \sigma$$

Reynolds number based on the speed of sound, **c**.

According to Buckingham Π Theorem, a unique correlation exists between the normalized flow resistance and the other non-dimensional parameters listed above.

Salikuddin [12] also obtained DC flow resistance data under conditions of high speed grazing flows at three different values of the air temperature. The author[13] analyzed some of these data to investigate the dependence on the above Reynolds number. It was shown that these data collapsed well on a single correlation between the normalized values of flow resistance and the through-flow velocity, (**u/c**). There was no clear trend in regard to variations in the Reynolds number. Thus, it was demonstrated that the "Normalized DC flow resistance" is not dependent on temperature except through the air density and the speed of sound used in the normalizing process.

In previous work [2, 3], the increase in acoustic Resistance was correlated in the following manner.

$$\Delta R^* = F\{M, \delta^*/d\}/\sigma$$

where

ΔR* is the increase in normalized acoustic Resistance under grazing flow conditions relative to no grazing flow conditions

δ*/d ratio of boundary layer displacement thickness, **δ***, and the diameter, **d,** of the perforations in the face sheet of the acoustic liner

σ Open area ratio (**OAR**) or porosity of the face sheet.

F{M, δ*/d **}** is a function to be determined from the correlation of the measured data.

The correlation developed by GE, is of the following form.

$$R^*\{M, \sigma, (\delta^*/d),.(u/c)\} = F_1\{M, \sigma, (\delta^*/d)\} + F_2\{M, \sigma\}\,(u/c) \qquad \ldots\ldots \quad (14)$$

3.1 Correlation for the metallic perforated face sheets

First consider the test data from samples # 1, #2, #3, #4, #9 and #10. All these samples have holes of 0.039 inch diameter. Also for these tests, there is no variation in the boundary layer thickness to hole diameter ratio, (δ^*/d). Thus these data can be used determine a correlation between **R***, **M**, **(u/c)** , and the porosity **σ**. Sample #5 has holes of 0.090 inch diameter. Also Samples #6, #7 and #11 have holes of 0.050 inch diameter. Therefore, the data from these samples, together with the data for samples with 0.039 inch diameter holes, were used to obtain a correlation between **R*** and **(δ^*/d)**.

The final Calibration of all the data from the perforated metallic face sheets is as follows:

$$F_1\left\{M, \sigma, \frac{\delta^*}{d}\right\} = \alpha_1\{M\}\,\sigma^{\beta_1\{M\}}\left\{\frac{\delta^*}{d}\right\}^{\beta_2\{M\}} \qquad (15)$$

$$\alpha_1\{M\} = 0.0713\,M + 0.3181\,M^2 \qquad (16a)$$

$$\beta_1\{M\} = -1.423 + 0.733\,M - 0.367\,M^2 \qquad (16b)$$

$$\beta_2\{M\} = -0.347 + 0.118\,M \qquad (16c)$$

$$F_2\{M, \sigma\} = \alpha_2\{M\}\,\sigma^{\beta_3\{M\}} \qquad (17)$$

$$\alpha_2\{M\} = 0.53\,e^{-4.95\,M} \qquad (18a)$$

$$\beta_3\{M\} = -2.08 - 2.395\,M + 1.633\,M^2 \qquad (18b)$$

Thus

$$R^*\left\{M, \sigma, \frac{\delta^*}{d}, \frac{u}{c}\right\} = \alpha_1\{M\}\,\sigma^{\beta_1\{M\}}\left\{\frac{\delta^*}{d}\right\}^{\beta_2\{M\}} + \alpha_2\{M\}\,\sigma^{\beta_3\{M\}}\left\{\frac{u}{c}\right\} \qquad (19)$$

Note that the first term, $F_1\{M, \sigma, \delta^*/d\}$ represents the so-called "intercept" or the linear term, which is independent of the flow velocity through the perforated sheet. The second term, $F_2\{M, \sigma\}$, represents the "non-linear" term or the "slope", which shows sensitivity to the normalized flow velocity, (u/c), through the perforated sheet.

In Figure 30, the linear part of the correlation (the intercept) is compared with the measured data from all the metallic treatment samples. Note that the magnitude of the deviation of the measured data from the correlation increases with the grazing flow Mach number.

Figure 31a shows a histogram of the data scatter from the predictions of the linear (intercept) normalized resistance (ρc) of the metallic face sheet samples. It shows that all

data, except one measurement, lies within ±0.5ρc of the predicted value. Note that the distribution of the data scatter is very similar to the "Normal" distribution. This means that the data scatter is largely caused by random errors in the measurement process.

Figure 31b shows a plot of the residuals against the fitted values, as determined by regression analysis of the predicted and the measured data. The correlation between the predicted values and the corresponding measured data is 98.8%.

3.2 Correlation for the perforated face sheets made from composite materials

The composite treatment samples #12 and #14 were manufactured by B. F. Goodrich and by GE (Albuquerque plant) respectively. Figure 32 shows the linear part of the normalized resistance data from tests on these samples compared with predictions using the correlation defined by equations 15 through 19. Note that the measured values of the normalized resistance, R*, are slightly less than the corresponding predicted values for both the test samples. However, the differences between the measured and the predicted data are within the data scatter described in section 3.1 above. A statistical analysis, called "two sample T-Test," on the data from the metallic perforated sheets and from Samples #12 & #14 was performed. It showed that within 95% confidence interval, the above two sets of data belonged to a single distribution. This means that the correlation developed from data measured with metallic perforates can be used for composite perforates represented by samples #12 and #14.

The samples #15A and 15B were made of Graphite-Epoxy face sheet, perforated by means of a "Pin-Less" process, by Middle River Aircraft Systems. The face sheet also had an "erosion resistant coating" which significantly affected the hole shapes at the edges, as illustrated in the schematic sketch below.

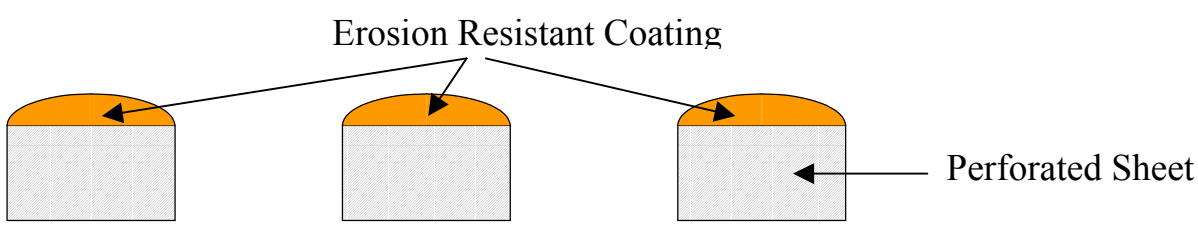

Figure 33 shows a comparison of the measured values of the normalized linear part of the resistance with the corresponding predicted values, using the correlation defined in equations 15 through 19. It is clear that the measured resistance values are significantly less than the predicted values, especially at grazing flow Mach numbers greater than 0.2. It is believed that this effect is caused by the change in the hole shape due to the erosion resistant coating. This is an important finding. It means that to some extent the normalized resistance of a perforated sheet of given porosity may be controlled, under grazing flow conditions, by using surface coatings. After a separate investigation into this phenomenon, MRAS obtained a US patent [14] for this ability to control the normalized resistance of a perforated face sheet under grazing flow conditions.

3.3 The Non-linearity Issue – Sensitivity to the Normalized Flow Velocity through the Face Sheet.

Figure 34 shows, for sample #1, the plots of the measured Normalized Resistance, R*, against the normalized flow velocity through the face sheet, at different values of the grazing flow Mach number. Note that the sensitivity of the measured value of R* to the normalized through flow velocity, (u/c), decreases with increasing values of the grazing flow Mach number. This observed trend is true for all face sheet samples tested under this research project.

For the data at each value of the grazing flow Mach number in Figure 34, a slope was defined. Thus for each grazing flow Mach number, the Normalized Resistance can be expressed as

$$R^*\{M)\} = \text{Intercept}\{M\} + \text{Slope}\{M\}\left\{\frac{u}{c}\right\}$$

The intercept is referred to as the linear part of the resistance. The slope represents the sensitivity to the flow velocity through the face sheet. It represents the nonlinearity of the porous face sheet. The test data from all the metallic face sheet samples were used to derive the correlation described by equations (17), (18a) & (18b).

Note that u/c=0.003 represents flow velocity of approximately 100cm/sec at 70°F (530°R). It can be seen that at grazing flow Mach numbers greater than 0.3, the non-linear effect may be negligible for low values of (u/c). Therefore, in treatment design calculations for aircraft engine nacelles, the non-linearity effect may be neglected when the grazing flow speeds are greater than 0.3. This eliminates the need to know the in-duct acoustic excitation levels (spectral data) for the purpose of liner design.

3.4 The Effects of the Boundary Layer Displacement Thickness, δ^*

The non-dimensional parameter of interest is the normalized displacement thickness, (δ^*/d). The measured boundary layer data are presented in Figure 35. Note that between the two values of grazing flow Mach number, there was very little change in mean value of the boundary layer displacement thickness. Consequently a mean value of $\delta^* = 0.057$ was used to compute values of (δ^*/d). Thus all the variation in this parameter was due to the variation in the hole-diameter.

Figure 36 compares the boundary layer effects predicted by the current correlation (equation 15) with those predicted by the Rice / Heidelberg correlation described in section 3.5. Note that the boundary layer effects predicted by the GE correlation are very close to those predicted by the Rice / Heidelberg correlation.

Figure 37 compares the boundary layer effects on the normalized Resistance, R*, at different values of the grazing flow Mach number. The data show that the effects of boundary layer thickness variation increase with the grazing flow Mach number.

3.5 Comparison with the correlation by Rice and Heidelberg

The simple correlation by Rice[2] is given by

$$\mathbf{oar.\Delta R_0^* = 0.3M} \qquad \ldots\ldots\ldots \qquad (20)$$

The more complex correlation by Rice and Heidelberg is given by

$$\mathbf{oar.\Delta R_0^* = M/\{2+1.256(\delta^*/d)\}} \qquad \ldots\ldots \qquad (21)$$

Comparisons of the Normalized Resistance, R*, calculated by the GE method (equation 19) and the Rice/Heidelberg method (equation 21) are shown in Figure 38. Data correspond to open area ratio (OAR) of 10% and two values of (**δ*/d**). Note that the Rice/Heidelberg correlation significantly under predicts the normalized resistance at grazing flow greater than Mach 0.4.

3.6 Grazing Flow Effects for Liners with Linear Face Sheets

Figure 29 shows data from a wiremesh-on-perforate type linear sample tested under Task Order 3. These data clearly indicated a significant increase in resistance due to high speed grazing flow. Additional tests were conducted on linear treatment samples taken from panels that were originally constructed under Task Order 25. These samples are described in the table below.

Panel ID	Description of the face sheet of acoustic liner.	R* (intercept)	POA of Perf. Sheet.	Dia (inch) of holes in Perf. Sheet	Perf Sheet Thickness (inch)
# 4-4.1	SDOF: Wiremesh-on-Perforate	2.24	34%	0.05	0.025
# 4-4.4	SDOF: Wiremesh screen bonded directly on honeycomb.	1.86	NA	NA	NA
# 5-5.1	SDOF: Wiremesh-on-Perforate	1.51	34%	0.05	0.025
# 5-5.4	SDOF: Wiremesh screen bonded directly on honeycomb.	1.11	NA	NA	NA
# 6-6.1	2DOF: Wiremesh-on-Perforate face sheet	0.95	34%	0.05	0.025

The measured Normalized Flow Resistance data from tests on samples from these panels are presented in Figures 39 through 43.

It can be seen that the effects of grazing flow on the normalized resistance of these so-called linear materials are quite significant, and therefore, should not be ignored.

Figure 44 shows the increase in normalized resistance, {R*(M)-R*(0)}, plotted against the grazing flow Mach number, M, for the above five samples. The data for the wiremesh-on-perforate samples from panels #5-5.1 and # 6-6.1 show significantly larger increase in resistance than the data for the "wiremesh only" samples from panels #4-4.4 and #5-5.4. The data from the wiremesh-on-perforate sample from panel #4-4.1 are closer to the data from the "wiremesh only" samples.

These data from the five linear face sheets are not sufficient to establish generalized correlation for such linear face sheet materials. However, in the absence of better data, the following correlation may be used to compute the increase in resistance of linear face sheets, for grazing flow Mach number values in the range: $0.3 < M < 0.8$.

For "Wiremesh-on-Perforate" type face sheets:

$$\{R^*(M) - R^*(0)\} = 0.07\,M + 1.61\,M^2 \qquad \ldots\ldots \quad (22)$$

For "Wiremesh Only" face sheets:

$$\{R^*(M) - R^*(0)\} = -0.36\,M + 1.41\,M^2 \qquad \ldots\ldots. \quad (23)$$

4.0 Discussion, Conclusions and Recommendations

A technique to measure DC flow resistance under grazing flow conditions has been developed under this contract. A number of liner samples with perforated face sheets have been tested. Eleven (11) of these liner samples were made with punched Aluminum sheet materials. Three samples were made of Fiberglas-Epoxy or Graphite-Epoxy face sheets. These composite sheets were made with three different processes representing manufacturing as follows

B. F. Goodrich	holes produced by drilling
GE Aircraft Engines	holes produced by pin-mandrel tools
Middle River Aircraft Systems	holes produced by "pin-less process"

In addition, a sample with a laser drilled (micro-porous) thin film bonded on a 34% porosity perforated face sheet was tested. This sample represented a new process to produce face sheets with micro-porous label.

Six samples with so-called linear face sheets were also tested. Four of these had "Wiremesh-on-Perforate" and two had "Wiremesh Only" face sheets.

All liner samples with perforated face sheets, were fabricated using the "sheet reticulation method" for bonding the honeycomb core to the face sheet. The analysis of the test data revealed several interesting results. These are discussed below.

Linearity or Sensitivity to the particle velocity normal to the liner surface

Hitherto, perforated sheet materials have been regarded "very non-linear" because they were considered to be very sensitive to the acoustic particle velocity. This conclusion was based on DC flow resistance characteristics measured without grazing flow. This non-linearity, was considered undesirable. Hence the extensive use of linear liners made with wiremesh screens bonded on high porosity perforated sheets. These liners were expensive to fabricate and were easily damaged due to ingestion of birds, ice impact and erosion.

The data measured under this contract has proved that liners with perforated face sheets become linear when they operate in the presence of high speed grazing airflow. In actual fact they become as linear as any linear liner at grazing flow Mach numbers above 0.5.

Sensitivity to Grazing Flow Velocity

Tests have shown that perforated sheet materials are significantly more sensitive to grazing flow velocity than laser drilled (micro-porous) or DynaRohr type (wiremesh-on-perforate) sheet materials. However, the tests have also demonstrated that the laser drilled or the DynaRohr type liners are not insensitive to grazing flow. In the past, for DynaRohr and micro-porous sheet materials, the grazing flow effects were assumed to negligible. The tests conducted under this contract have demonstrated that for these materials, the increase in Resistance due to grazing flow is quite significant and should be taken into account when designing such liners.

The tests on the samples from MRAS show that spraying of erosion resistant coating can significantly reduce the sensitivity to grazing flow. Therefore, we can not use the correlation developed for punched Aluminum sheet materials, to predict the resistance of a face-sheet that has a thick coat of paint on it. More tests are needed to understand and correlate the effects of spray coating of acoustic liners. The test method developed under this contract is an economical way of conducting such studies.

The Effects of Grazing Flow on Mass Reactance

We have demonstrated that grazing flow has a major impact on the value of the acoustic resistance of a liner made with perforated face sheets. Any scaling laws and methods based on impedance data acquired without grazing flow are not accurate under high speed grazing flow conditions. This has been shown conclusively for the acoustic resistance. It is believed that the mass reactance of liners will also be greatly affected by high speed grazing flow. This was shown, to a limited extent, by Kooi & Sarin [3]. There is a need to investigate and quantify this effect.

Conclusions

- A new correlation for the Resistance of acoustic liners, made with perforated face sheets, has been obtained. This correlation is based on data at grazing flow speeds up to Mach 0.8.
- The increase in resistance with grazing flow Mach number is bigger than predicted by correlations proposed by Rice and Heidelberg. This difference is more significant at grazing flow speeds above Mach 0.5.
- Non-linearity characteristics decrease with grazing flow Mach number. Effectively, liners with perforated face sheets become linear (insensitive to acoustic particle velocity) under engine operating conditions.
- Grazing flow effects on the Resistance of laser drilled (micro-porous) face sheets (sample #13), are much bigger than predicted by Heidelberg-Rice correlation at all grazing flow speeds.
- DynaRohr type liners with wiremesh-on-perforate face sheets, do show significant increase in Resistance with increasing grazing flow Mach number. This effect should be included in design considerations.

Recommendations

The following work is recommended for future research sponsored by NASA.

1. Conduct tests to measure the mass Reactance of face sheet materials under grazing flow conditions. These tests, as originally planned, will be conducted with the In-Situ method for Impedance measurement.
2. Evaluate and develop new liner concepts that can provide substantial increase in noise suppression over conventional single layer liners.

Nomenclature

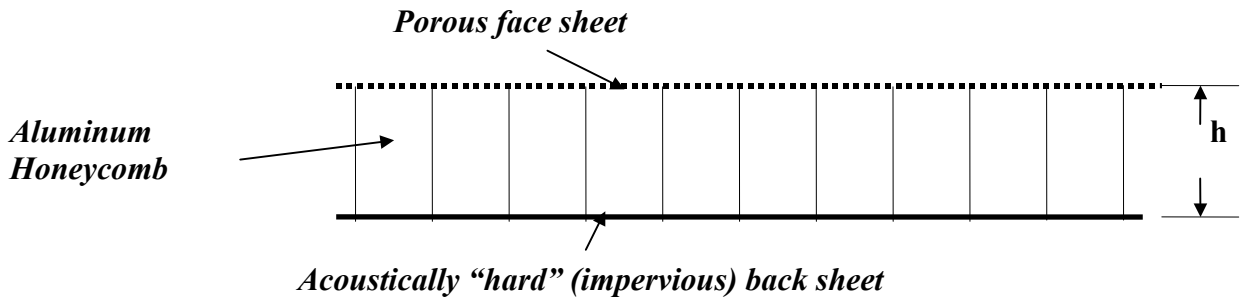

a - the intercept of the straight line relationship (Green's equation) for the Steady (DC) flow resistance of a porous sheet material (cgs Rayl)
b - the slope of the straight (green's equation)
c - speed of sound in air
d - diameter of perforations or holes (inch) in a perforated face-sheet
h - depth (inch) of the honeycomb core
s1 - spacing between adjacent holes in a row of the hole pattern of a perforated sheet
s2 - spacing between adjacent rows of holes
t - thickness of a face-sheet material
u - particle velocity (cm/s) of air flowing through the face sheet during a flow resistance test
oar - open area ratio or porosity of the hole pattern of a perforated sheet
rms - root-mean-squared value
C_d - discharge coefficient
M - Mach number of the grazing air flow over the test sample (V/c)
R - The steady flow Resistance (cgs Rayl); for a given porous test sample the flow resistance is given by Green's equation: $R(U) = a + bU$
R_0 - Value of resistance at $u = 0$; note that $R_0 = a_0$, the intercept of Green's equation
NLF - non-linearity factor -- The ratio of the flow resistance at two different values of flow velocity through the test sample. Thus $NLF_{150:20} = R(150)/R(20)$
R* - normalized or non-dimensional resistance; $R^* = R/(\rho c)$
R_0* - $R_0/(\rho c)$
U - particle velocity (cm/s) of air flowing through the face sheet during a flow resistance test
V - Grazing Flow Velocity
OAR - open area ratio or porosity of the hole pattern of a perforated sheet
δ - boundary layer thickness of the flow over the test sample
δ^* - boundary layer displacement thickness
μ - coefficient of viscosity
μ_0 - coefficient of viscosity at reference temperature
ρ - density of air flow over the test sample
ρ_0 - density of air at reference temperature and pressure
σ - open area ratio (oar) or porosity of the hole pattern of a perforated sheet
θ - boundary layer momentum thickness

The suffix 0 may denote reference conditions of temperature (70° F) and pressure (14.7 psia) or it may denote zero flow velocity through the porous sheet sample. Unless otherwise stated, all data presented in this report are normalized to the above reference temperature and pressure values.

References

1. R. E. Kraft, I. Yu and H. W. Kwan, NASA CR-1999-209120, "Acoustic Treatment Design Scaling Methods – Volume 2: Advanced Treatment Impedance Models for High Frequency Ranges." April 1999.

2. L. J. Heidelberg, E. J. Rice, and L. Homyak, " Experimental Evaluation of a Spinning-Mode Acoustic Treatment Design Concept for Aircraft Inlets," NASA Technical Paper 1613, 1980.

3. J. W. Kooi and S. L. Sarin, "An Experimental Study of the Acoustic Impedance of Helmholtz Resonator Arrays under a Turbulent Boundary Layer," paper AIAA-81-1998 presented at the 7th Aeronautics Conference in Palo Alto, California. October 1981.

4. A. A. Syed, "In-Situ Impedance Test Data," presentation during the "Orifice Impedance Model Workshop," in February 1998 in Chula Vista, California.

5. J. Yu, "Acoustic Liner Impedance Modeling with Grazing Flow," presentation during the "Orifice Impedance Model Workshop," in February 1998 in Chula Vista, California.

6. Data files generated in this study are archived on a CDROM entitled "Perforated Sheet Study Data - 2001." Individual files include "att-data.xls", "DC-resis-data.xls", "Dyna17-att.xls", "impedance data.doc", "NM-imp-data.xls" and "Perf1&3-att.xls."

7. A. A. Syed, "On the Prediction of Sound Attenuation in Acoustically Lined Circular Ducts," Doctoral Thesis, May 1980.

8. Communications between Asif Syed (GE), Jerry Bielak (Boeing), Jia Yu (BFG) and Mike Jones and Tony Parrott (NASA LaRC). Big differences between the Boeing's method and the GE/BFG method for the Acoustic resistance of perforated face sheet materials were pointed out. Jerry Bielak, in his presentation during the "Orifice Impedance Model Workshop," in February 1998 in Chula Vista, California.

9. R. E. Motsinger, A. A. Syed, and M. B. Manley, "The Measurement of the Steady Flow Resistance of Porous Materials," AIAA-83-0779, 8th Aeroacoustics Conference in Atlanta Georgia, April 19983

10. G. H. Fisk, A. A. Syed and R. E. Motsinger of General Electric Co. and M. C. Joshi and R. E. Kraft of Douglas Aircraft Co., "Measurement of Acoustic Modes and Wall Impedance in a Turbofan Exhaust Duct," AIAA –83-0733, AIAA 8th Aeroacoustic Conference in Atlanta, Georgia, April 11-13, 1983.

11. An oral review of the work completed under this contract was held on 5 October 1999 at NASA LaRC. Presentations by made by Asif Syed from GE and Dr. H. W. Kwan from BF Goodrich.

12. M. Salikuddin et al, NASA Contract NAS3-26617 & NAS3-27235, "Acoustic Characteristics of Various Treatment Panel Designs Specific to HSCT Mixer-Ejector Application," HSR/CPC Program Coordination Memo No. GE99-030-N, November 1999.

13. A. A. Syed, "Correlation of Steady (DC) Flow Resistance Data in the presence of High Speed Grazing Flows," Technical note prepared in September 2001 and communicated to Michael G. Jones of NASA LaRC, on 15 December 2001.

14. C. E. Swindlehurst, R. B. Plunkett, J. F. Lennon, "Acoustic Liner and Method of Making an Acoustic Liner," US Patent Number 6,206,136 B1, March 27, 2001.

Table 1.

Matrix of Proposed Acoustic Treatment Panels with Perforated Face Sheets for Impedance Measurements under Grazing Flow conditions.

No.	Candidates	Initial Open Area Ratio (POA)*	Availability	Hole Diameter ¥ ***d*** (inch)	Plate thickness ***t*** (inch)	Core Depth (GE/NASA) ***h*** (inch)
1	Base liner	8.7	Yes	.039	.025	1.5/1.5
2	Min **POA**	6.4	Yes	.039	.025	1.5/1.5
3	Max **POA**	15	Yes	.039	.025	1.5/1.5
4	Min ***d***	13.2	yes	.039	.025	1.5/1.5
5	Max ***d***	13.0	yes	.093	.032	1.5/1.5
6	Min ***t***	7.3	Yes	0.05	.02	1.5/1.5
7	Max ***t***	7.3	Yes	0.05	.04	1.5/1.5
9	Max ***h***	8.7	Yes	.039	.025	0.75/3
10	Special 1	10.5	Yes	.039	.028	1.5/1.5
11	Special 2	8.7	Yes	.050	.045	1.5/1.5
12	Composite	8.3	Yes	0.062	0.028	1.5/1.5
13	PU film	18/34	Yes	.062/0.005	.015/.032	1.5/1.5
14	GE (pin-mandrel)	9%	Yes	0.062	0.030	1.5 / 1.5
15A	MRAS (pin-less)	9%	Yes	0.062	0.030	1.5 / 1.5
15B*	MRAS (pin-less)	9%	Yes	0.062	0.030	1.5 / 1.5

Porous Face Sheet

Honeycomb Core

Impervious back sheet

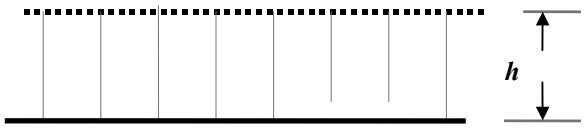

* **Note: The dimensions of the panel (15A) made for the GE/BFG ducts were incorrect. Therefore, MRAS made a second set (panel plus samples) for GE only. NASA LaRC received the set with panel #15A.**

Table 2

Steady Flow Resistance Data from tests conducted at the BF Goodrich plant in Chula Vista, California.

Sample	Measured Data (Input)								Estimated Data (Output)					
Configuration	THK	SP	PTN		INT	SLP	R(105)	NLF	DIA	POA	INT	SLP	R(105)	NLF
	inch	inch	inch		Rayl		Rayl		inch		Rayl		Rayl	
					Unprimed									
	0.025	0.126	Stagger	Entry	-0.39	0.134	**13.63**	11.58	.0377	8.13%	0.49	0.125	**13.63**	8.52
	0.025	0.126	Stagger	Exit	0.31	0.121	**12.96**	9.00	.0382	8.32%	0.47	0.119	**12.96**	8.51
	0.025	0.126	Stagger	Average	-0.04	**0.128**	13.30	10.29	.0374	7.99%	0.51	**0.129**	14.04	8.52
1					**Primed**									
	0.025	0.126	Stagger	Entry	0.26	0.119	**12.77**	9.11	.0382	8.32%	0.48	0.117	**12.77**	8.47
	0.025	0.126	Stagger	Exit	1.24	0.101	**11.82**	6.56	.0389	8.65%	0.44	0.108	**11.82**	8.47
	0.025	0.126	Stagger	Average	0.75	**0.110**	12.30	7.84	.0388	8.59%	0.45	**0.110**	12.00	8.47
					Bonded									
	0.025	0.126	Stagger	Average	0.53	0.119	**13.06**	8.39	.0379	8.21%	0.49	0.120	**13.06**	8.47
					Unprimed									
	0.025	0.146	Stagger	Entry	-0.83	0.255	**25.92**	11.80	.0374	5.95%	0.69	0.240	**25.92**	8.88
	0.025	0.146	Stagger	Exit	-1.32	0.277	**27.75**	12.81	.0367	5.74%	0.74	0.257	**27.75**	8.87
	0.025	0.146	Stagger	Average	-1.08	**0.266**	26.84	12.31	.0364	5.64%	0.76	**0.266**	28.69	8.87
2					**Primed**									
	0.025	0.146	Stagger	Entry	-0.64	0.246	**25.22**	11.36	.0376	6.00%	0.68	0.234	**25.22**	8.86
	0.025	0.146	Stagger	Exit	-0.14	0.240	**25.06**	10.30	.0376	6.02%	0.68	0.232	**25.06**	8.86
	0.025	0.146	Stagger	Average	-0.39	**0.243**	25.14	10.83	.0372	5.89%	0.71	**0.243**	26.18	8.86
					Bonded									
	0.025	0.146	Stagger	Average	0.62	0.245	**26.39**	9.04	.0370	5.83%	0.72	0.244	**26.39**	8.84
					Unprimed									
	0.025	0.096	Stagger	Entry	0.39	0.036	**4.20**	6.89	.0381	14.26%	0.28	0.037	**4.20**	7.55
	0.025	0.096	Stagger	Exit	0.56	0.033	**3.97**	5.85	.0388	14.79%	0.26	0.035	**3.97**	7.61
	0.025	0.096	Stagger	Average	0.48	**0.035**	4.09	6.37	.0387	14.74%	0.26	**0.035**	3.96	7.58
3					**Primed**									
	0.025	0.096	Stagger	Entry	0.48	0.035	**4.10**	6.33	.0383	14.47%	0.27	0.036	**4.10**	7.57
	0.025	0.096	Stagger	Exit	0.71	0.032	**4.00**	5.31	.0385	14.59%	0.27	0.036	**4.00**	7.54
	0.025	0.096	Stagger	Average	0.60	**0.034**	4.05	5.82	.0389	14.92%	0.26	**0.034**	3.84	7.55
					Bonded									
	0.025	0.096	Stagger	Average	0.86	0.042	**5.28**	5.44	.0359	12.66%	0.36	0.047	**5.28**	7.53
					Unprimed									
	0.025	0.103	Stagger	Entry	0.41	0.052	**5.84**	7.47	.0378	12.21%	0.33	0.053	**5.84**	7.86
	0.025	0.103	Stagger	Exit	0.53	0.050	**5.79**	6.88	.0379	12.25%	0.33	0.052	**5.79**	7.86
	0.025	0.103	Stagger	Average	0.47	**0.051**	5.82	7.18	.0379	12.29%	0.32	**0.052**	5.76	7.86
4					**Primed**									
	0.025	0.103	Stagger	Entry	0.54	0.047	**5.44**	6.72	.0384	12.59%	0.31	0.049	**5.44**	7.82
	0.025	0.103	Stagger	Exit	0.78	0.044	**5.35**	5.74	.0385	12.70%	0.31	0.048	**5.35**	7.83
	0.025	0.103	Stagger	Average	0.66	**0.046**	5.40	6.23	.0388	12.85%	0.30	**0.047**	5.22	7.83
					Bonded									
	0.025	0.103	Stagger	Average	0.83	0.051	**6.18**	5.95	.0371	11.77%	0.36	0.055	**6.18**	7.80

Table 2 (continued)

Steady Flow Resistance Data from tests conducted at the BF Goodrich plant in Chula Vista, California.

Sample	Measured Data (Input)								Predicted Data (Output)					
Configuration	THK	SP	PTN		INT	SLP	R(105)	NLF	DIA	POA	INT	SLP	R(105)	NLF
	inch	inch	inch		Rayl		Rayl		inch		Rayl		Rayl	
					Unprimed									
	0.032	0.250	Stagger	Entry	-0.77	0.077	**7.34**	18.89	.0893	11.57%	0.08	0.069	**7.34**	9.51
	0.032	0.250	Stagger	Exit	-0.82	0.080	**7.62**	19.34	.0884	11.34%	0.08	0.072	**7.62**	9.51
	0.032	0.250	Stagger	Average	-0.80	**0.079**	7.48	19.12	.0864	10.83%	0.09	**0.079**	8.38	9.51
5					Primed									
	0.032	0.250	Stagger	Entry	-0.52	0.073	**7.10**	15.07	.0896	11.66%	0.08	0.067	**7.10**	9.50
	0.032	0.250	Stagger	Exit	-0.51	0.073	**7.15**	14.98	.0894	11.60%	0.08	0.067	**7.15**	9.50
	0.032	0.250	Stagger	Average	-0.52	**0.073**	7.13	15.03	.0877	11.16%	0.09	**0.073**	7.75	9.50
					Bonded									
	0.032	0.250	Stagger	Average	-0.89	0.073	**6.78**	24.21	.0905	11.89%	0.08	0.064	**6.78**	9.49
					Unprimed									
	0.020	0.175	Stagger	Entry	-2.07	0.225	**21.58**	17.63	.0480	6.82%	0.29	0.203	**21.58**	9.40
	0.020	0.175	Stagger	Exit	-2.22	0.227	**21.66**	18.56	.0479	6.80%	0.29	0.203	**21.66**	9.39
	0.020	0.175	Stagger	Average	-2.15	**0.226**	21.62	18.10	.0467	6.46%	0.33	**0.226**	24.05	9.39
6					Primed									
	0.020	0.175	Stagger	Entry	-1.22	0.204	**20.23**	13.84	.0488	7.04%	0.27	0.190	**20.23**	9.39
	0.020	0.175	Stagger	Exit	-0.92	0.196	**19.66**	12.80	.0491	7.14%	0.27	0.185	**19.66**	9.39
	0.020	0.175	Stagger	Average	-1.07	**0.200**	19.95	13.32	.0481	6.85%	0.29	**0.201**	21.39	9.39
					Bonded									
	0.020	0.175	Stagger	Average	-1.29	0.202	**19.89**	14.22	.0488	7.06%	0.28	0.187	**19.89**	9.38
					Unprimed									
	0.040	0.175	Stagger	Entry	0.32	0.175	**18.73**	9.24	.0475	6.67%	0.61	0.173	**18.73**	8.66
	0.040	0.175	Stagger	Exit	0.87	0.166	**18.32**	8.15	.0477	6.75%	0.59	0.169	**18.32**	8.65
	0.040	0.175	Stagger	Average	0.60	**0.171**	18.53	8.70	.0475	6.69%	0.60	**0.172**	18.63	8.66
7					Primed									
	0.040	0.175	Stagger	Entry	0.53	0.164	**17.74**	8.76	.0480	6.83%	0.58	0.163	**17.74**	8.63
	0.040	0.175	Stagger	Exit	0.95	0.152	**16.95**	7.87	.0486	6.98%	0.56	0.156	**16.95**	8.63
	0.040	0.175	Stagger	Average	0.74	**0.158**	17.35	8.32	.0484	6.94%	0.57	**0.158**	17.16	8.63
					Bonded									
	0.040	0.175	Stagger	Average	0.11	0.171	**18.10**	9.72	.0477	6.75%	0.60	0.167	**18.10**	8.63
					Unprimed									
	0.025	0.126		Entry	-0.35	0.131	**13.45**	11.45	.0377	8.13%	0.50	0.123	**13.45**	8.49
	0.025	0.126		Exit	0.52	0.116	**12.71**	8.38	.0383	8.38%	0.47	0.117	**12.71**	8.50
	0.025	0.126		Average	0.09	**0.124**	13.08	9.92	.0376	8.09%	0.50	**0.125**	13.57	8.50
9					Primed									
	0.025	0.126		Entry	1.09	0.104	**11.95**	6.91	.0388	8.60%	0.45	0.110	**11.95**	8.48
	0.025	0.126		Exit	-0.01	0.124	**13.01**	10.05	.0380	8.23%	0.49	0.119	**13.01**	8.47
	0.025	0.126		Average	0.54	**0.114**	12.48	8.48	.0384	8.44%	0.46	**0.113**	12.38	8.47
					Bonded									
	0.025	0.126		Average	1.22	0.108	**12.59**	6.75	.0382	8.35%	0.48	0.115	**12.59**	8.46

Note: The parameters for the face sheet for treatment panel No. 8 are the same as those for panel No. 9.

Table 2 (continued)

Steady Flow Resistance Data from tests conducted at the BF Goodrich plant in Chula Vista, California.

Sample	Measured Data (Input)								Predicted Data (Output)					
Configuration	THK	SP	PTN		INT	SLP	R(105)	NLF	DIA	POA	INT	SLP	R(105)	NLF
	inch	inch	inch		Rayl		Rayl		inch		Rayl		Rayl	
10					**Unprimed**									
	0.028	0.115		Entry	0.20	0.081	**8.74**	9.04	.0380	9.92%	0.44	0.079	**8.74**	8.02
	0.028	0.115		Exit	0.60	0.076	**8.59**	7.46	.0382	10.00%	0.44	0.078	**8.59**	8.02
	0.028	0.115		Average	0.40	**0.079**	8.67	8.25	.0380	9.90%	0.45	**0.079**	8.77	8.02
					Primed									
	0.028	0.115		Entry	0.58	0.076	**8.59**	7.53	.0380	9.90%	0.45	0.077	**8.59**	7.96
	0.028	0.115		Exit	1.00	0.070	**8.39**	6.26	.0382	10.01%	0.44	0.076	**8.39**	7.96
	0.028	0.115		Average	0.79	**0.073**	8.49	6.90	.0385	10.18%	0.43	**0.073**	8.12	7.96
					Bonded									
	0.028	0.115		Average	0.80	0.078	**9.00**	6.94	.0375	9.65%	0.48	0.081	**9.00**	7.94
11					**Unprimed**									
	0.045	0.160		Entry	0.58	0.114	**12.59**	8.17	.0472	7.89%	0.58	0.114	**12.59**	8.17
	0.045	0.160		Exit	0.86	0.108	**12.18**	7.44	.0476	8.03%	0.56	0.111	**12.18**	8.17
	0.045	0.160		Average	0.72	**0.111**	12.39	7.81	.0476	8.02%	0.57	**0.111**	12.21	8.17
					Primed									
	0.045	0.160		Entry	0.64	0.110	**12.14**	7.98	.0475	8.00%	0.57	0.110	**12.14**	8.14
	0.045	0.160		Exit	1.04	0.104	**11.98**	7.01	.0477	8.07%	0.56	0.109	**11.98**	8.15
	0.045	0.160		Average	0.84	**0.107**	12.06	7.50	.0479	8.14%	0.55	**0.107**	11.77	8.15
					Bonded									
	0.045	0.160		Average	-0.02	0.117	**12.21**	10.08	.0474	7.94%	0.59	0.111	**12.21**	8.11
12					**Composite Perforate**									
	0.028	0.191		Average	-0.51	**0.115**	11.53	12.59	.0594	8.78%	0.21	**0.115**	12.25	9.25
					Bonded									
	0.028	0.191		Average	-0.05	0.111	**11.61**	10.21	.0602	9.00%	0.20	0.109	**11.61**	9.24

R(U) = INT + SLP * U

where U is the mean flow velocity through the perforated face sheet (cm/s); R(U) is the steady (DC) flow resistance (cgs Rayl) at flow velocity U. The column headers of Table 2 are provided below:

THK = Sheet Thickness
SP = Hole Spacing
PTN = Hole Pattern
INT = Intercept
SLP = Slope
R(105) = Flow Resistance at 105 cm/sec
NLF = Nonlinearity Factor = R(200)/R(20)
DIA = Hole Diameter
POA = Percent Open Area

Table 3
Boundary Thickness data measured over the test sample.

Sample Number	Mach Number	Displacement Thickness	Momentum Thickness	Hole Diameter d
2	0.323	0.0595	0.0475	0.0380
3	0.288	0.0497	0.0413	0.0380
5	0.320	0.0550	0.0439	0.0900
6	0.320	0.0600	0.0483	0.0480
7	0.321	0.0646	0.0521	0.0480
9	0.326	0.0645	0.0519	0.0380
12	0.288	0.0438	0.0357	0.0650
13	0.323	0.0622	0.0496	0.0480
14	0.324	0.0605	0.0484	0.0540
15	0.326	0.0601	0.0483	0.0400
2	0.545	0.058	0.047	0.038
5	0.544	0.057	0.046	0.090
6	0.546	0.059	0.047	0.048
7	0.545	0.059	0.048	0.048
9	0.543	0.059	0.047	0.038
12	0.485	0.052	0.043	0.065
13	0.549	0.059	0.048	0.048
14	0.552	0.054	0.043	0.054
15	0.552	0.059	0.047	0.040

FIGURE 1.

Diagram of a treatment panel to be tested in the rectangular flow ducts at GEAE and BFGoodrich.

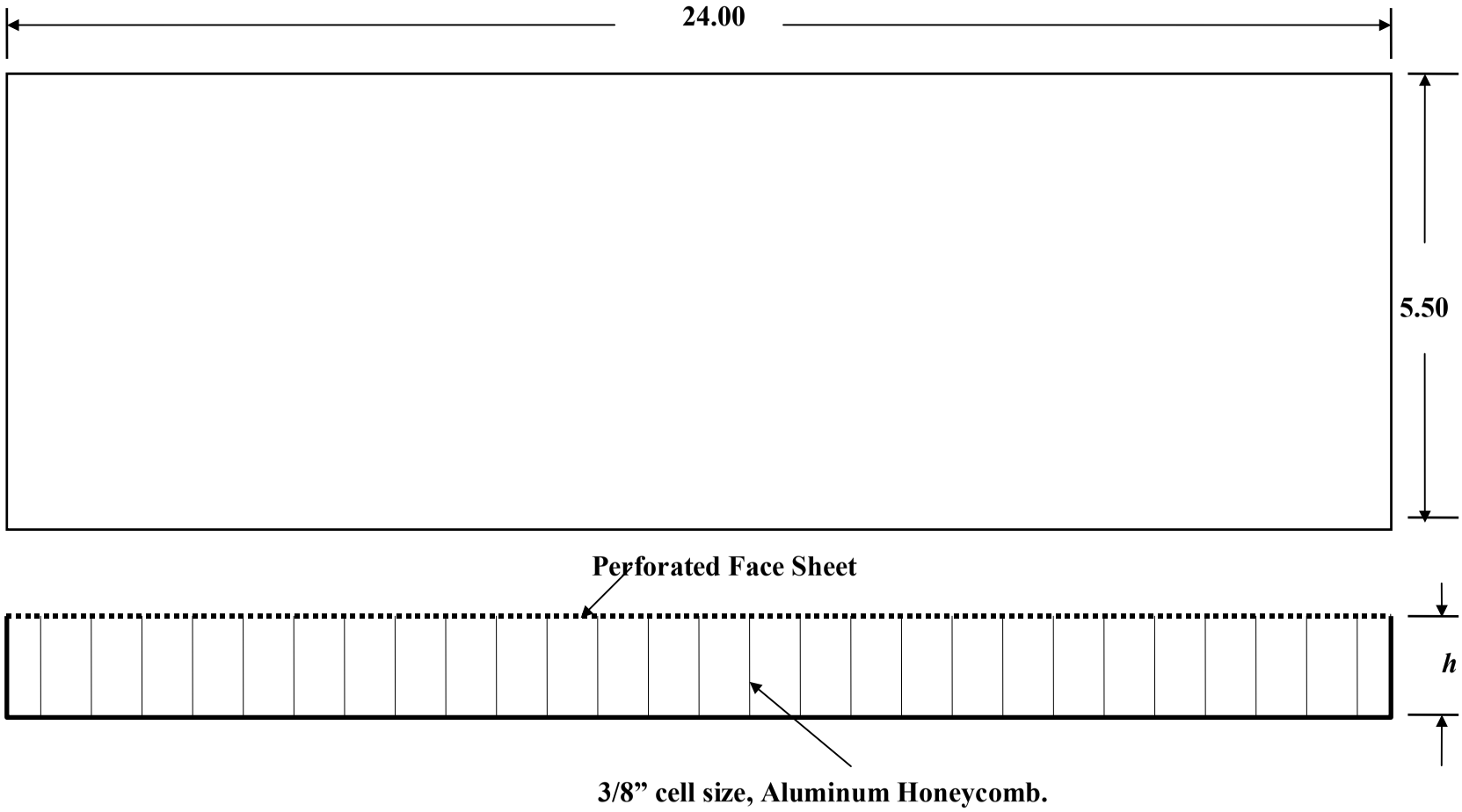

All dimensions are in inches.
For definition of treatment parameters, see Table 1.

FIGURE 2.
Diagram of a treatment panel to be tested in the rectangular flow ducts at NASA Langley Research Center.

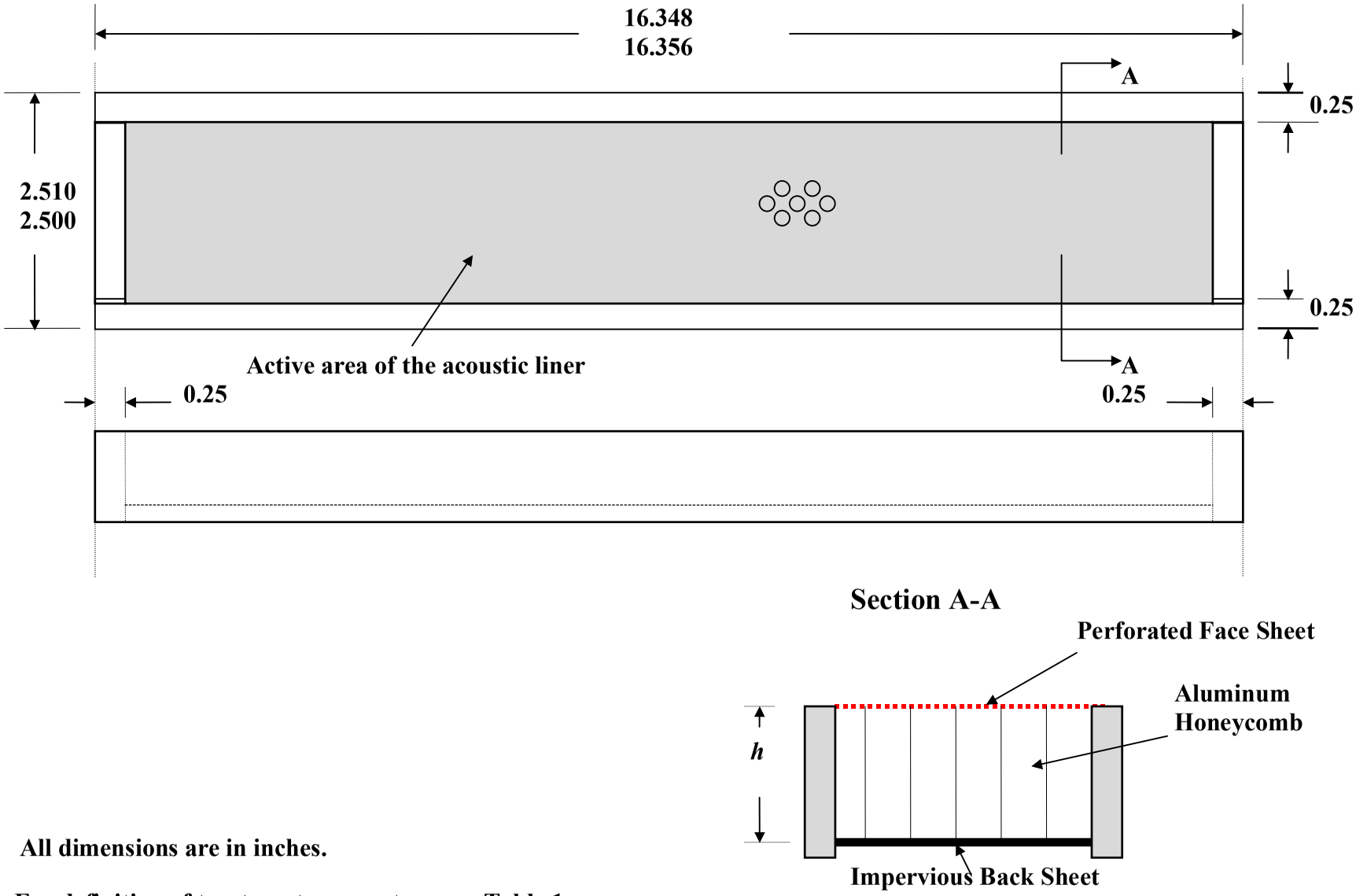

All dimensions are in inches.

For definition of treatment parameters, see Table 1.

FIGURE 3. THE INSERTION LOSS METHOD – SCHEMATIC DIAGRAM OF THE FLOW DUCT TEST APPARATUS AT BF Goodrich PLANT IN CHULA VISTA, CALIFORNIA.

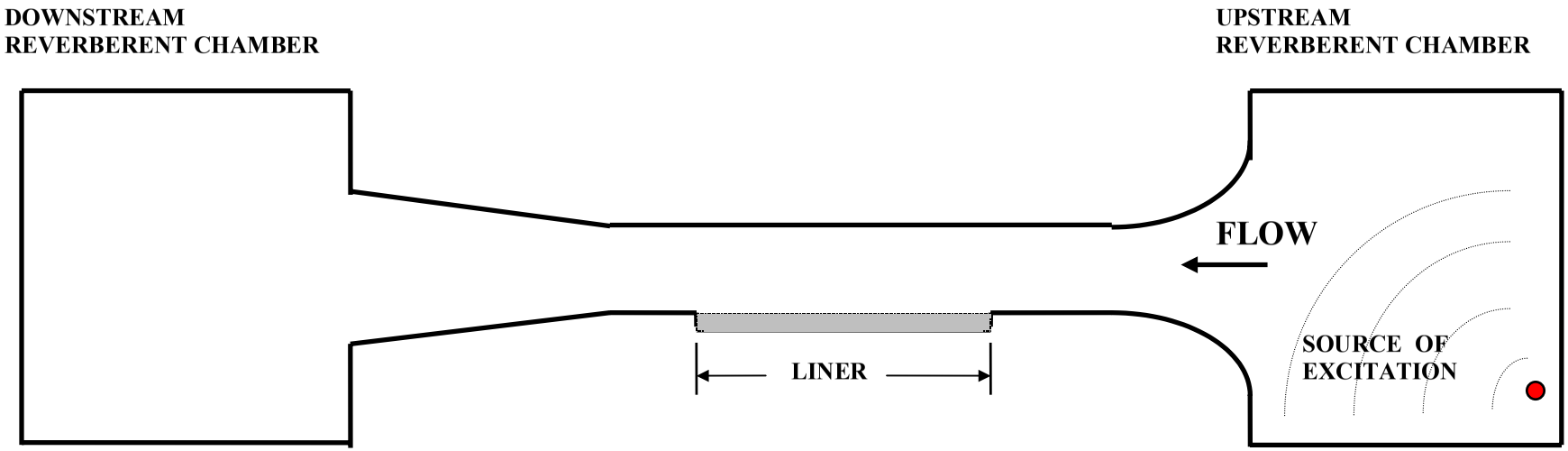

Figure 4a

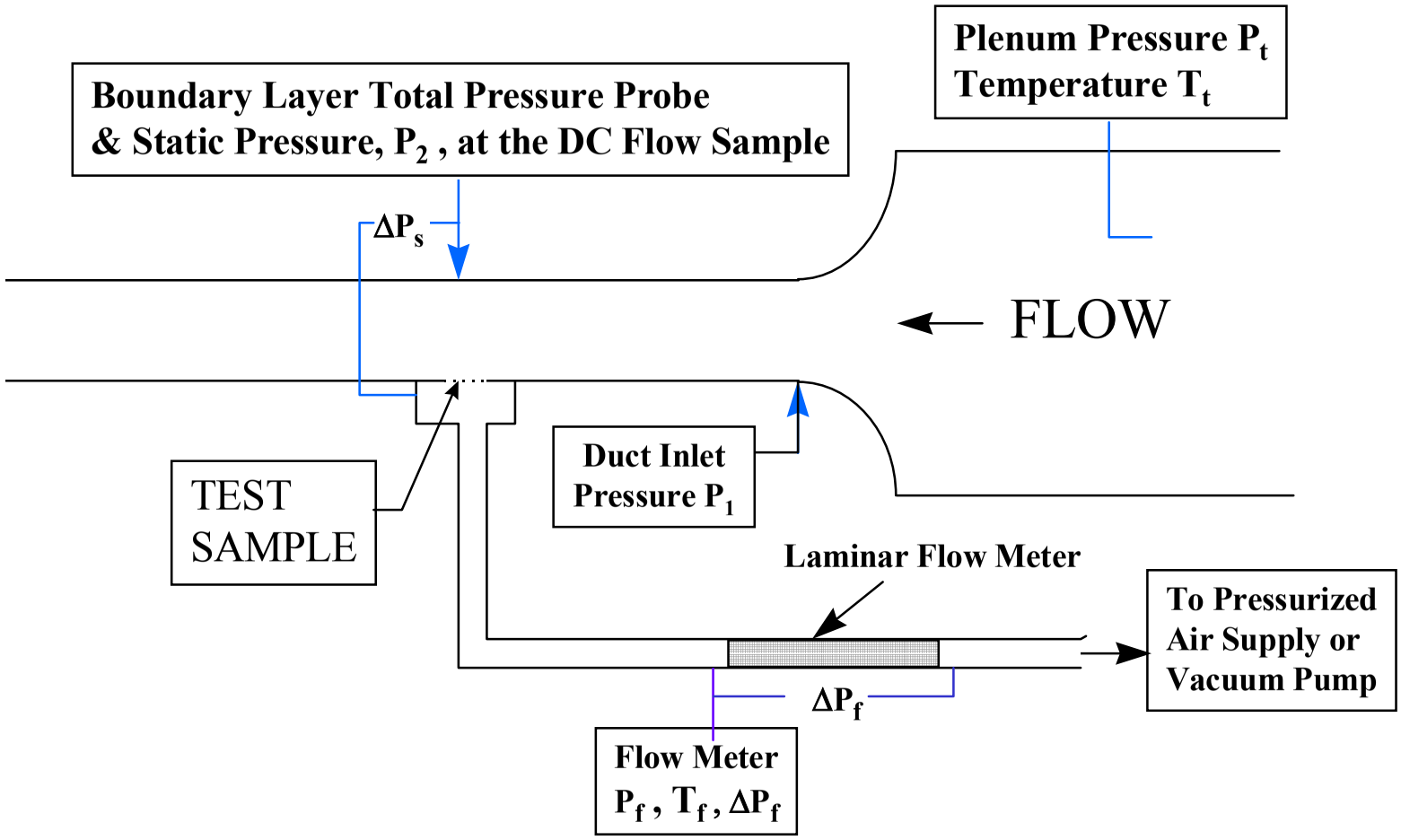

SCHEMATIC DIAGRAM OF THE FLOW DUCT APPARATUS USED FOR DC FLOW MEASUREMENTS IN HIGH SPEED GRAZING FLOWS.

Figure 4b
Schematic Diagram of the installation of the treatment sample for DC flow testing in the Flow Duct apparatus.

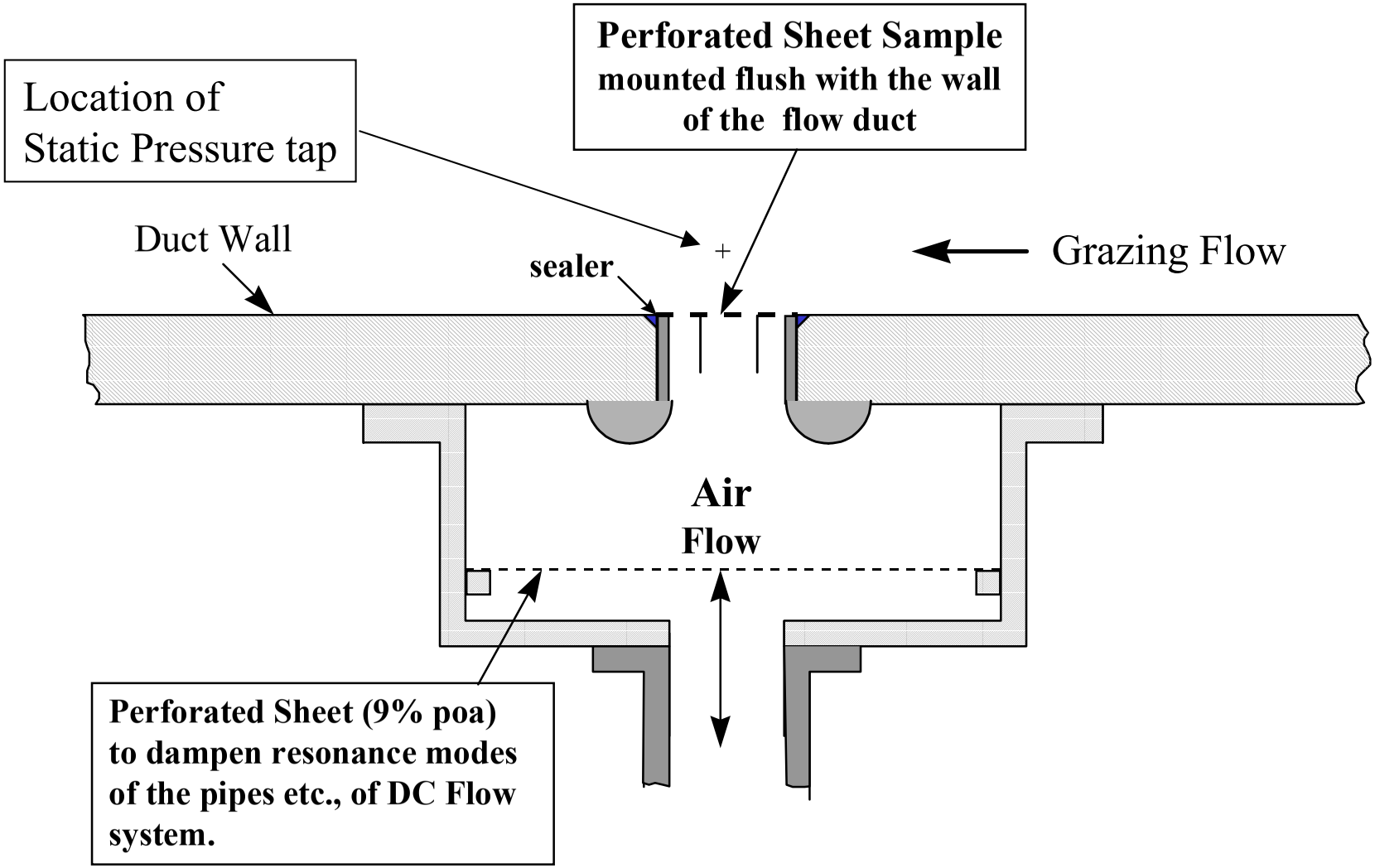

Figure 4c

Schematic Diagram of the Data Acquisition System used in the DC Flow tests conducted in the Flow Duct.

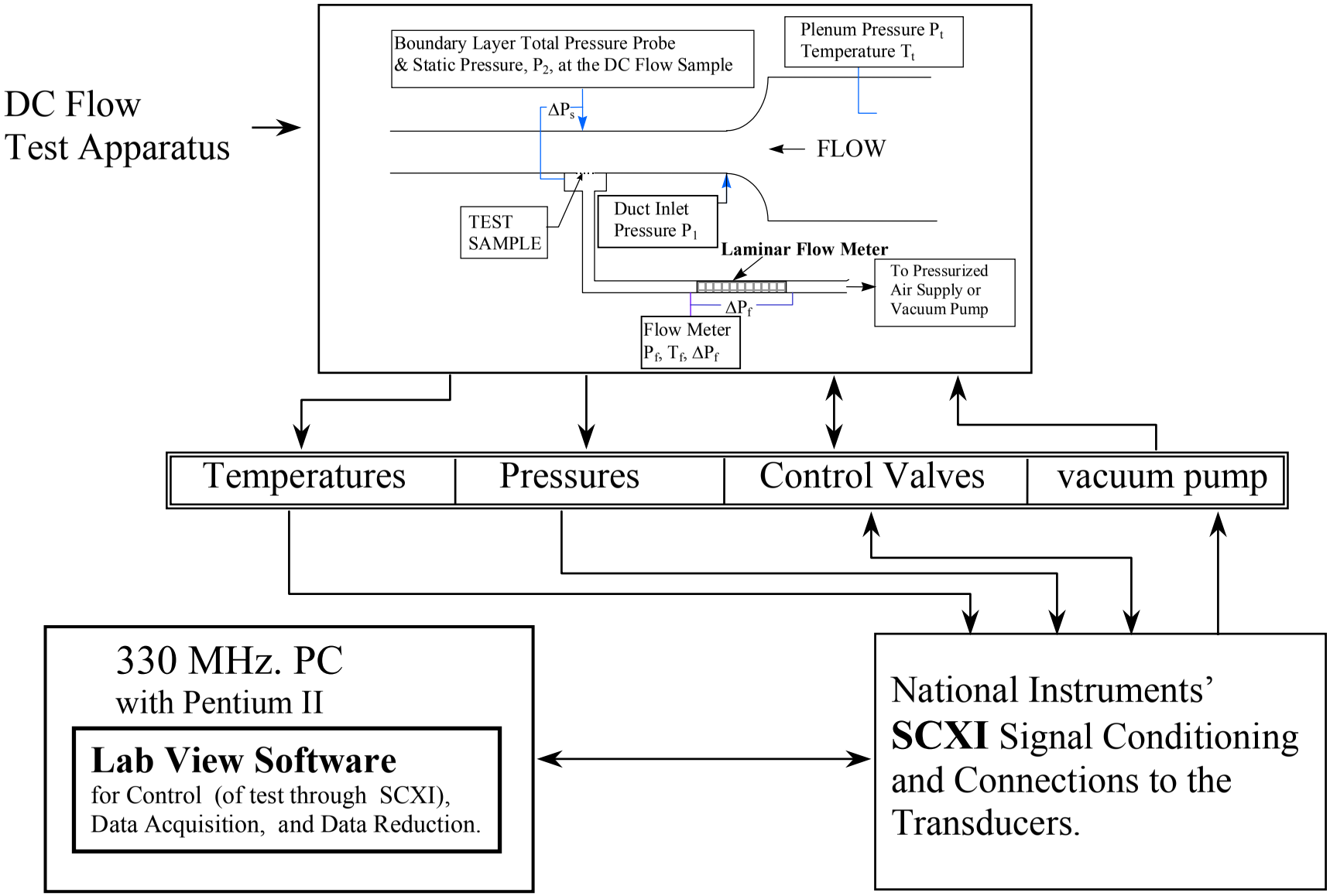

Figure 5
A Photograph of the Flow Duct Facility set up to measure the DC Flow Resistance of Porous Face Sheet Samples.

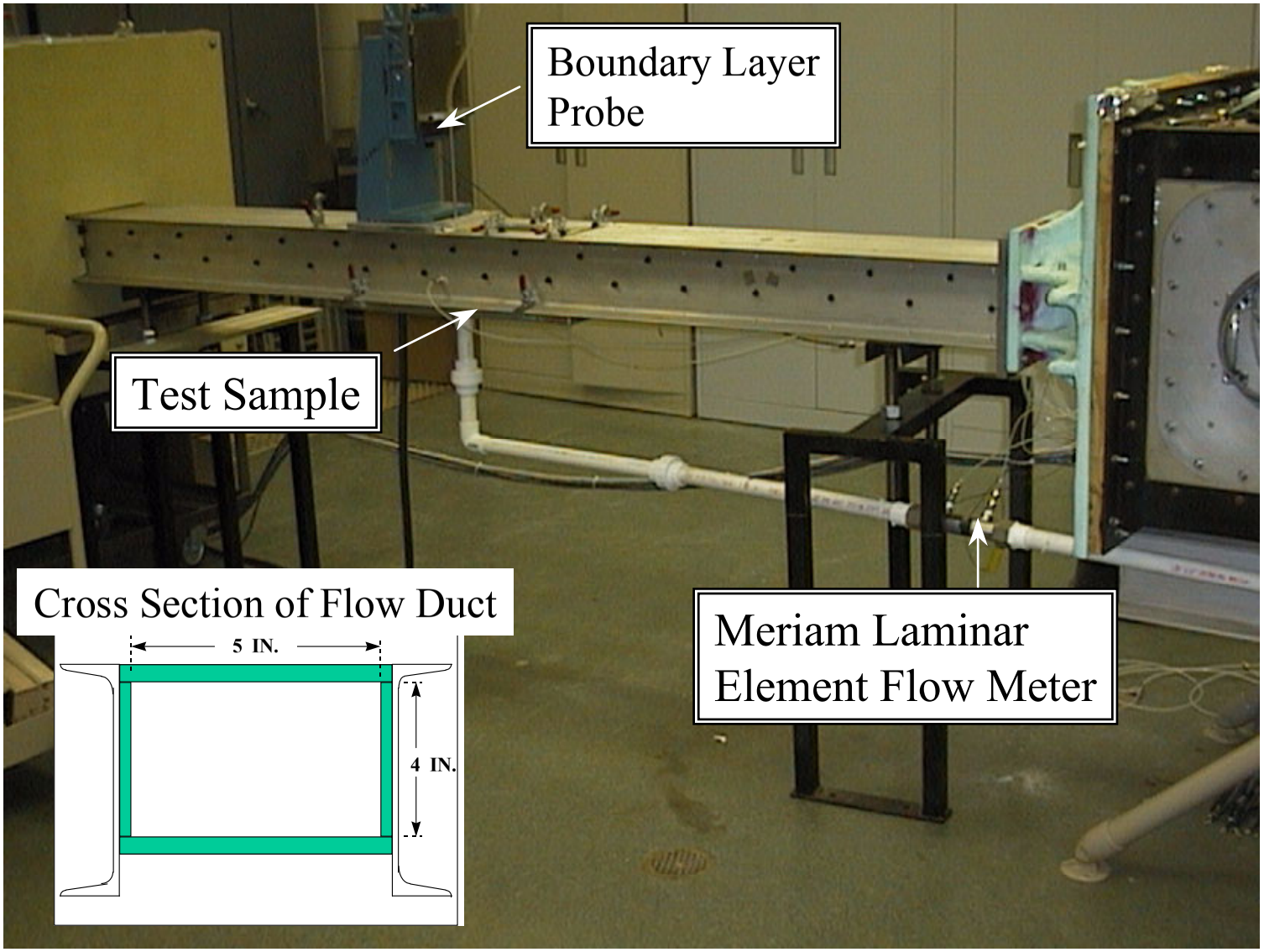

Figure 6

DC Flow Resistance Data Measured with Sample No. 3
Grazing Flow Mach No. = 0.0

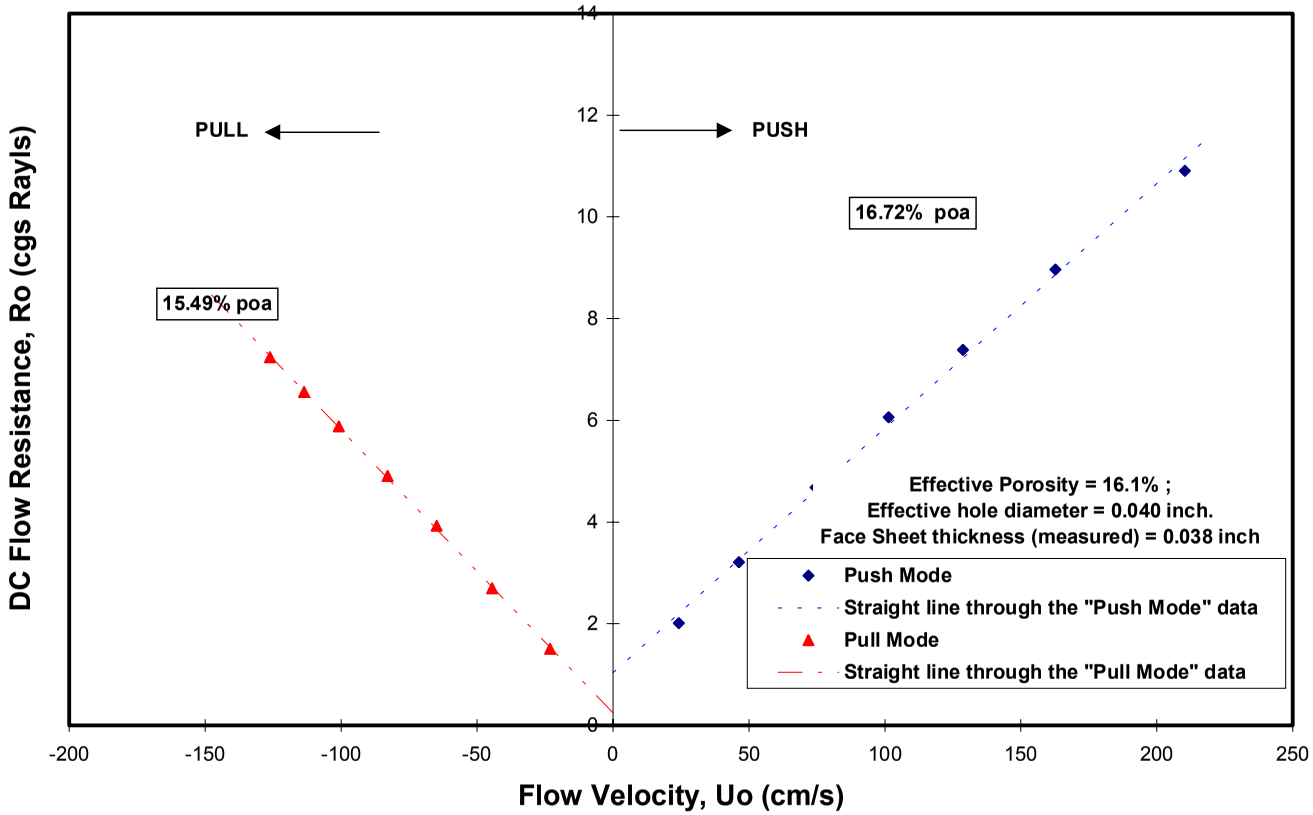

Push Mode		Pull Mode	
Uo	Ro	Uo	Ro
24.21	2.01	-23.16	1.51
46.35	3.21	-44.47	2.70
74.45	4.68	-64.84	3.93
101.33	6.06	-82.86	4.91
128.69	7.39	-100.89	5.88
162.78	8.96	-113.66	6.56
210.35	10.91	-126.18	7.24

Porosity, based on the mean value of the slope = 16.1%

Figure 7

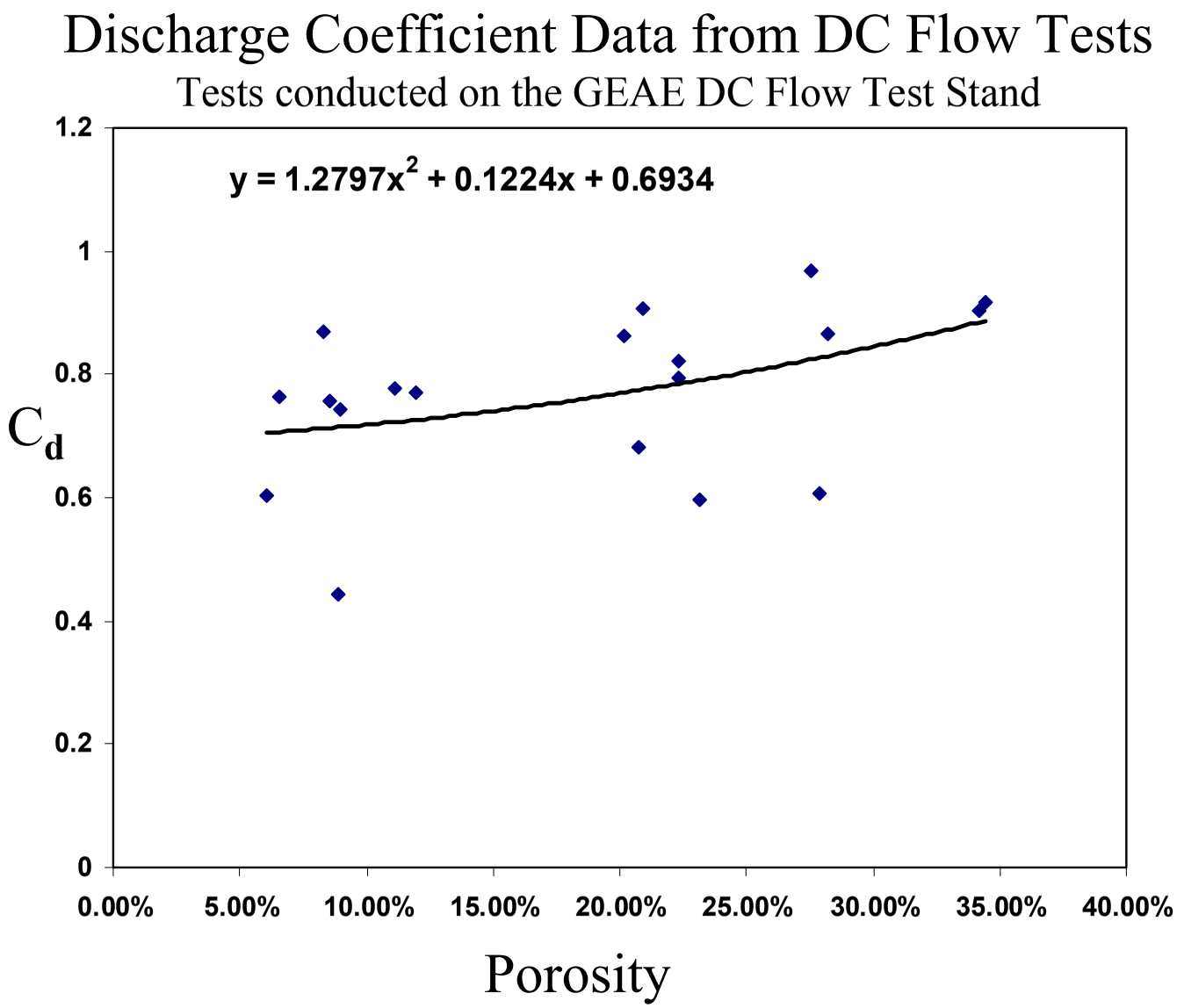

Porosity	Discharge Coefficient
11.95%	0.772
8.98%	0.744
6.53%	0.763
8.31%	0.869
20.90%	0.908
23.19%	0.596
27.88%	0.606
11.14%	0.778
34.40%	0.916
28.22%	0.865
20.20%	0.861
20.77%	0.682
8.91%	0.443
22.36%	0.794
22.36%	0.821
34.17%	0.903
27.58%	0.967
6.08%	0.604
8.57%	0.758

Figure 8
Statistical Analysis of Discharge Coefficient Data.

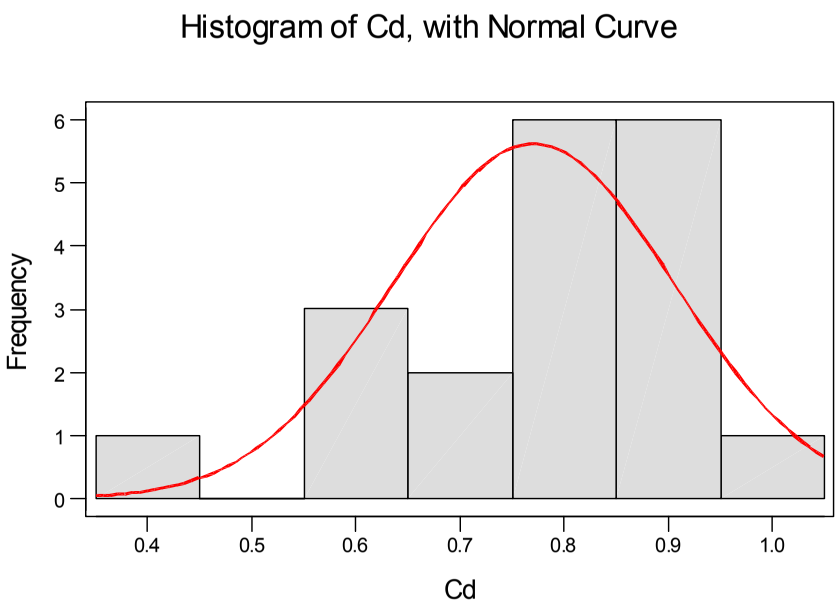

Mean Cd = 0.7711
Std. Deviation = 0.1349

$$C_d = 1.2797\,\sigma^2 + 0.1224\,\sigma + 0.6934$$

Mean Deviation from Polynomial = 0.0
Std. Deviation = 0.1212

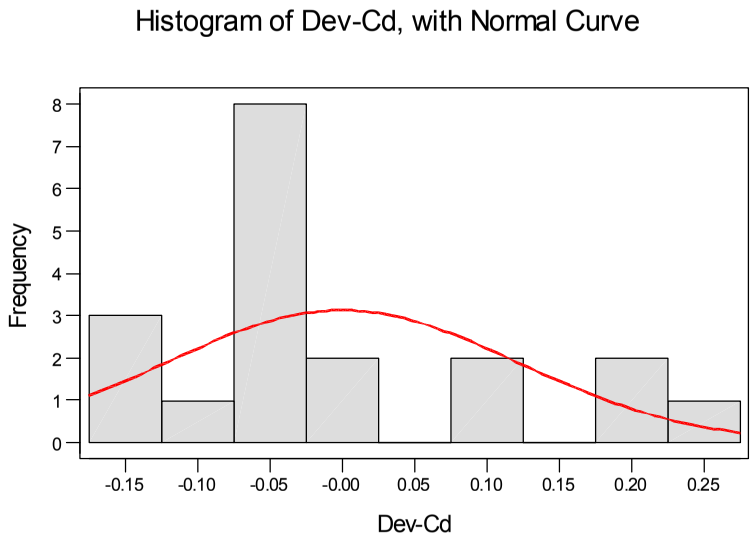

Figure 9

Data measured on Sample #3 on five different days.
Mach 0.0

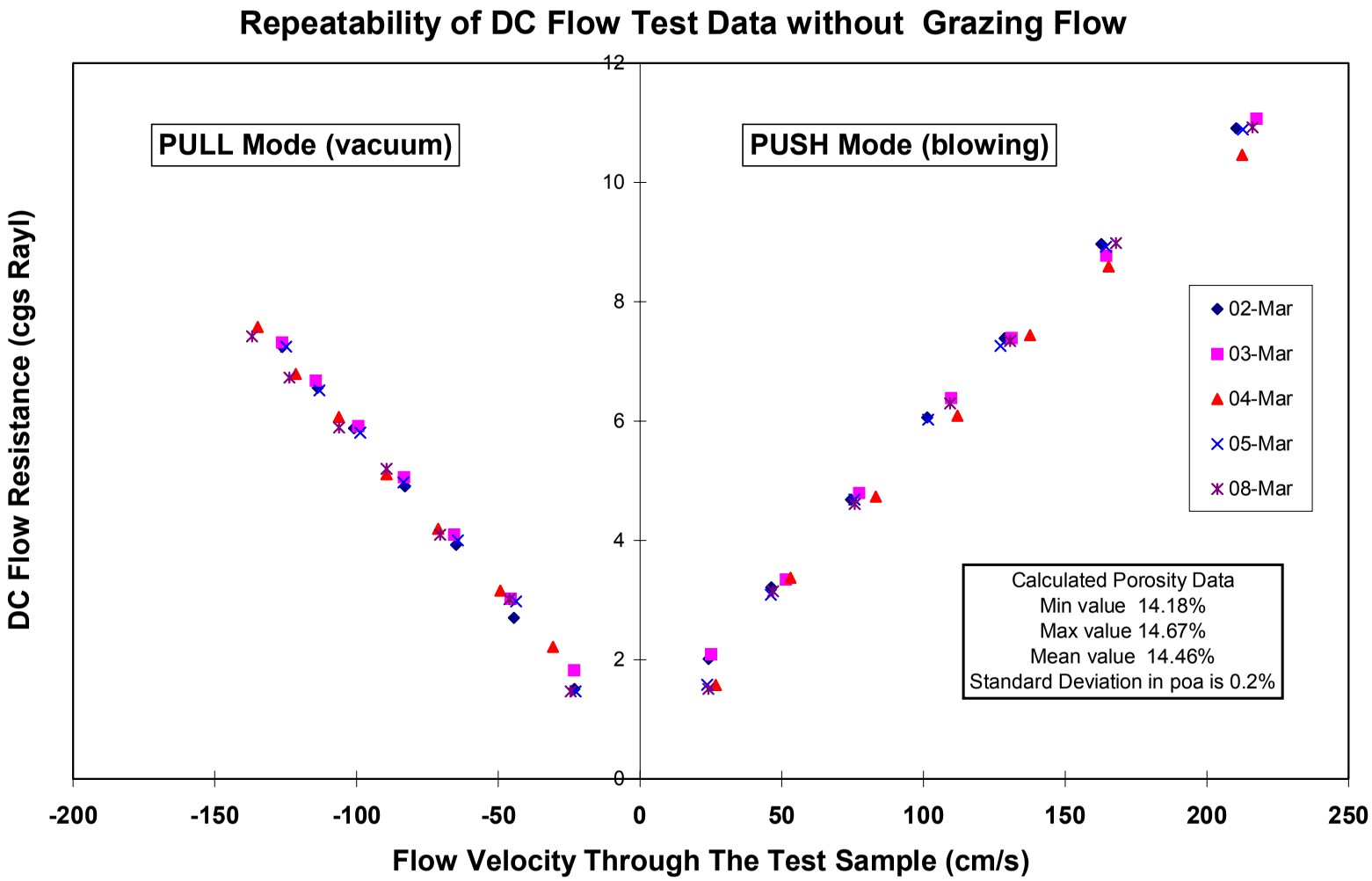

Figure 10

Data showing the repeatability of measurements without grazing flow.

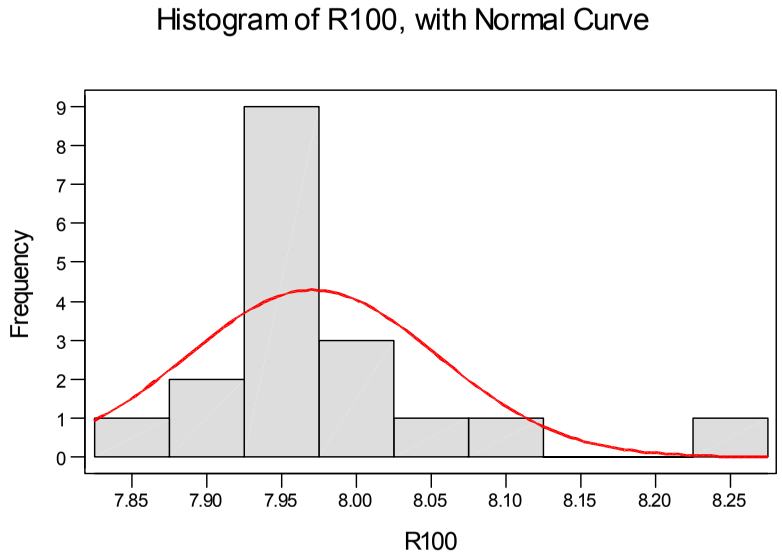

Statistical Data from 18 different DC Flow tests on sample #4 at Mach 0.0

	R100	POA (%)
Mean	7.97	12.04
St Dev.	0.08	0.09
Max	8.24	12.32
Min	7.86	11.95

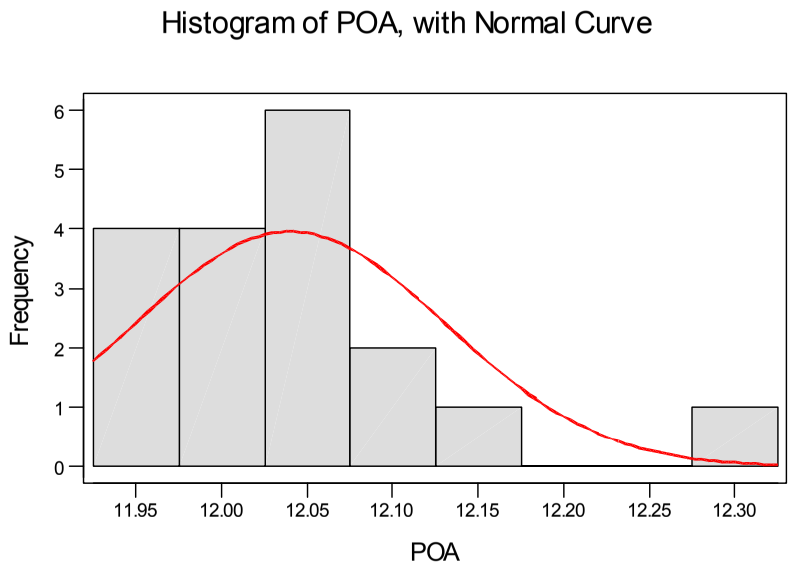

Measured physical porosity value from hole pattern is between 11.4% and 12.7%

Figures 11a and 11b

Illustration of the procedure used in reducing measured DC Flow Data

Under Grazing Flow Conditions at Mach 0.3

Figure 11a:
Plots of the Pressure drop (inches of H_2O) measured across the sample against the measured velocity (cm/s) of airflow through the sample.

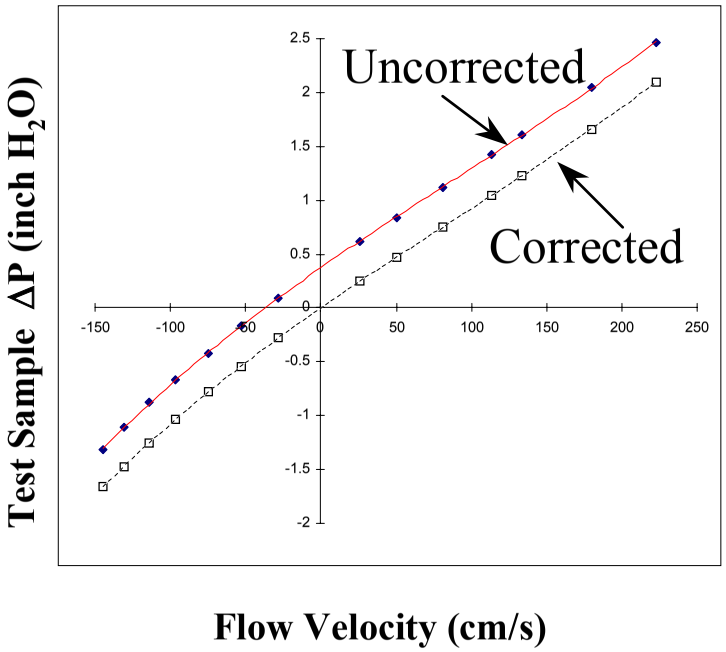

Figure 11b:
Plots of the DC Flow Resistance (cgs Rayl) against the measured velocity (cm/s) of airflow through the sample.

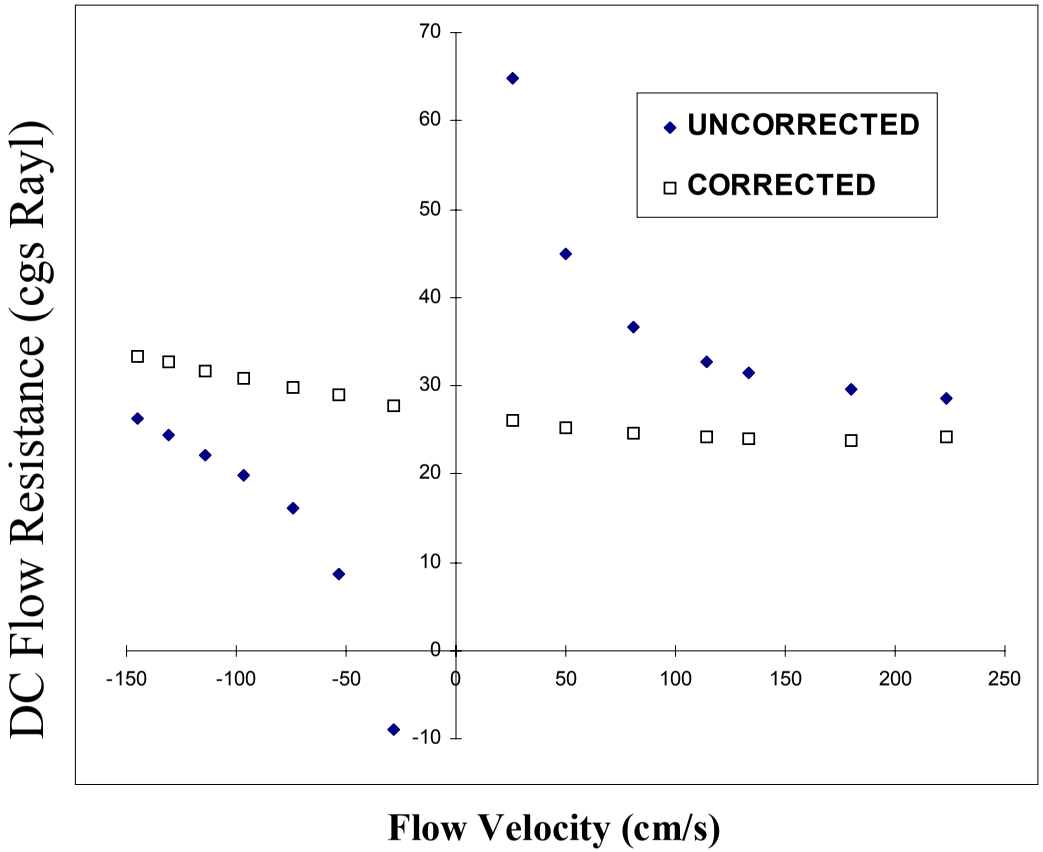

Figure 12

DC Flow Resistance Data from a Test Sample with a Perforated Face Sheet under grazing Flow Conditions.

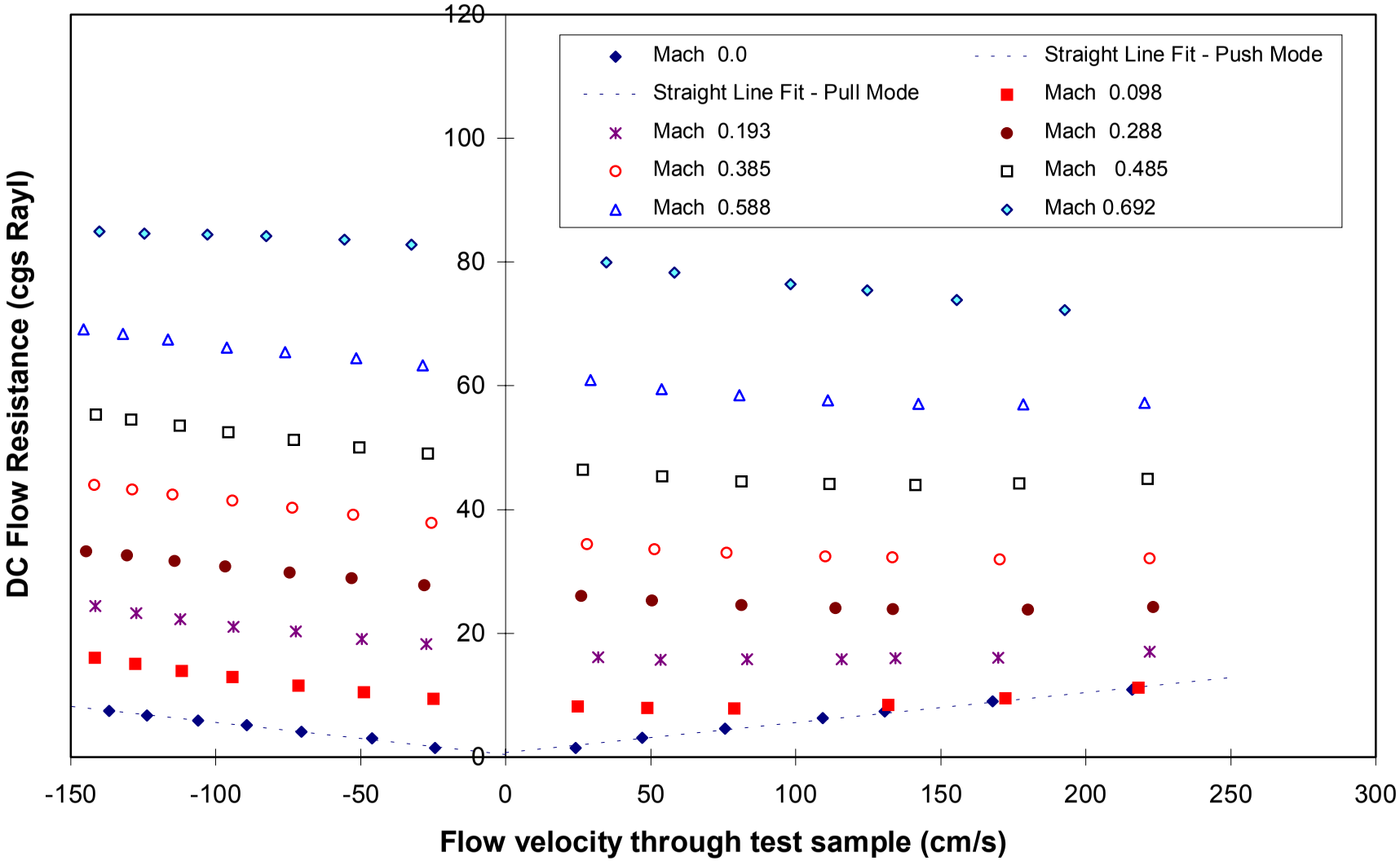

Figure 13a
Polynomial fit through DC Flow Resistance Data
(Data from test sample #3 at Grazing Flow Mach number of 0.3)

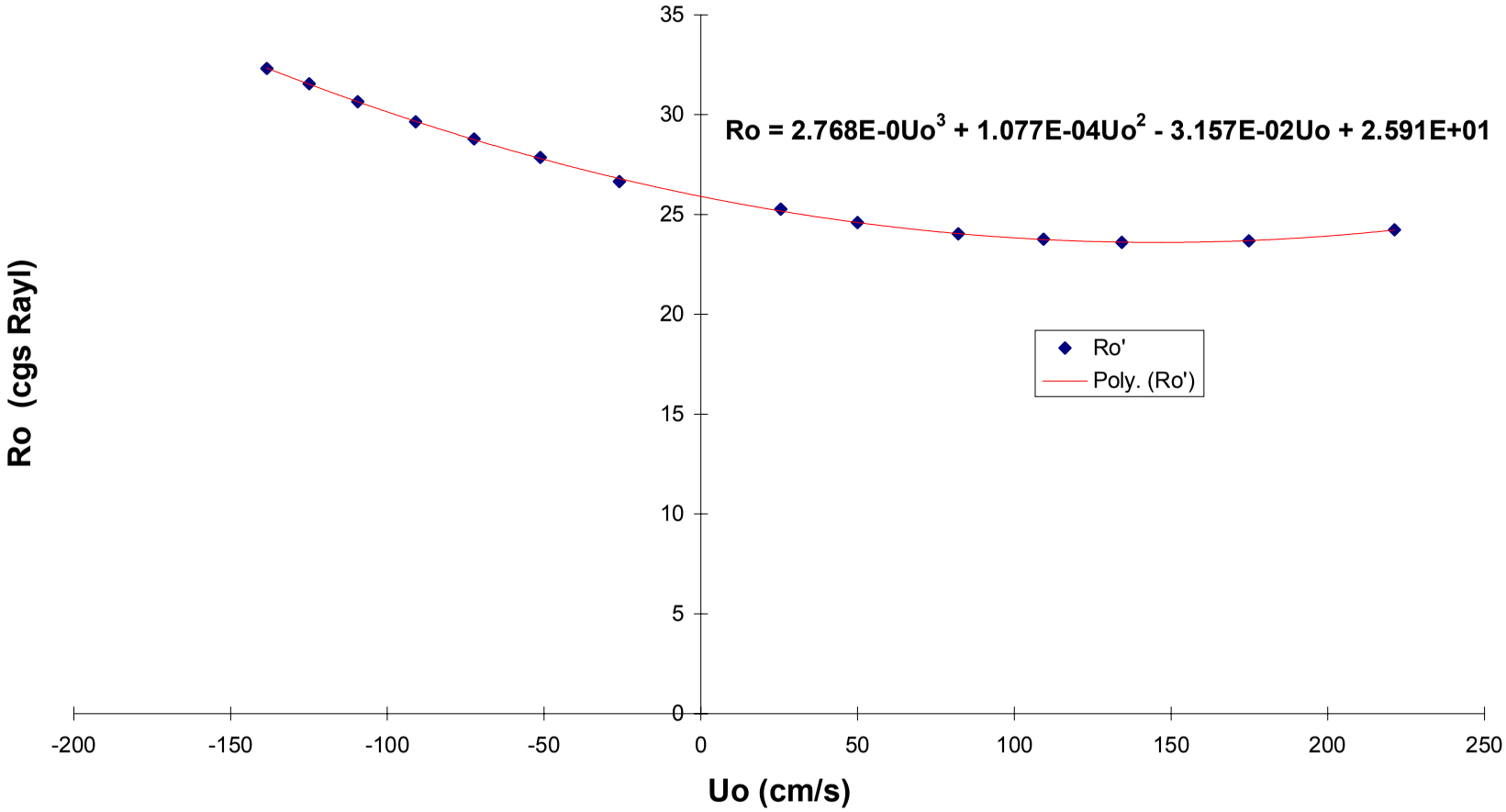

Figure 13b
Calculation of rms particle velocity from a set of values during one oscillation cycle.

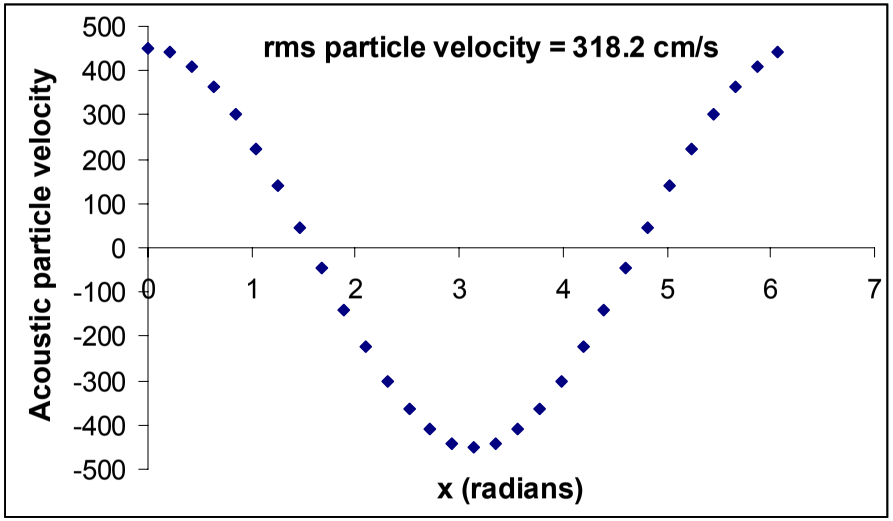

Figure 13c
Calculation of rms resistance from a set of values computed using the Polynomial fit of Figure 13a and the particle velocities of Figure 13b.

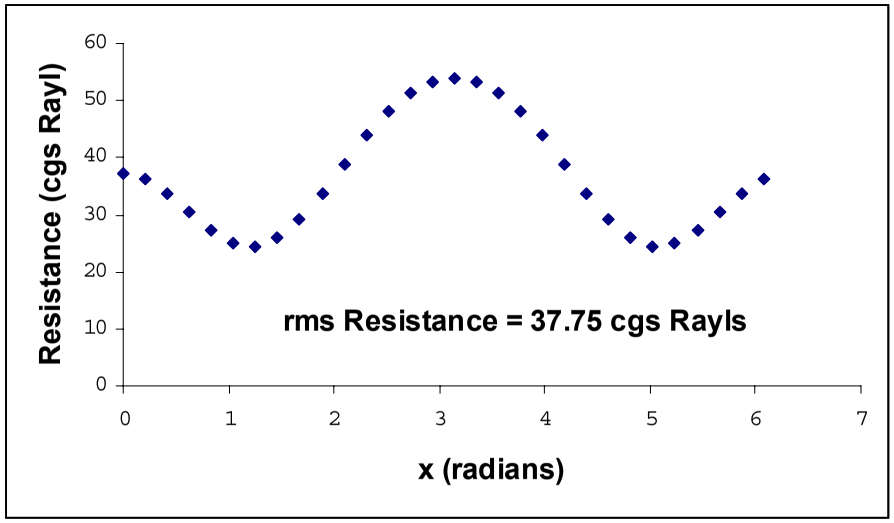

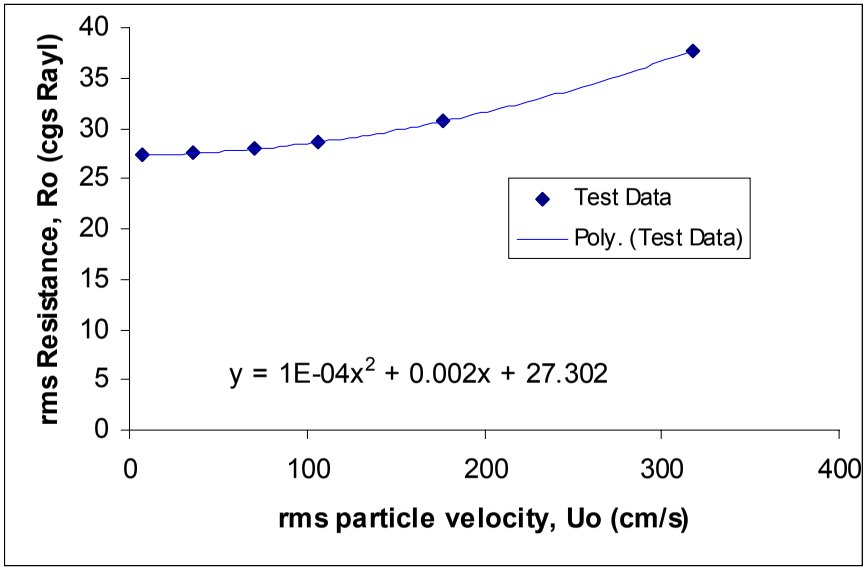

Figure 13d
Plot of rms Resistance values against rms particle velocity values. Corresponding to each rms value of particle velocity, a value of rms resistance was computed as illustrated in Figures 13b and 13c.

Figure 14
Typical Boundary Layer Measurements over the test sample.

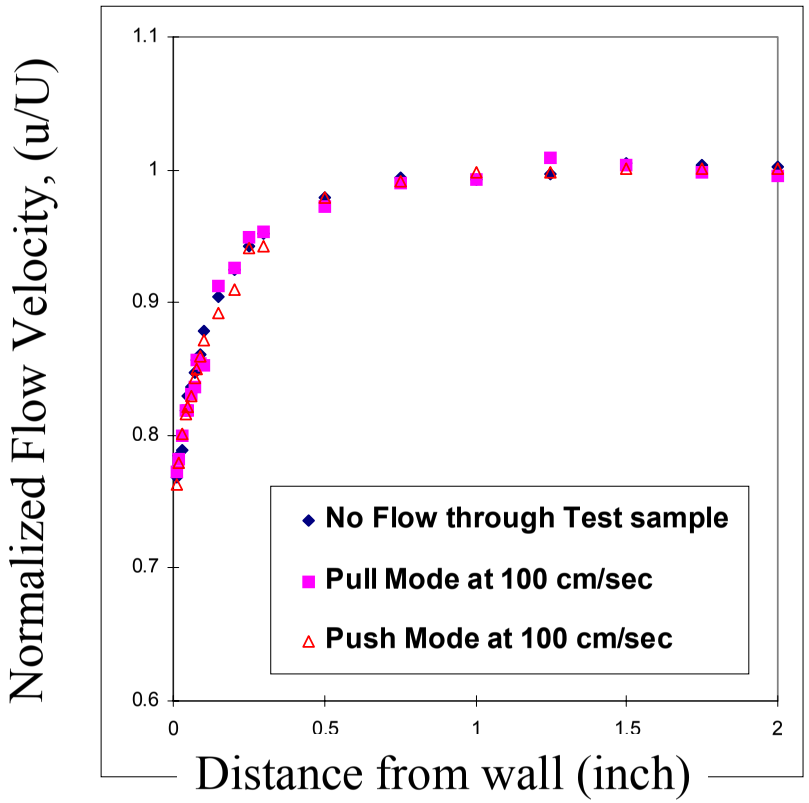

Boundary Layer Thickness (inch)	No Flow Through Sample	PULL Mode at 100 cm/s	PUSH Mode at 100 cm/s
δ^*	0.045	0.044	0.047
θ	0.040	0.040	0.042

Figure 15. DC Flow Resistance Data for Sample No. 1

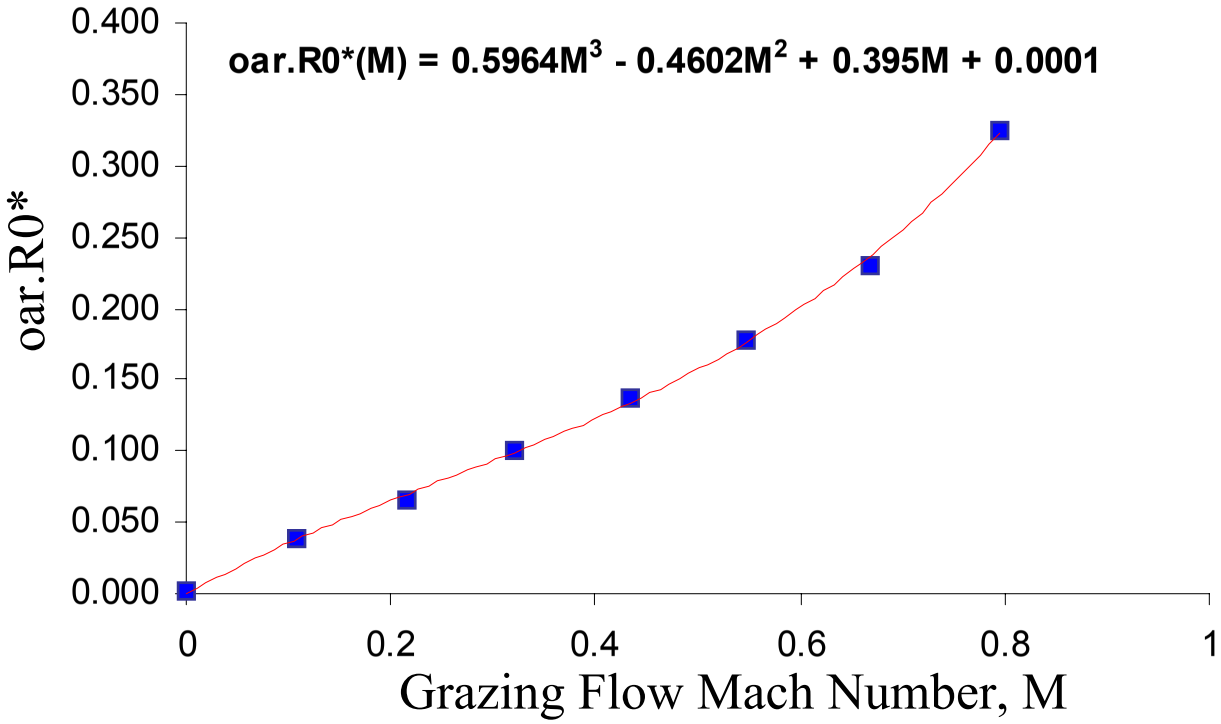

Sample # 1

Hole Diameter	**0.038**
Porosity	**8.30%**
sheet thickness	**0.037**

Mach N0.	R0	R0*	oar*R0*	NLF150/20
0	0.60	0.014	0.001	6.43
0.109	18.94	0.458	0.038	1.69
0.215	33.03	0.799	0.066	1.39
0.322	50.00	1.210	0.100	1.21
0.433	68.10	1.648	0.137	1.12
0.547	88.79	2.148	0.178	1.07
0.669	114.93	2.781	0.231	1.07
0.794	161.63	3.911	0.325	1.00

oar - open area ratio
R0* - normalized resistance

Figure 16. DC Flow Resistance Data for Sample No. 2

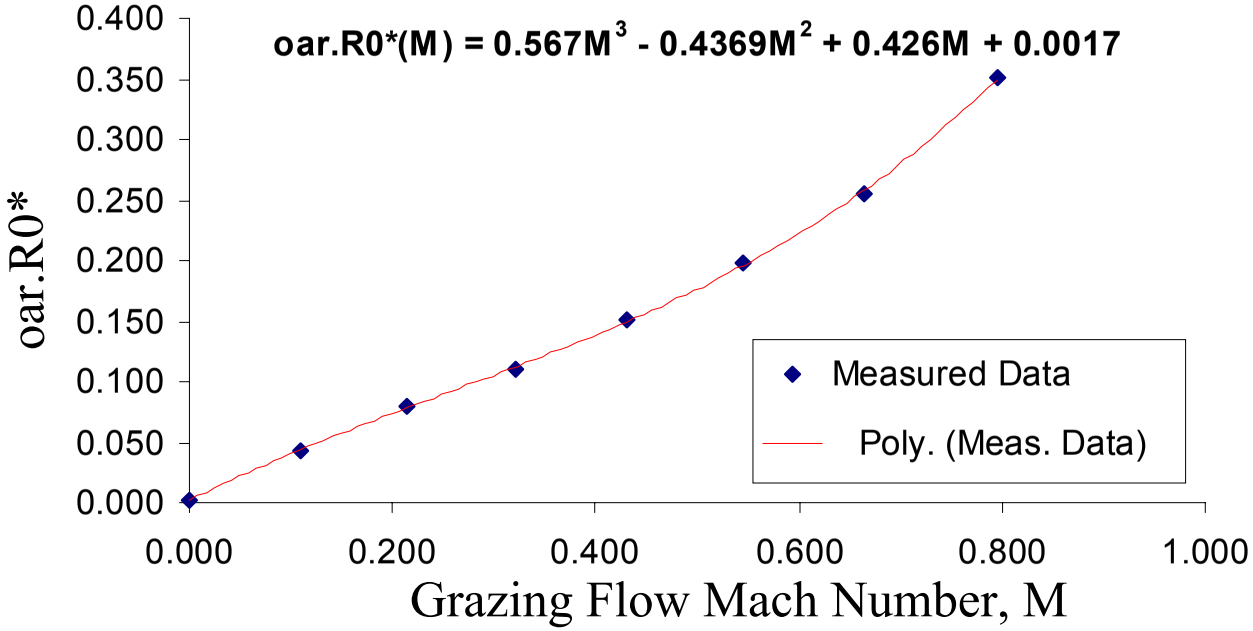

Sample # 2

Hole Diameter	**0.038**
Porosity	**6.50%**
sheet thickness	**0.037**

Mach No	R0	R0*	oar.R0*	NLF150:20
0.000	1.63	0.04	0.003	5.68
0.109	26.715	0.65	0.042	3.38
0.214	50.507	1.22	0.079	1.60
0.322	70.429	1.70	0.111	1.46
0.431	96.449	2.33	0.152	1.23
0.545	125.86	3.04	0.198	1.13
0.665	161.85	3.92	0.254	1.07
0.795	222.96	5.39	0.351	1.06

oar - open area ratio
R0* - normalized resistance

Figure 17a. DC Flow Resistance Data for Sample No. 3

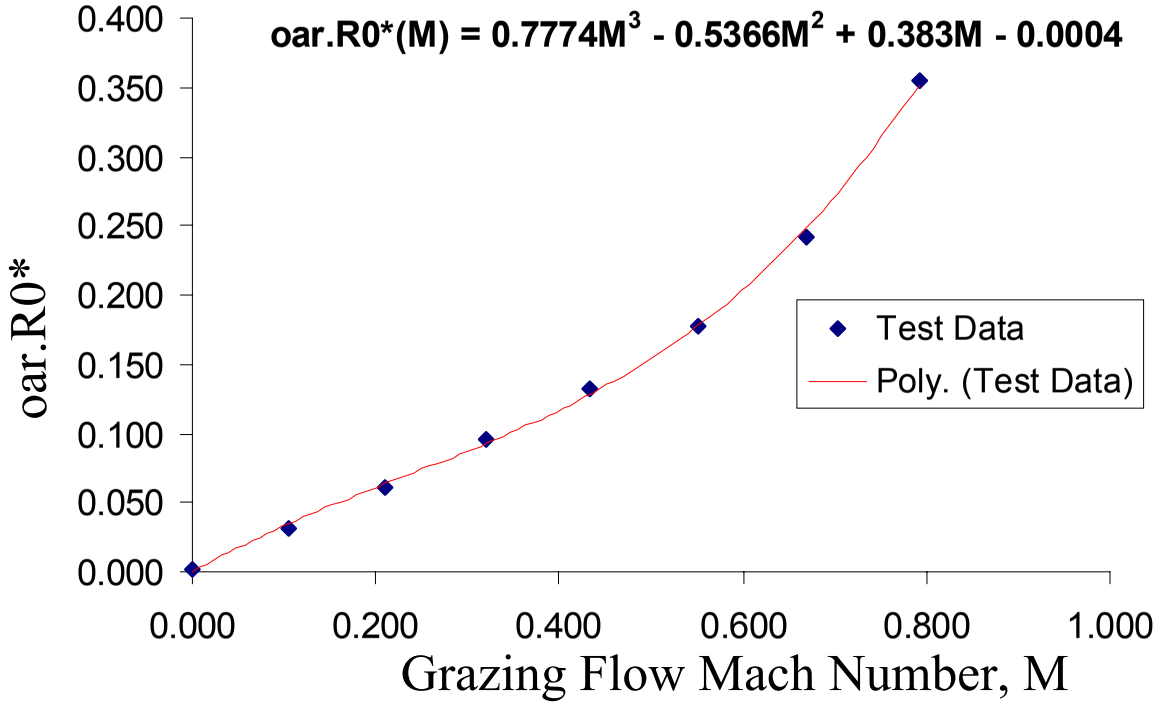

Sample # 3

Hole Diameter	**0.038**
Porosity	**14.46%**
sheet thickness	**0.037**

Mach N0.	R0	R0*	oar*R0*	NLF150/20
0.000	0.61	0.015	0.002	5.04
0.104	8.76	0.212	0.031	1.51
0.211	17.34	0.419	0.061	1.14
0.320	27.34	0.661	0.096	1.08
0.434	37.59	0.909	0.132	1.05
0.550	50.72	1.227	0.178	1.04
0.669	69.08	1.671	0.242	1.02
0.792	101.19	2.448	0.355	1.00

oar - open area ratio
R0* - normalized resistance

Figure 17b. DC Flow Resistance Data for Sample No. 3 (Repeat Test)

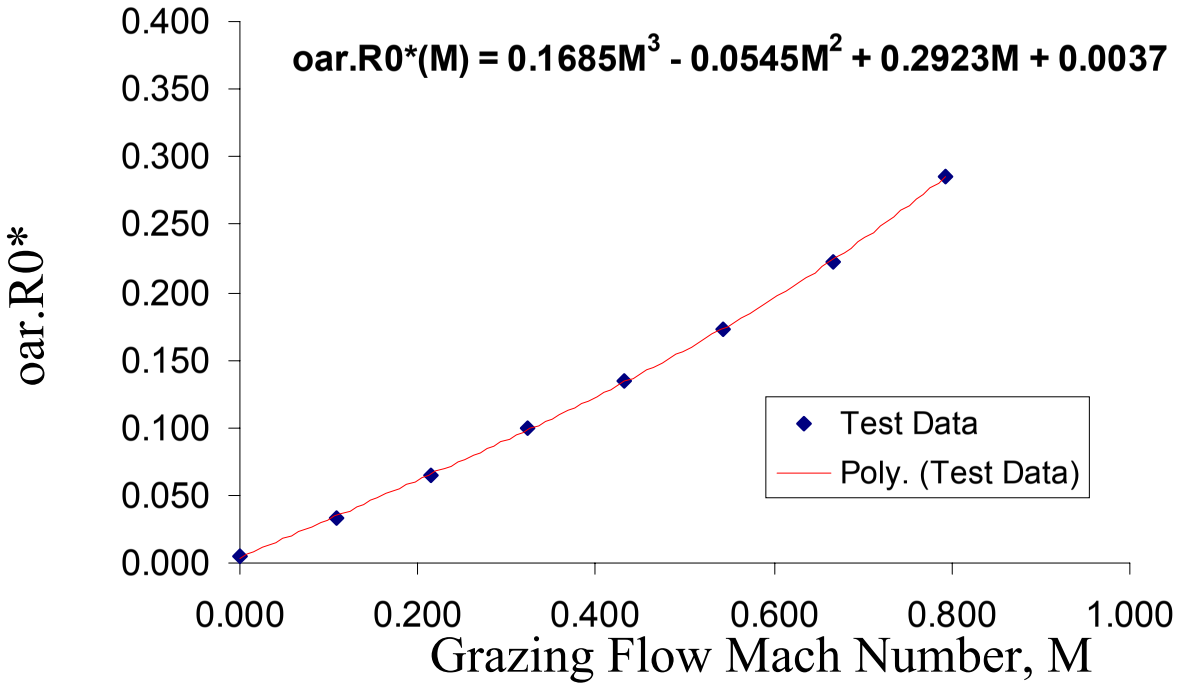

Sample # 3 **Repeat Test**

Hole Diameter	0.038
Porosity	14.62%
sheet thickness	0.037

Mach N0.	R0	R0*	oar*R0*	NLF150/20
0.000	1.28	0.031	0.005	5.81
0.108	9.43	0.228	0.033	1.43
0.216	18.40	0.445	0.065	1.14
0.323	27.96	0.676	0.099	1.06
0.431	38.08	0.921	0.135	1.02
0.544	48.96	1.184	0.173	1.02
0.666	62.83	1.520	0.222	1.00
0.793	80.80	1.955	0.286	1.00

oar - open area ratio
R0* - normalized resistance

Figure 17c. DC Flow Resistance Data for Sample No. 3
Comparison of data from repeat tests.

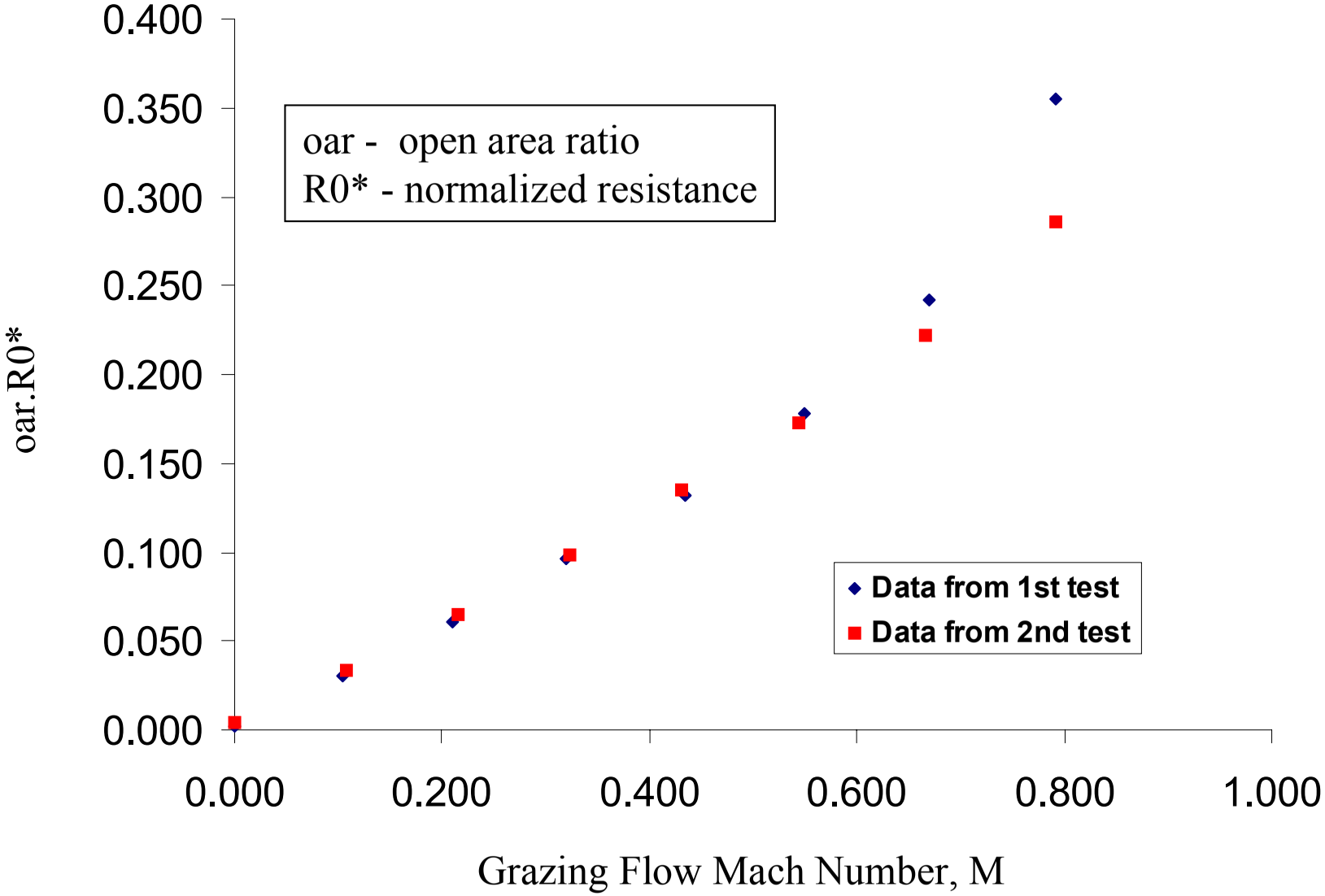

Figure 18. DC Flow Resistance Data for Sample No. 4

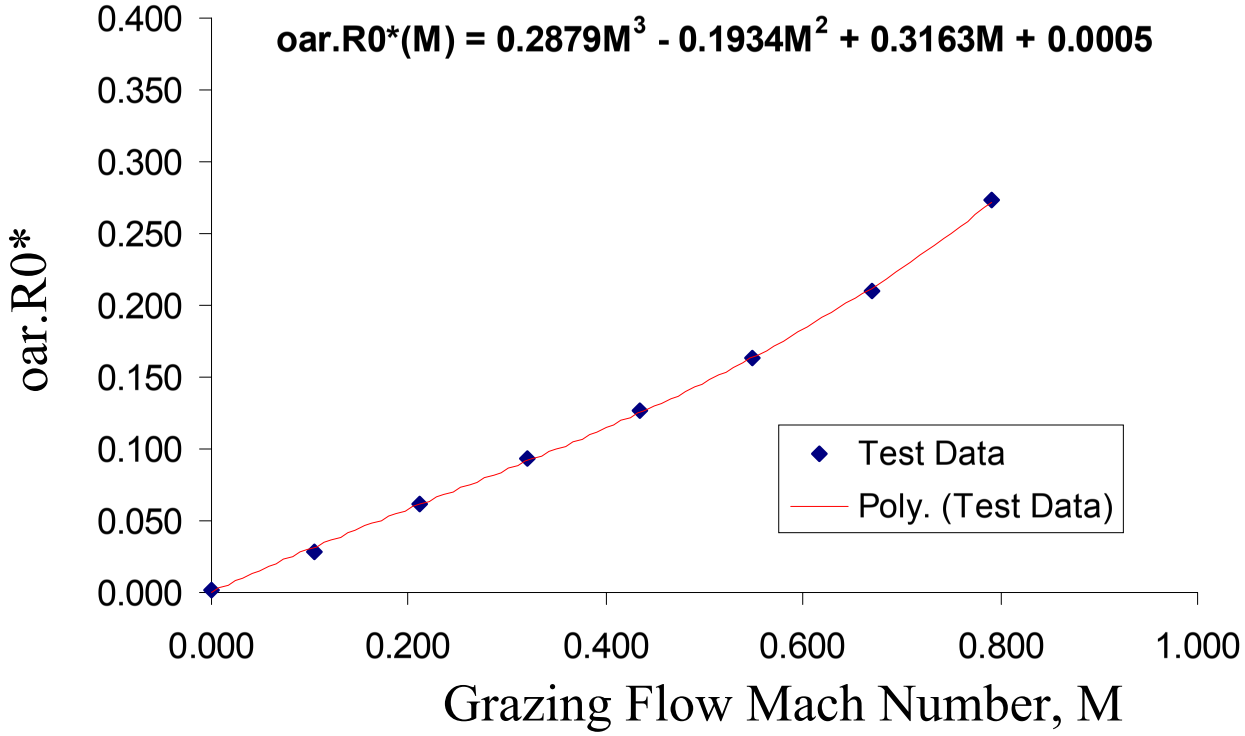

Sample # 4

Hole Diameter	**0.038**
Porosity	**12.04%**
sheet thickness	**0.037**

Mach N0.	R0	R0*	oar*R0*	NLF150/20
0.000	0.81	0.020	0.002	5.16
0.104	9.57	0.231	0.028	2.20
0.211	21.10	0.510	0.061	1.27
0.320	32.16	0.778	0.094	1.17
0.434	43.21	1.045	0.126	1.07
0.550	55.91	1.353	0.163	1.06
0.669	72.15	1.745	0.210	1.04
0.791	93.82	2.270	0.273	1.02

oar - open area ratio
R0* - normalized resistance

Figure 19. DC Flow Resistance Data for Sample No. 5

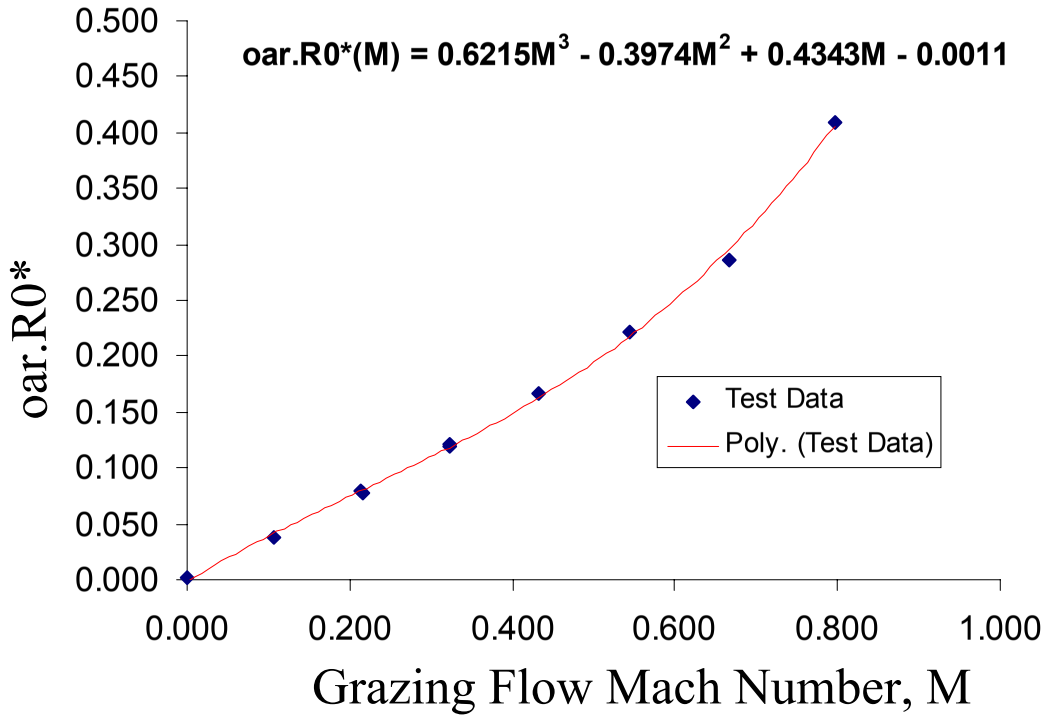

Sample # 5

Hole Diameter	**0.038**
Porosity	**13.32%**
sheet thickness	**0.037**

Mach N0.	R0	R0*	oar*R0*	NLF150/20
0.000	0.60	0.015	0.002	5.30
0.108	11.68	0.283	0.038	1.52
0.215	23.90	0.578	0.077	1.18
0.213	24.50	0.593	0.079	1.12
0.322	37.00	0.895	0.119	1.08
0.322	37.40	0.905	0.121	1.06
0.432	51.86	1.254	0.167	1.02
0.545	68.55	1.658	0.221	1.01
0.666	88.81	2.148	0.286	1.00
0.796	127.20	3.077	0.410	1.00

oar - open area ratio
R0* - normalized resistance

Figure 20. DC Flow Resistance Data for Sample No. 6

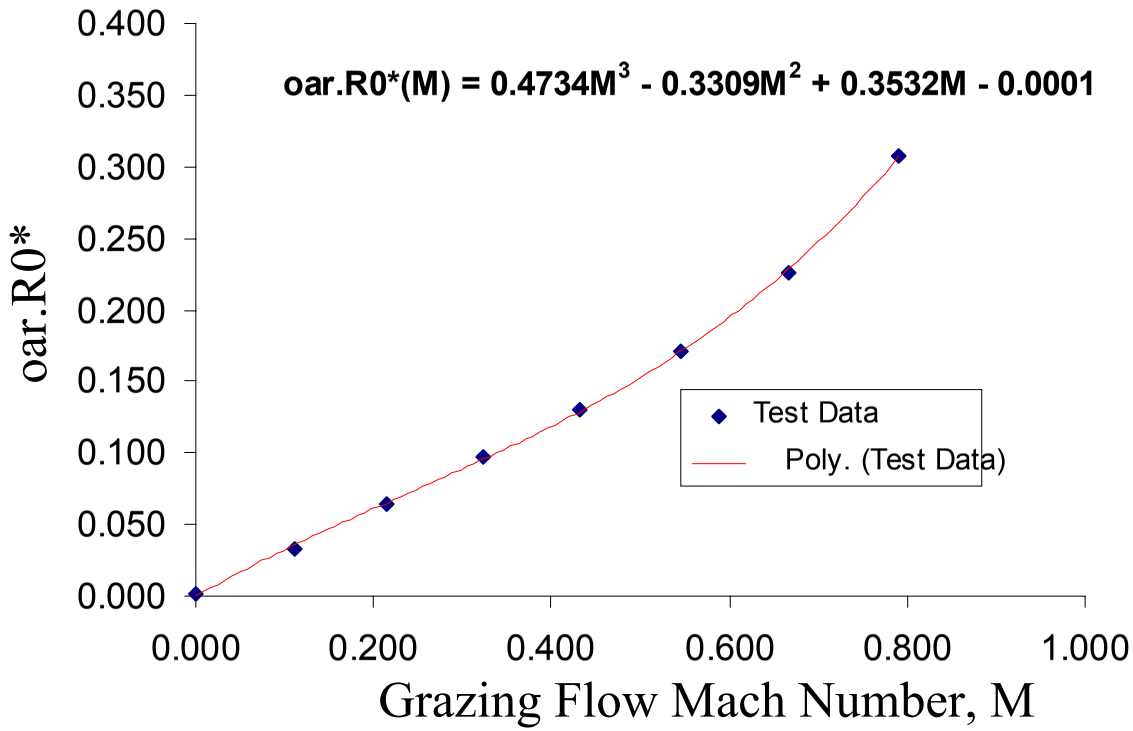

Sample # 6

Hole Diameter	**0.048**
Porosity	**7.35%**
sheet thickness	**0.037**

Mach N0.	R0	R0*	oar*R0*	NLF150/20
0.000	0.58	0.014	0.001	6.66
0.110	18.77	0.454	0.033	2.32
0.215	36.78	0.890	0.065	1.44
0.324	54.84	1.326	0.097	1.25
0.432	73.72	1.783	0.130	1.19
0.545	96.65	2.338	0.171	1.11
0.667	128.30	3.104	0.227	1.07
0.791	174.29	4.216	0.308	1.04

oar - open area ratio
R0* - normalized resistance

Figure 21. DC Flow Resistance Data for Sample No. 7

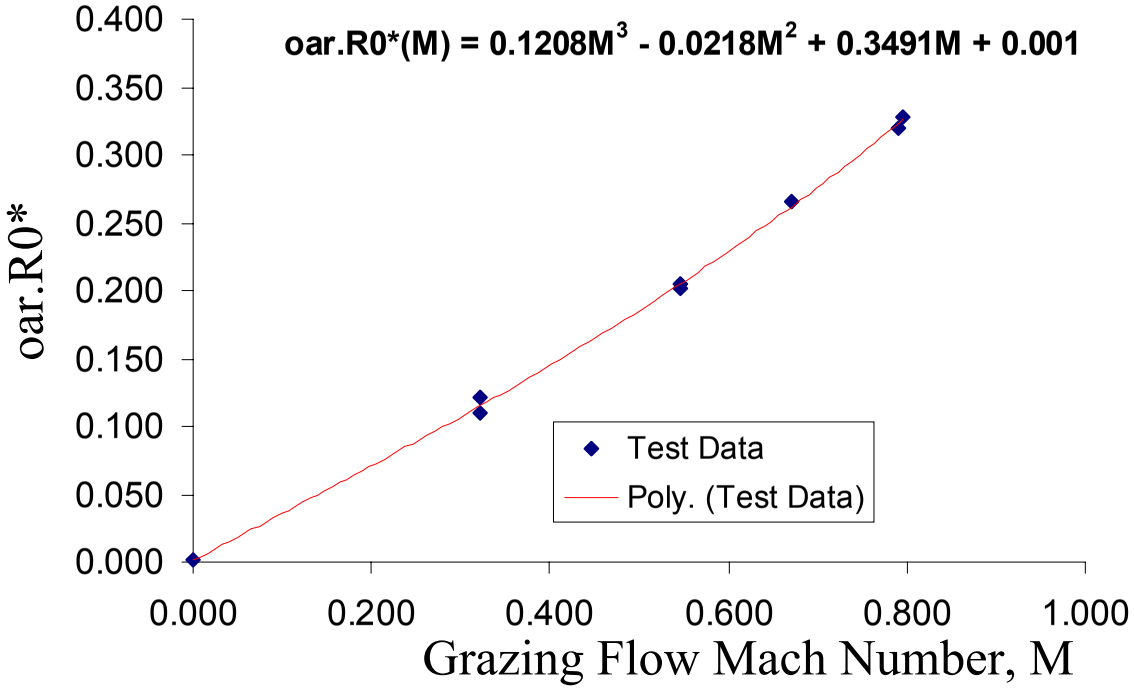

Sample # 7

Hole Diameter	**0.048**
Porosity	**7.70%**
sheet thickness	**0.051**

Mach N0.	R0	R0*	oar*R0*	NLF150/20
0.000	0.48	0.012	0.001	6.72
0.322	64.60	1.563	0.121	1.12
0.322	58.65	1.419	0.110	1.17
0.547	109.10	2.639	0.205	1.05
0.545	107.70	2.605	0.202	1.03
0.671	141.10	3.413	0.265	1.03
0.796	174.90	4.231	0.328	1.02
0.790	170.20	4.117	0.319	1.07

oar - open area ratio
R0* - normalized resistance

Figure 22. DC Flow Resistance Data for Sample No. 9

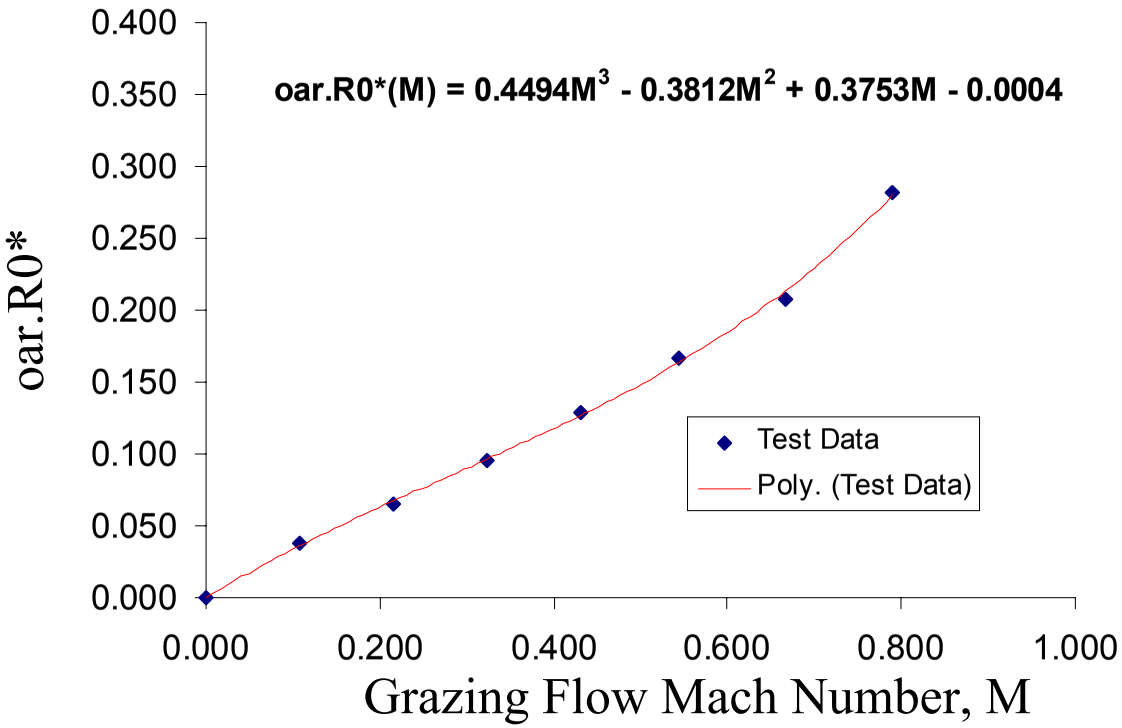

Sample # 9

Hole Diameter	**0.038**
Porosity	**7.70%**
sheet thickness	**0.035**

Mach N0.	R0	R0*	oar*R0*	NLF150/20
0.000	-0.03	-0.001	0.000	7.57
0.109	18.77	0.454	0.037	1.70
0.215	32.49	0.786	0.065	1.42
0.323	47.74	1.155	0.095	1.18
0.430	65.15	1.576	0.130	1.09
0.545	83.83	2.028	0.167	1.07
0.666	104.34	2.524	0.207	1.04
0.790	141.81	3.430	0.282	0.98

oar - open area ratio
R0* - normalized resistance

Figure 23. DC Flow Resistance Data for Sample No. 10

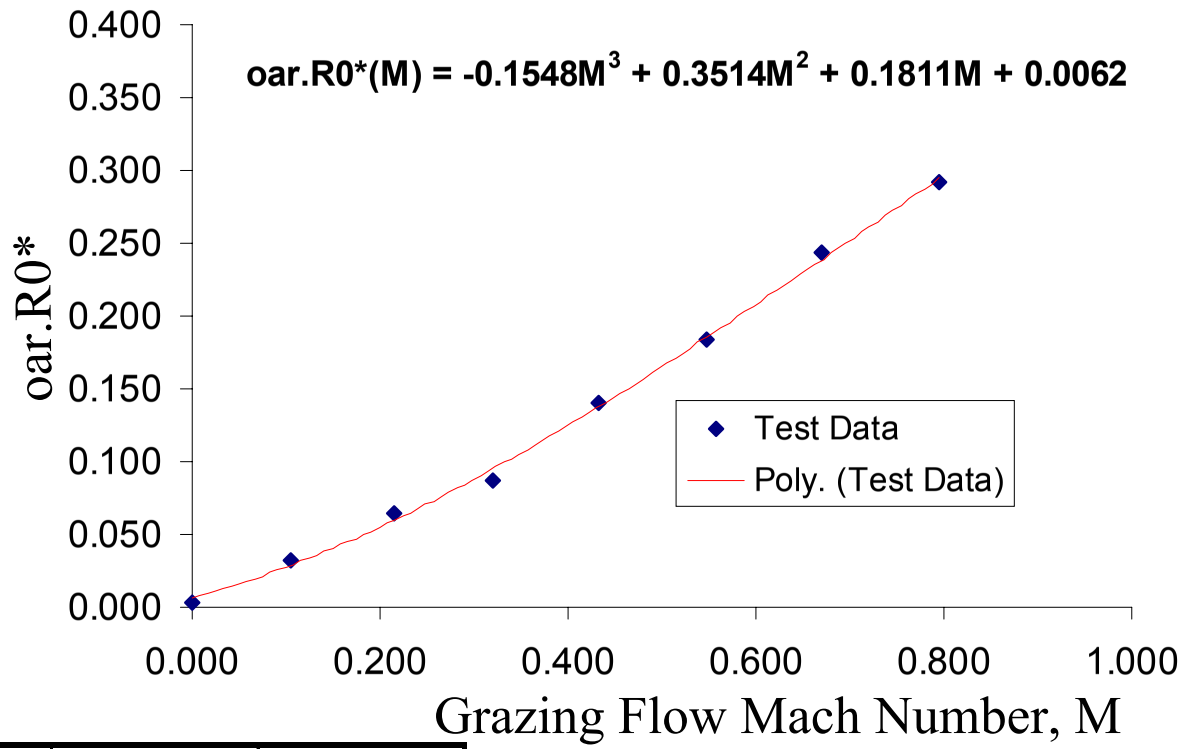

Sample # 10

Hole Diameter	**0.038**
Porosity	**10.77%**
sheet thickness	**0.038**

Mach N0.	R0	R0*	oar*R0*	NLF150/20
0.000	1.37	0.033	0.004	4.69
0.104	12.58	0.304	0.033	2.09
0.215	24.62	0.595	0.064	1.34
0.321	33.30	0.806	0.087	1.18
0.433	53.86	1.303	0.140	1.06
0.547	70.28	1.700	0.183	1.05
0.669	93.24	2.255	0.243	1.01
0.796	112.34	2.717	0.293	1.02

oar - open area ratio
R0* - normalized resistance

Figure 24. DC Flow Resistance Data for Sample No. 11

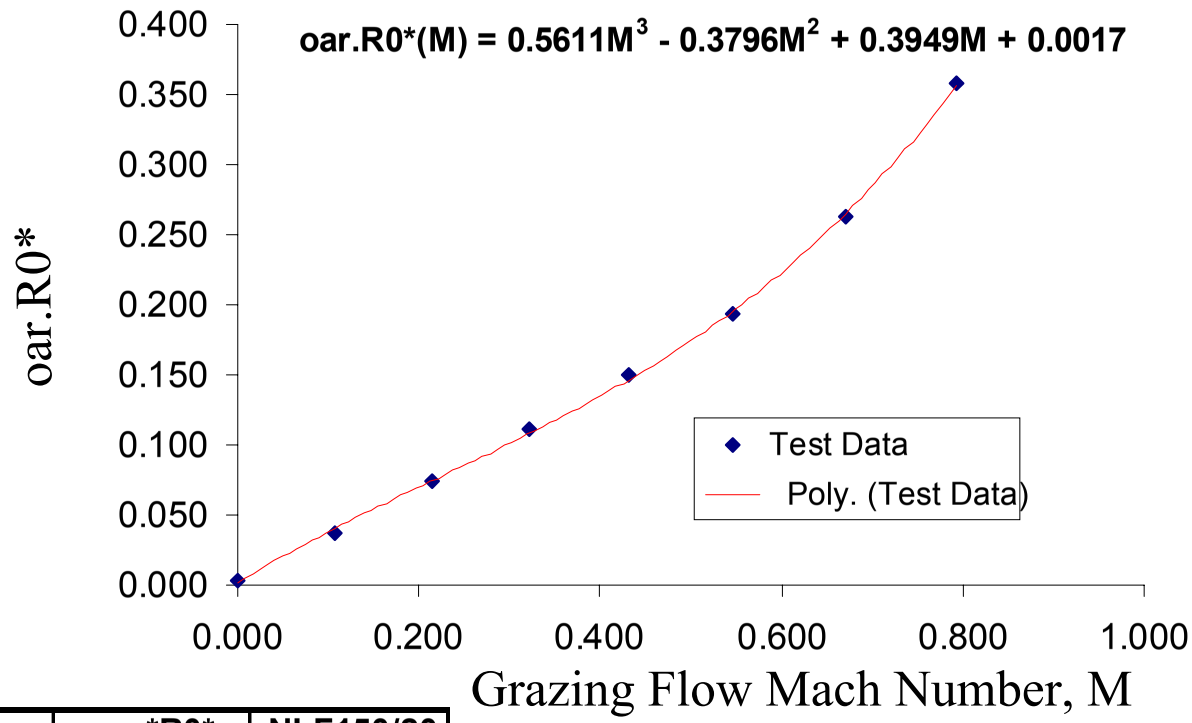

Sample # 11

Hole Diameter	0.048
Porosity	8.80%
sheet thickness	0.054

Mach N0.	R0	R0*	oar*R0*	NLF150/20
0.000	1.88	0.046	0.004	4.83
0.108	17.08	0.413	0.036	2.41
0.215	34.81	0.842	0.074	1.27
0.322	52.17	1.262	0.111	1.12
0.431	70.27	1.700	0.150	1.09
0.547	90.98	2.201	0.194	1.05
0.670	123.17	2.979	0.262	1.01
0.794	168.15	4.067	0.358	1.00

oar - open area ratio
R0* - normalized resistance

Figure 25. DC Flow Resistance Data for Sample No. 12

Graphite-Epoxy Composite Perforated Face Sheet.
This sample represents the manufacturing process at B. F. Goodrich (BFG).

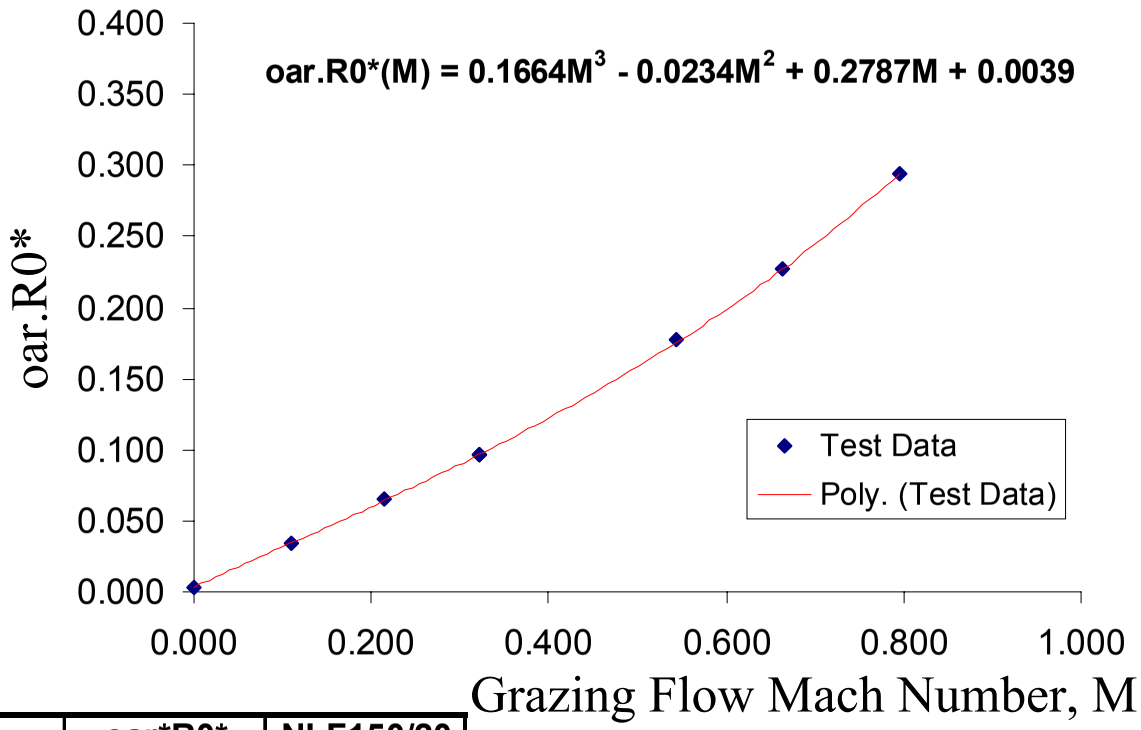

Sample # 12

Hole Diameter	**0.065**
Porosity	**7.50%**
sheet thickness	**0.037**

Mach N0.	R0	R0*	oar*R0*	NLF150/20
0.000	1.88	0.045	0.003	6.76
0.109	19.26	0.466	0.035	1.95
0.214	35.97	0.870	0.065	1.39
0.322	52.85	1.278	0.096	1.16
0.322	52.94	1.281	0.096	1.16
0.545	97.56	2.360	0.177	1.06
0.665	125.32	3.031	0.227	1.03
0.795	162.33	3.927	0.294	1.02

oar - open area ratio
R0* - normalized resistance

Figure 26. DC Flow Resistance Data for Sample No. 13

This face sheet had a thin micro-porous (PU) film bonded on a 34% porosity perforated sheet. The PU film had laser drilled holes of 0.005 inch diameter. Sample manufactured by BFG.

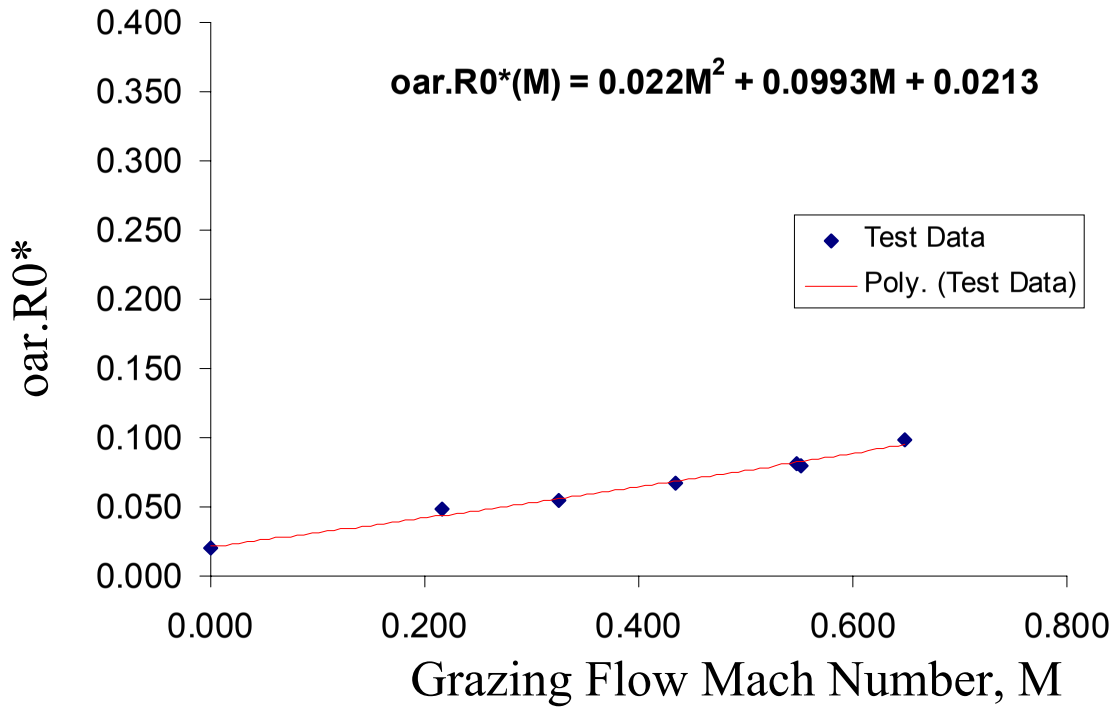

Sample # 13

Hole Diameter	**0.005**
Porosity	**2.02%**
sheet thickness	**0.05**

Mach N0.	R0	R0*	oar*R0*	NLF150/20
0.000	40.61	0.98	0.020	4.63
0.217	97.84	2.37	0.048	3.36
0.324	113.17	2.74	0.055	2.52
0.434	138.16	3.34	0.068	3.14
0.552	164.58	3.98	0.080	2.41
0.547	164.69	3.98	0.080	2.06
0.649	200.67	4.85	0.098	1.56
0.791	209.15	5.06	0.102	1.54

oar - open area ratio
R0* - normalized resistance

Figure 27a. DC Flow Resistance Data for Sample No. 14a

1st sample from panel # 14.

This Fiberglas-Epoxy face sheet was manufactured by GEAE using the pin-mandrel tooling process.

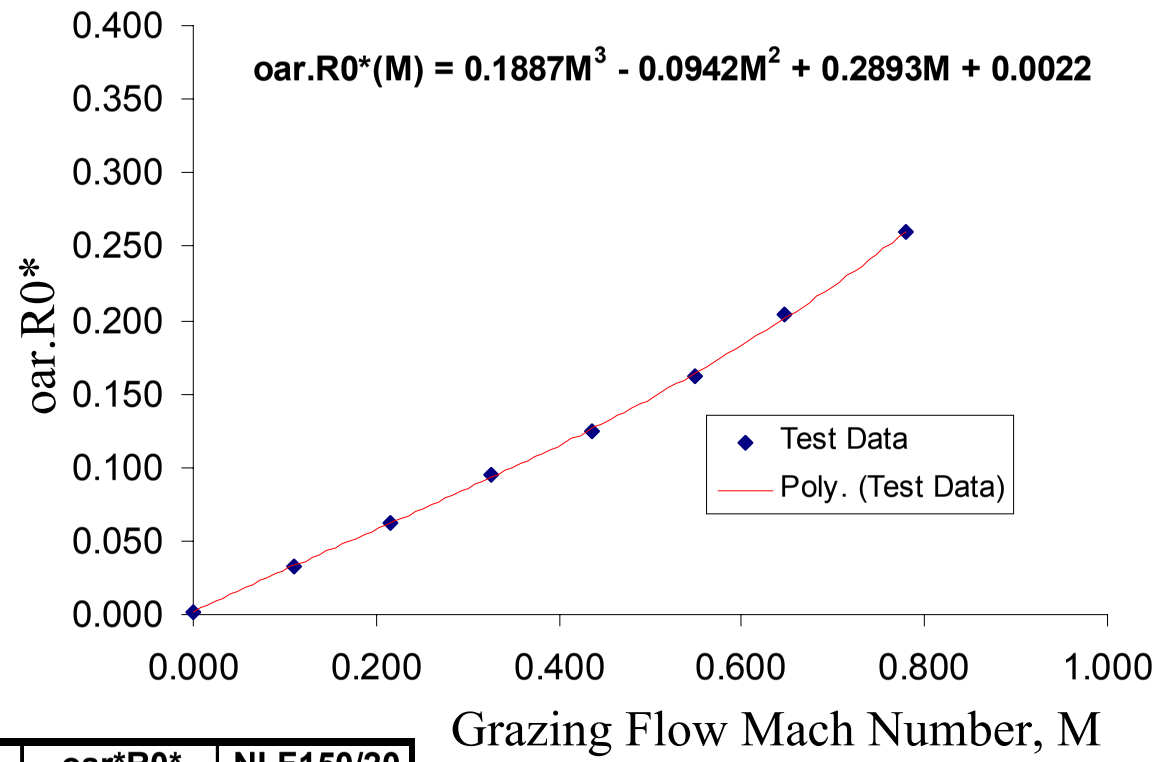

Sample #14a

Hole Diameter	**0.055**
Porosity	**8.00%**
sheet thickness	**0.05**

Mach N0.	R0	R0*	oar*R0*	NLF150/20
0.000	1.09	0.03	0.002	5.87
0.111	17.18	0.42	0.033	1.74
0.216	32.25	0.78	0.062	1.49
0.326	49.11	1.19	0.095	1.27
0.436	64.12	1.55	0.124	1.13
0.550	84.07	2.03	0.162	1.07
0.646	105.36	2.55	0.204	1.06
0.780	134.12	3.24	0.259	1.02

oar - open area ratio
R0* - normalized resistance

Figure 27b. DC Flow Resistance Data for Sample No. 14b

2nd sample from panel # 14.

This Fiberglas-Epoxy face sheet was manufactured by GEAE using the pin-mandrel tooling process.

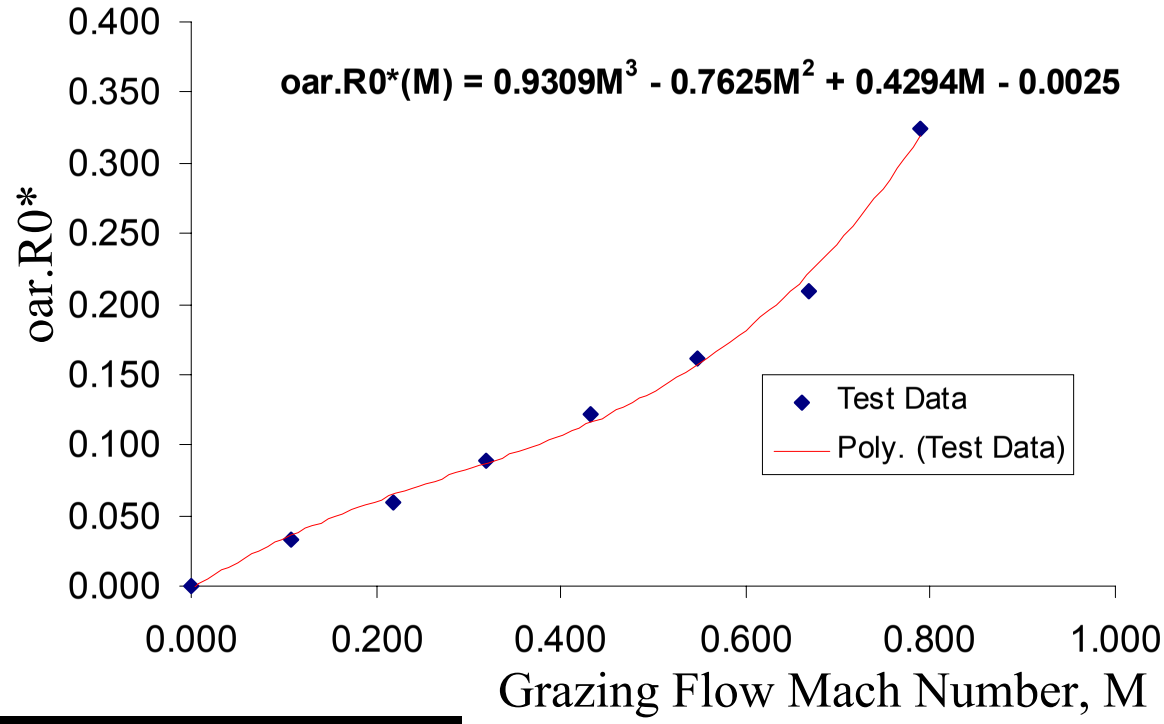

Sample # 14b

Hole Diameter	**0.057**
Porosity	**8.96%**
sheet thickness	**0.05**

Mach N0.	R0	R0*	oar*R0*	NLF150/20
0.000	0.09	0.00	0.000	5.49
0.108	15.39	0.37	0.033	1.65
0.218	27.37	0.66	0.059	1.37
0.319	41.03	0.99	0.089	1.19
0.433	56.52	1.37	0.123	1.09
0.547	74.46	1.80	0.161	1.07
0.668	96.23	2.33	0.209	1.06
0.789	149.53	3.62	0.324	1.01

oar - open area ratio
R0* - normalized resistance

Figure 27c. DC Flow Resistance Data for Samples No. 14a & 14b

Comparison of data for two samples from the same panel.

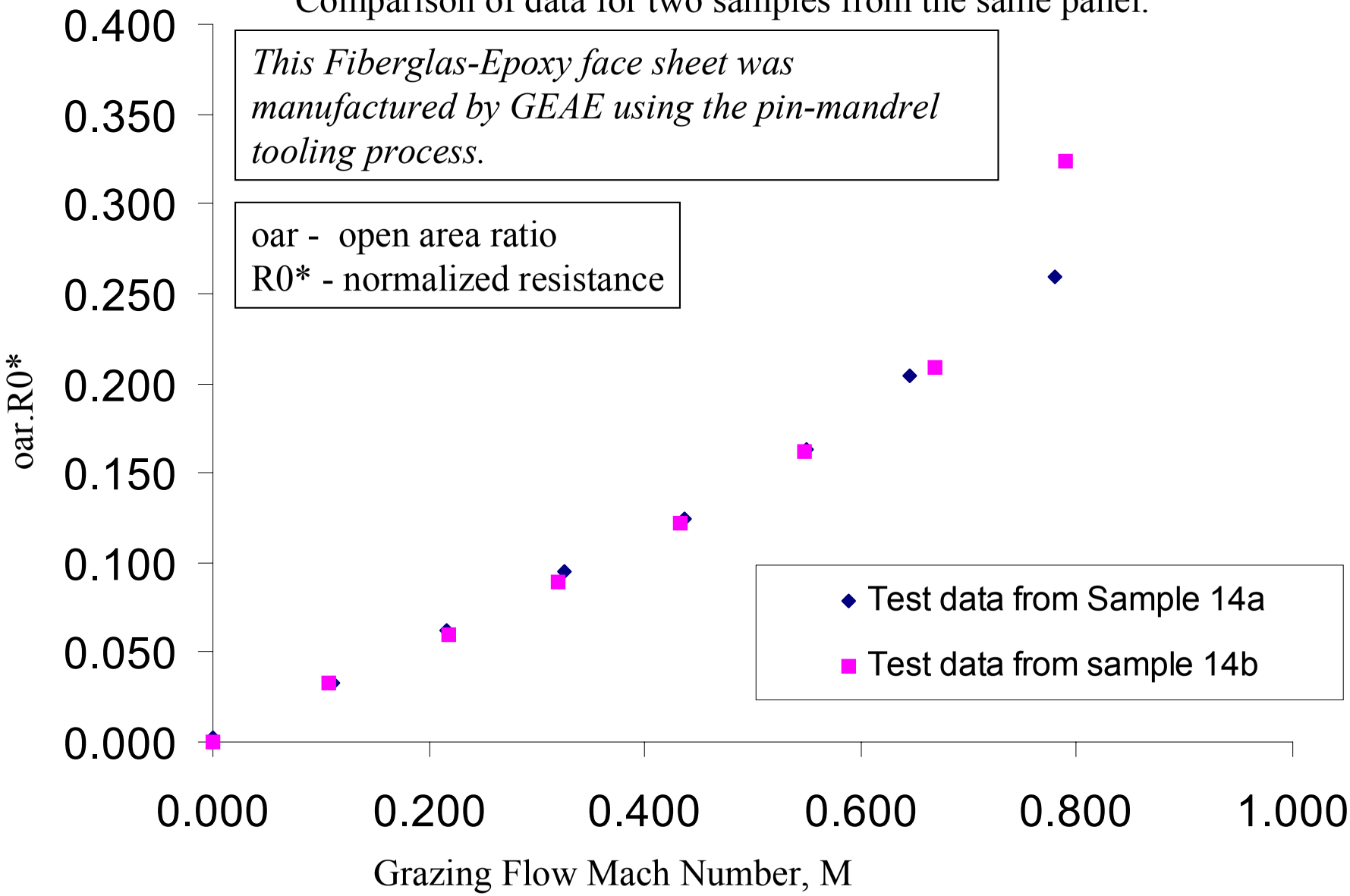

Figure 28a. DC Flow Resistance Data for Sample No. 15-1

This Graphite-Epoxy face sheet was fabricated by Middle River Aircraft Systems. The perforations were produced by the "pin-less" process. Face sheet was also coated for erosion resistance.

Sample # 15-1

Hole Diameter	**0.047**
Porosity	**10.70%**
sheet thickness	**0.04**

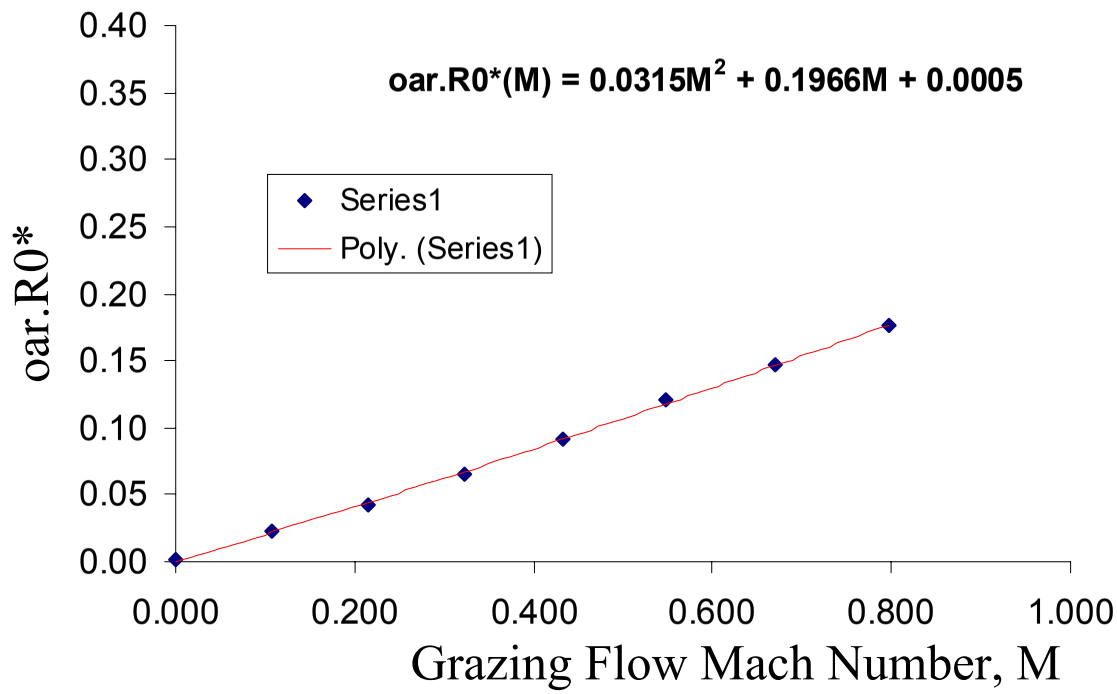

Mach N0.	R0	R0*	oar*R0*	NLF150/20
0.000	0.51	0.0123	0.0013	6.0843
0.108	8.74	0.2114	0.0226	1.8457
0.215	16.48	0.3986	0.0426	1.3007
0.323	25.20	0.6096	0.0652	1.2172
0.433	35.61	0.8614	0.0921	1.1465
0.548	46.52	1.1253	0.1203	1.0755
0.669	56.58	1.3687	0.1463	1.0974
0.797	68.02	1.6454	0.1759	1.0452

oar - open area ratio
R0* - normalized resistance

Figure 28b. DC Flow Resistance Data for Sample No. 15-2

This Graphite-Epoxy face sheet was fabricated by Middle River Aircraft Systems. The perforations were produced by the "pin-less" process. Face sheet was also coated for erosion resistance.

Sample # 15-2

Hole Diameter	**0.04**
Porosity	**10.93%**
sheet thickness	**0.04**

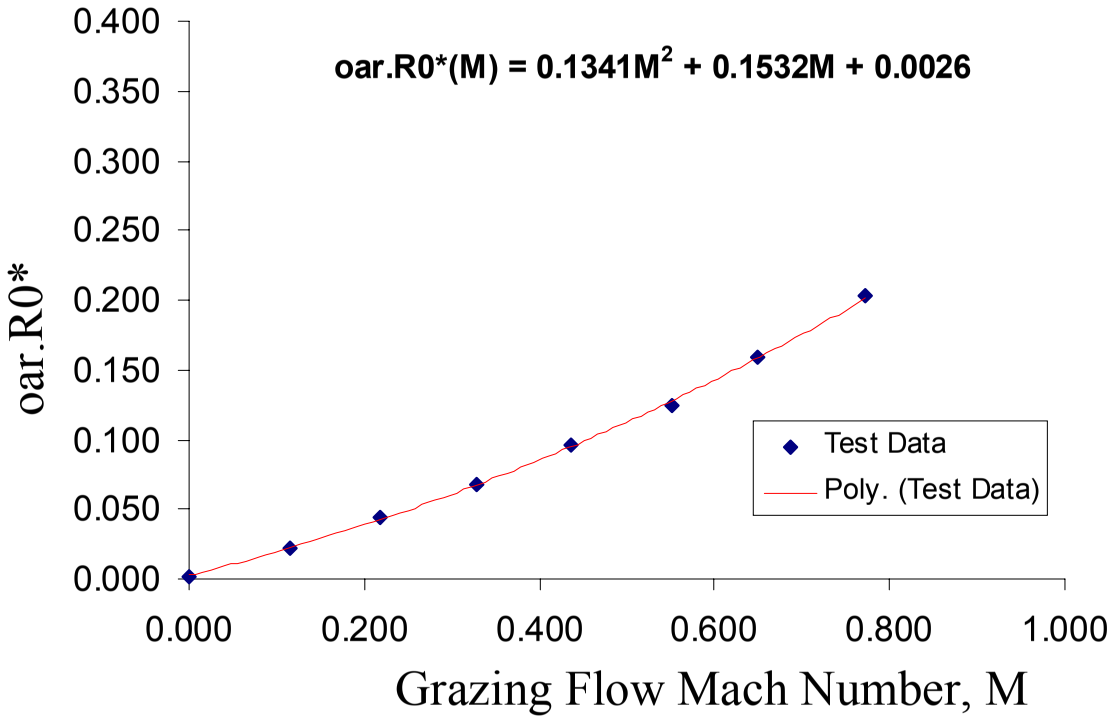

Mach N0.	R0	R0*	oar*R0*	NLF150/20
0.000	0.44	0.01	0.001	6.20
0.114	8.58	0.21	0.023	1.86
0.219	16.65	0.40	0.044	1.30
0.328	25.84	0.63	0.068	1.19
0.437	36.21	0.88	0.096	1.06
0.551	46.84	1.13	0.124	1.06
0.649	60.18	1.46	0.159	1.04
0.773	76.56	1.85	0.202	1.01

oar - open area ratio
R0* - normalized resistance

Figure 28c. DC Flow Resistance Data for Samples No. 15-1 & 15-2
Comparison of data from two panels made to the same design specification.

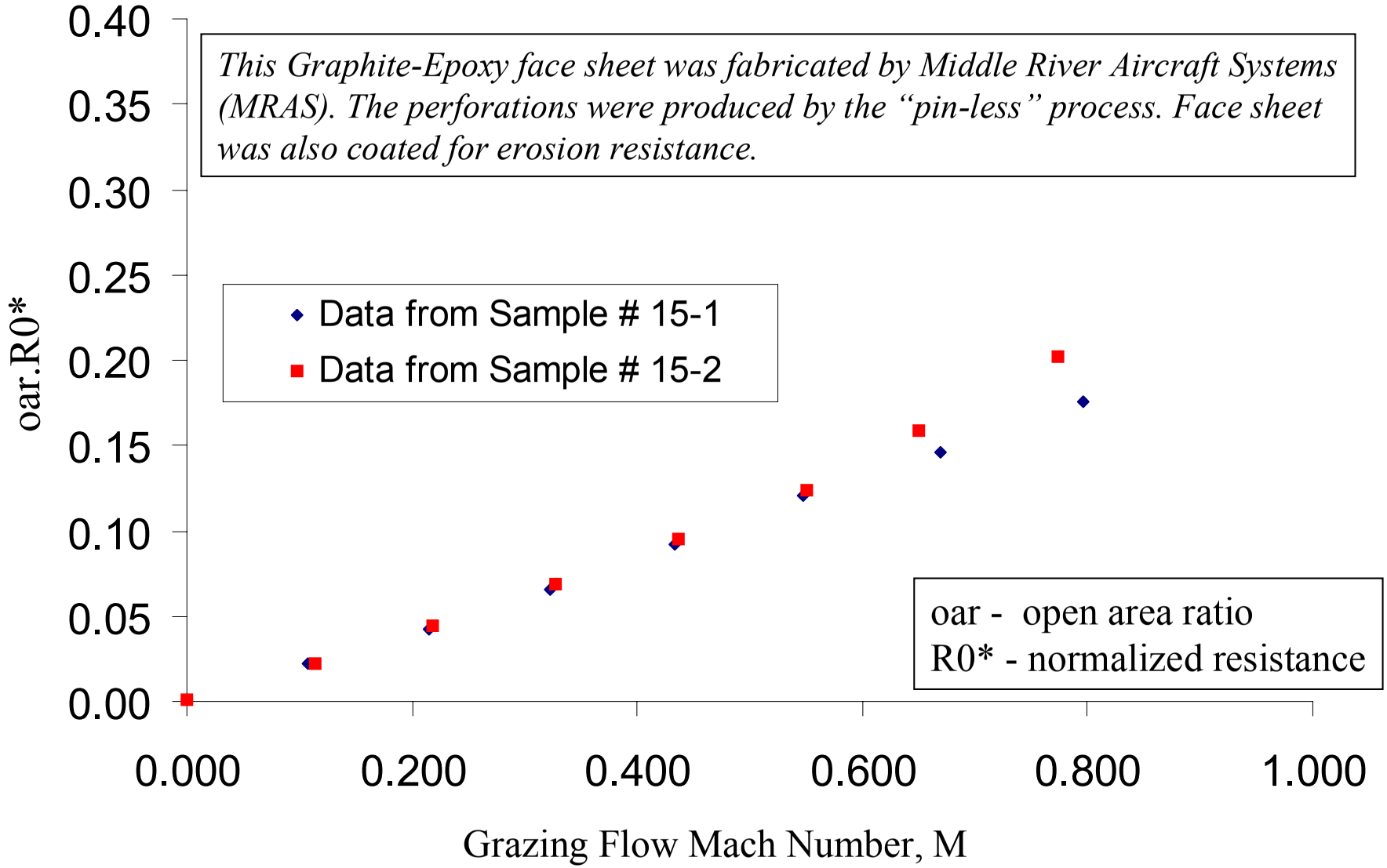

Figure 29. DC Flow Resistance Data for a liner sample with a "wiremesh-on-perforate type" linear face sheet.

Mach	R0	R0*	NLF150/20
0.000	41.31	1.00	1.25
0.110	46.15	1.12	1.15
0.217	45.79	1.11	1.10
0.325	48.74	1.18	1.09
0.436	52.015	1.26	1.04
0.553	58.49	1.41	1.04
0.648	68.86	1.67	1.01
0.760	87.31	2.11	0.97

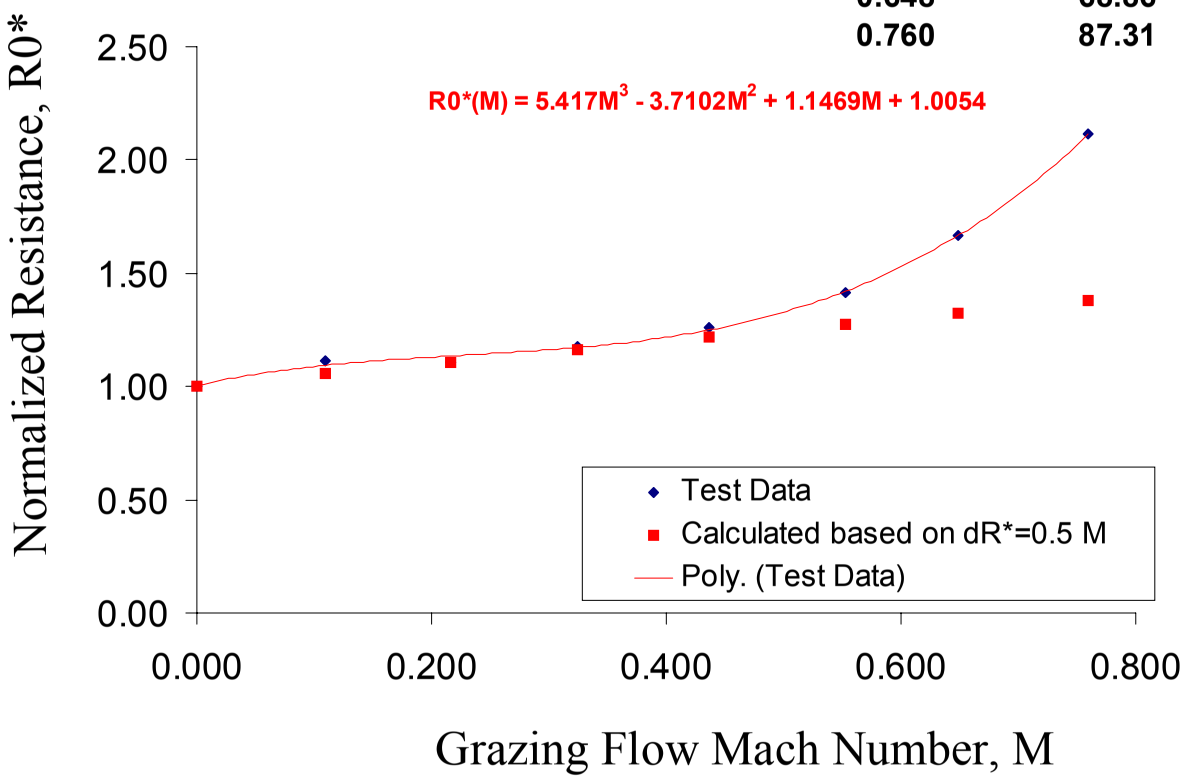

Figure 30

Comparison of the Correlation function, $\alpha_1(M)$ with measured data from all liner samples with metallic perforated face sheets.

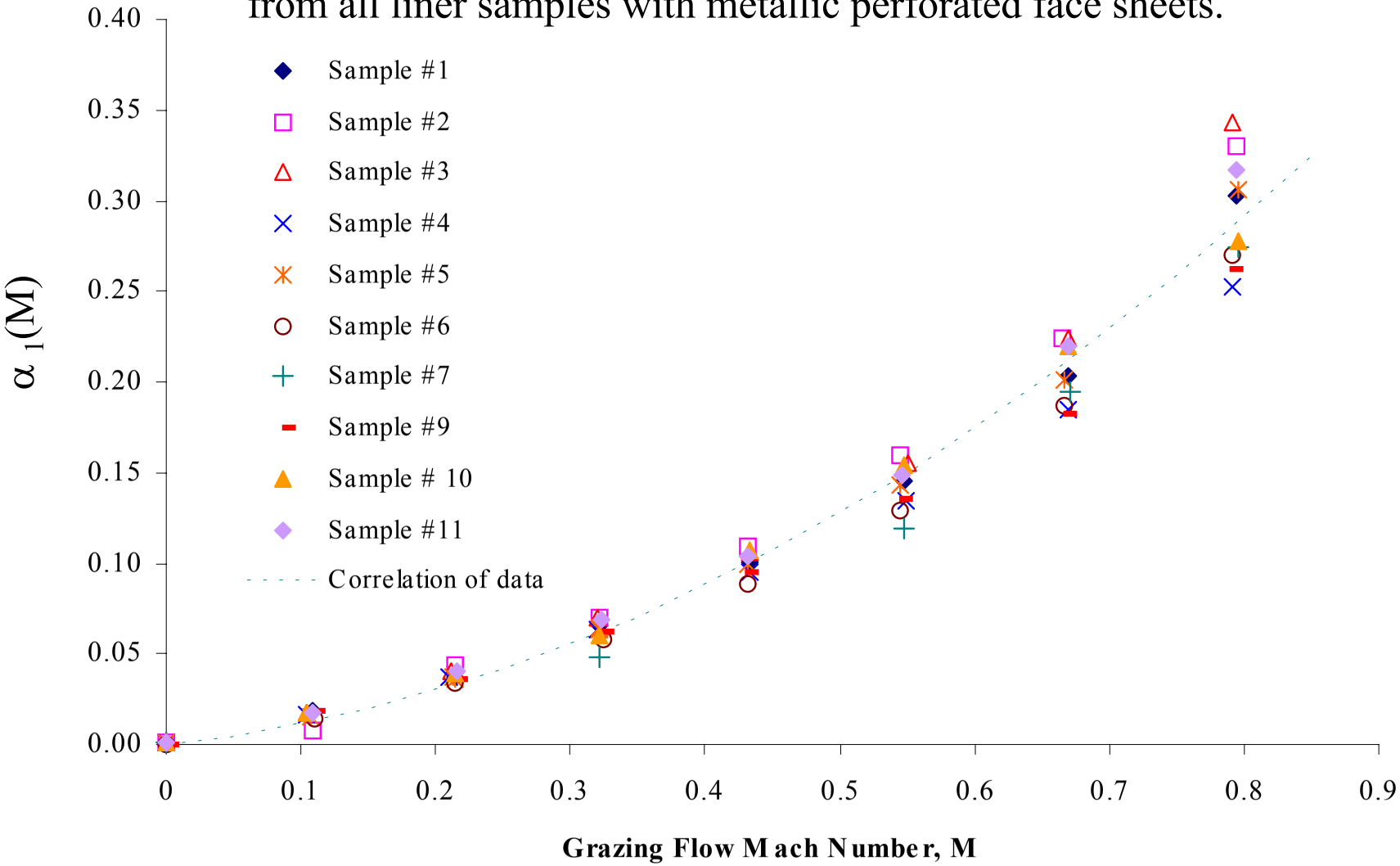

Figure 31a

Histogram of the difference between the Measured and the Predicted (from the correlation) values of the Normalized Resistance, R*(M, u/c=0), with the Normal Distribution Curve.

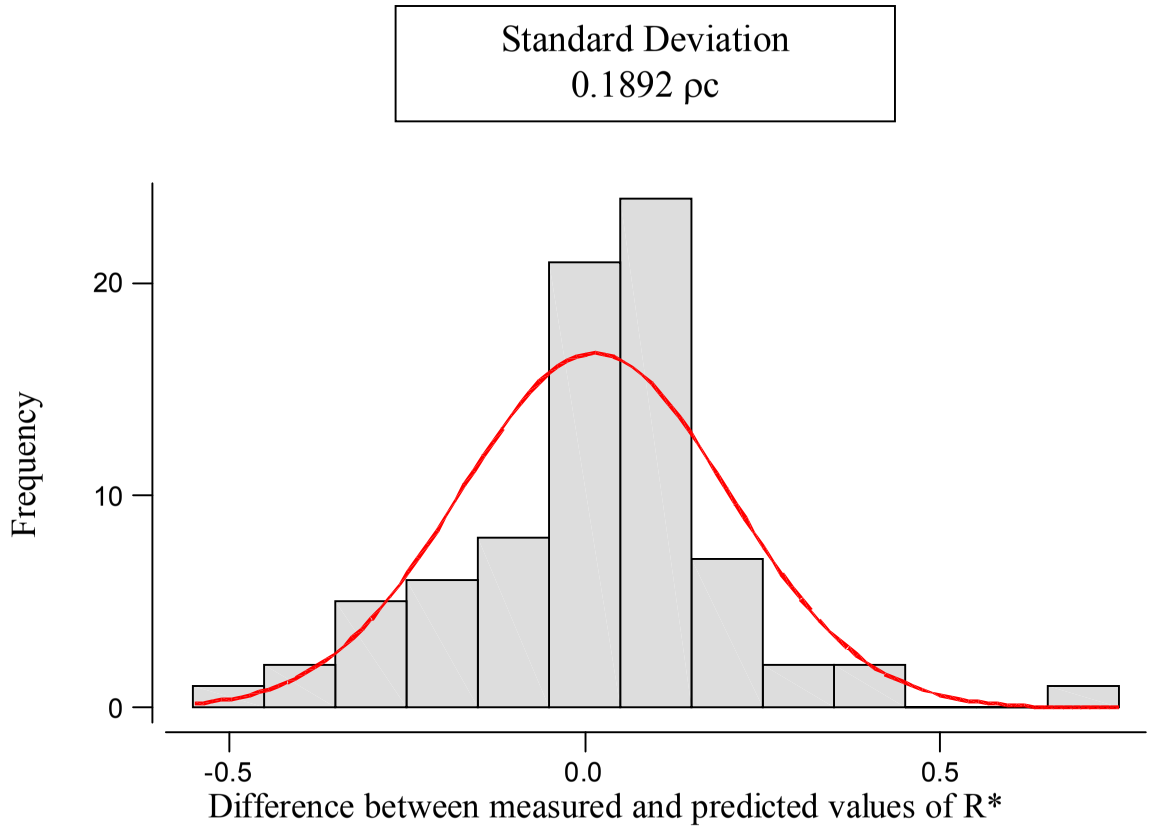

Figure 31b

Regression Analysis of the Predicted and the Measured Resistance (ρc) Data

Residuals Versus the Fitted Values

(response is Correlated)

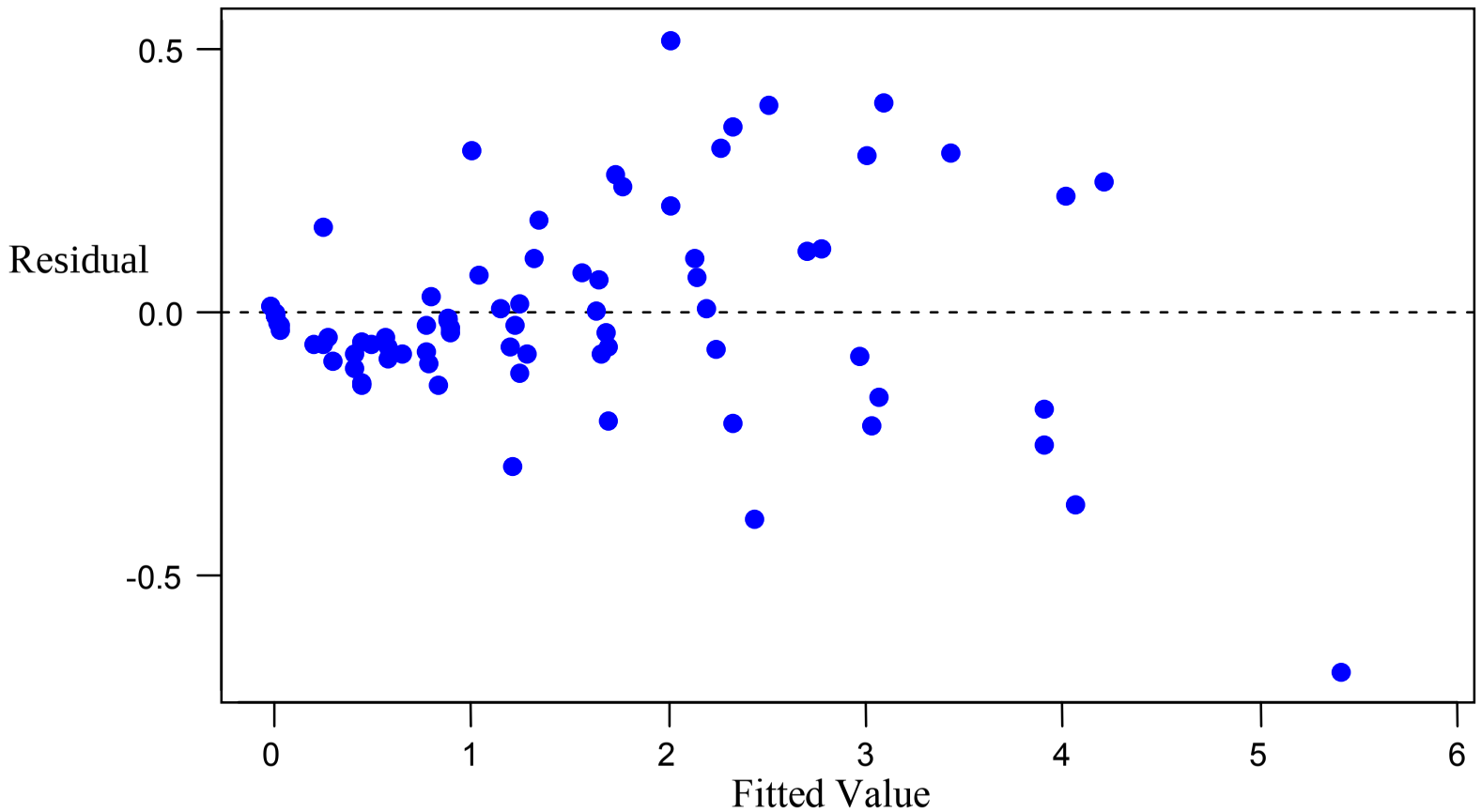

The regression equation is

Predicted Data = - 0.0146 + 1.00 Measured Data

Figure 32

Comparison of the Predicted and the Measured Flow Resistance Data from Tests on the Composite Liner from B. F. Goodrich (BFG) and from GE Albuquerque.

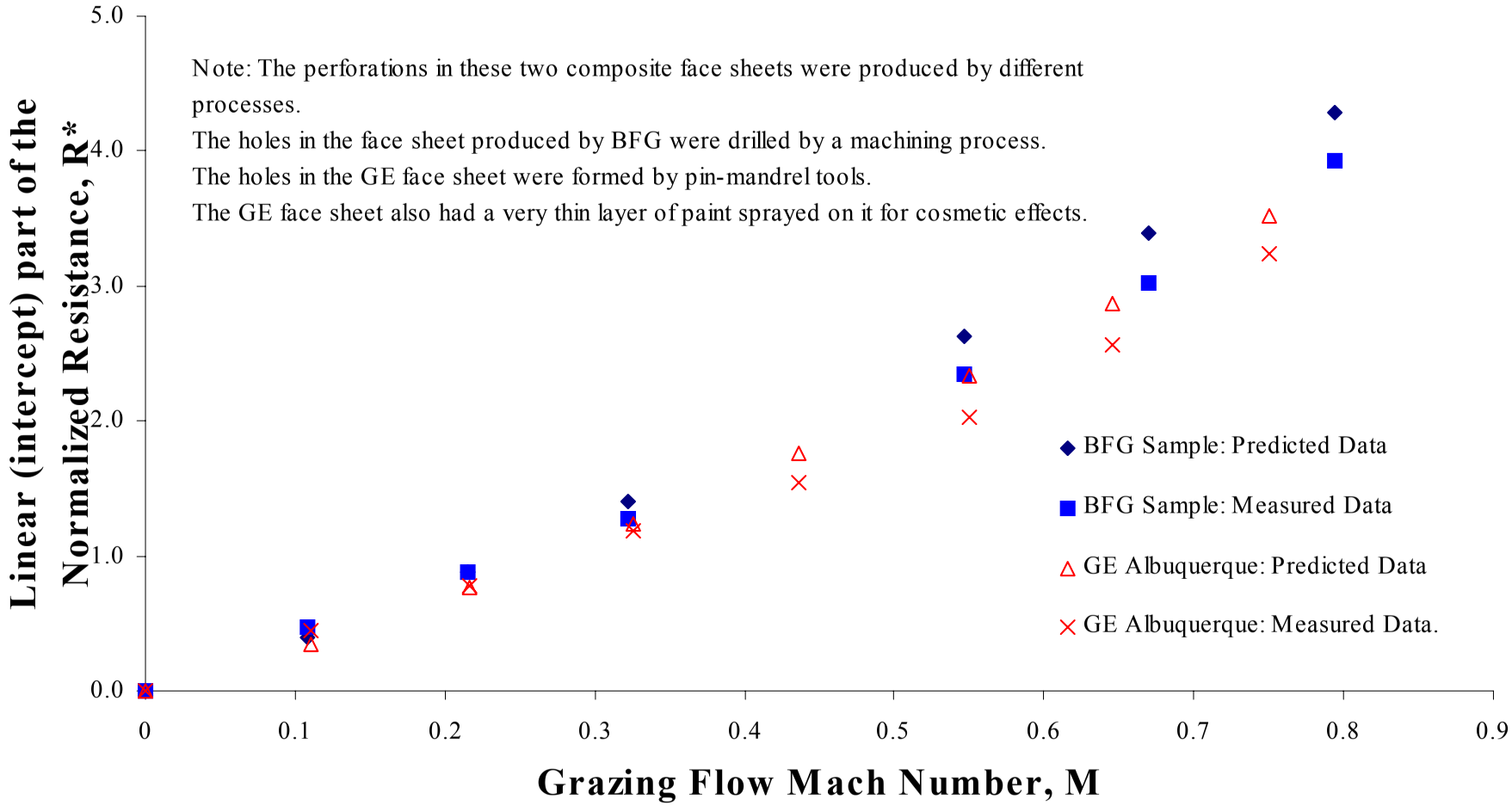

Figure 33
Comparison of the Predicted and the Measured Flow Resistance Data from Tests on the Composite Liner from Middle River Aircraft Systems.

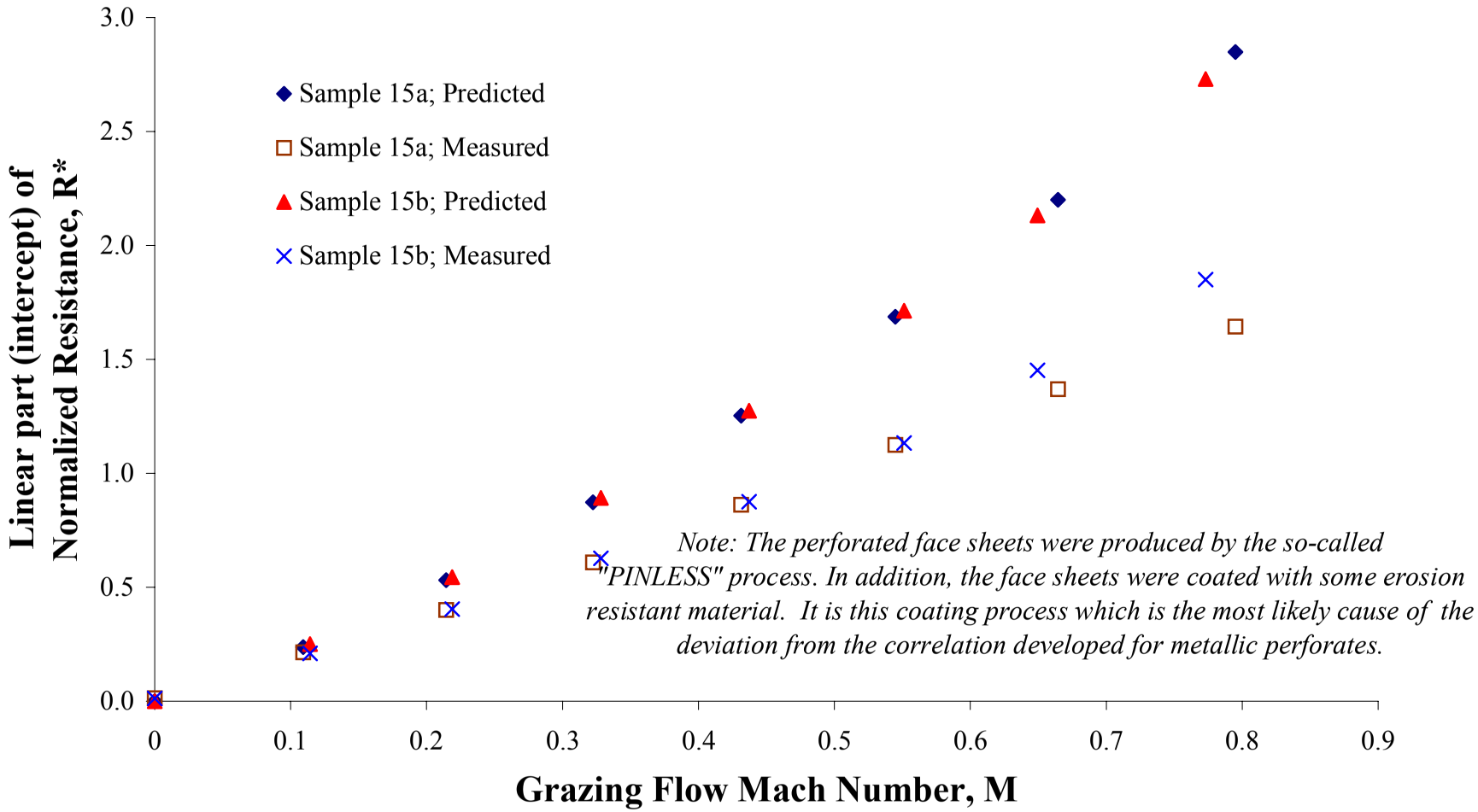

Figure 34
The Sensitivity to (u/c) with increasing values of the Grazing Flow Mach Number.
The Plots are for the Metallic Perforated Face Sheet Sample #1.

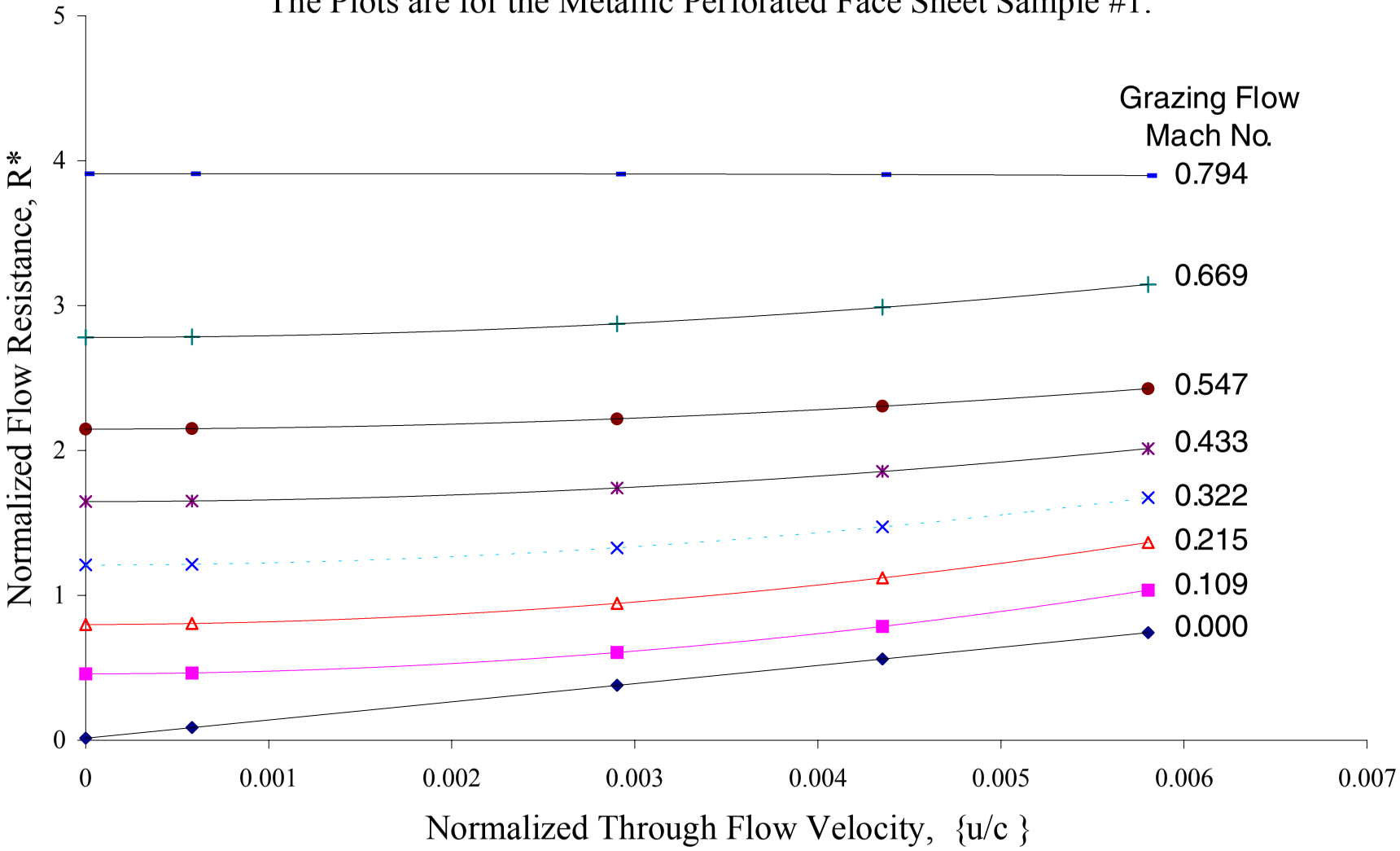

Figure 35
Boundary Layer Thickness Data at Nominal Flow Mach Numbers of 0.3 and 0.5.

Sample Number	Mach Number	δ^* (inch)	θ (inch)	Hole-diameter (inch)
2	0.323	0.060	0.047	0.038
3	0.288	0.050	0.041	0.038
5	0.320	0.055	0.044	0.090
6	0.320	0.060	0.048	0.048
7	0.321	0.065	0.052	0.048
9	0.326	0.065	0.052	0.038
12	0.288	0.044	0.036	0.065
13	0.323	0.062	0.050	0.048
14	0.324	0.060	0.048	0.054
15	0.326	0.060	0.048	0.040
2	0.545	0.058	0.047	0.038
5	0.544	0.057	0.046	0.090
6	0.546	0.059	0.047	0.048
7	0.545	0.059	0.048	0.048
9	0.543	0.059	0.047	0.038
12	0.485	0.052	0.043	0.065
13	0.549	0.059	0.048	0.048
14	0.552	0.054	0.043	0.054
15	0.552	0.059	0.047	0.040

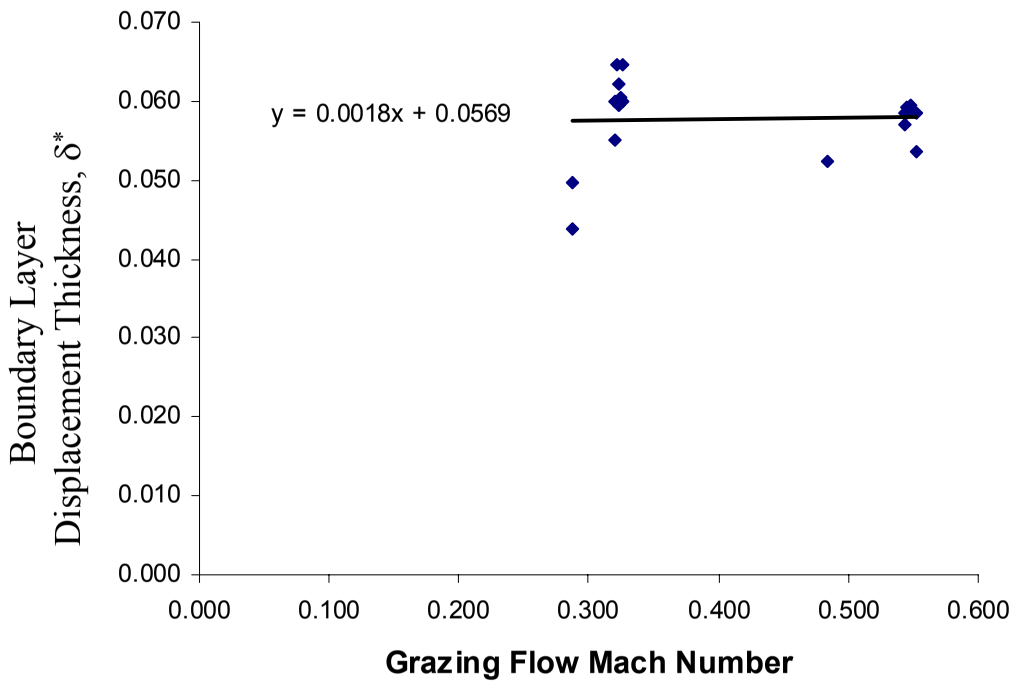

δ^* is the Boundary Layer Displacement Thickness
θ is the Boundary Layer Momentum Thickness

Figure 36
The Effects of the Boundary Layer Displacement Thickness on the Linear Part (intercept) of Normalized Resistance.

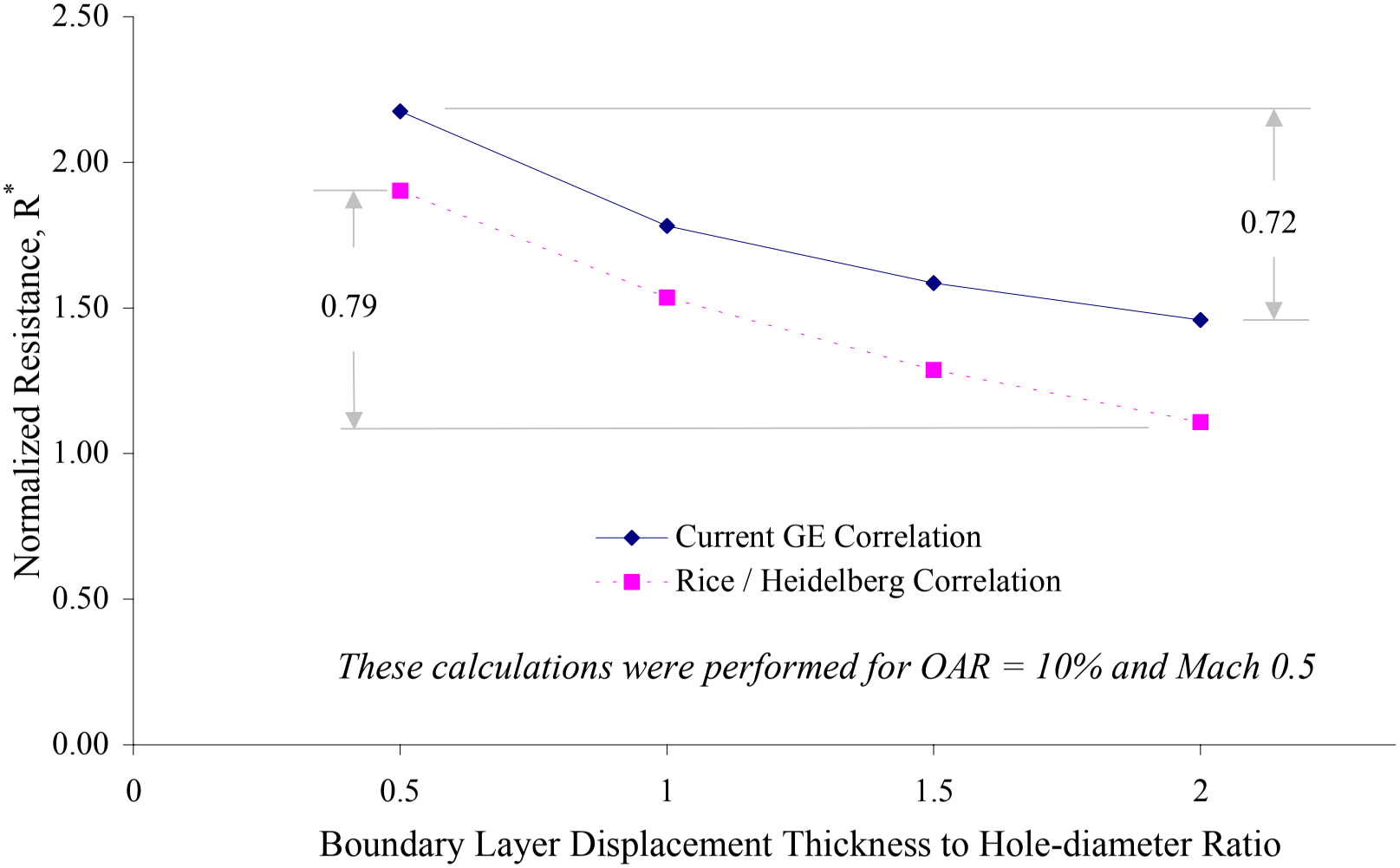

Figure 37

The Effects of changes in the Boundary Layer Displacement Thickness at Different Flow Mach Number Values

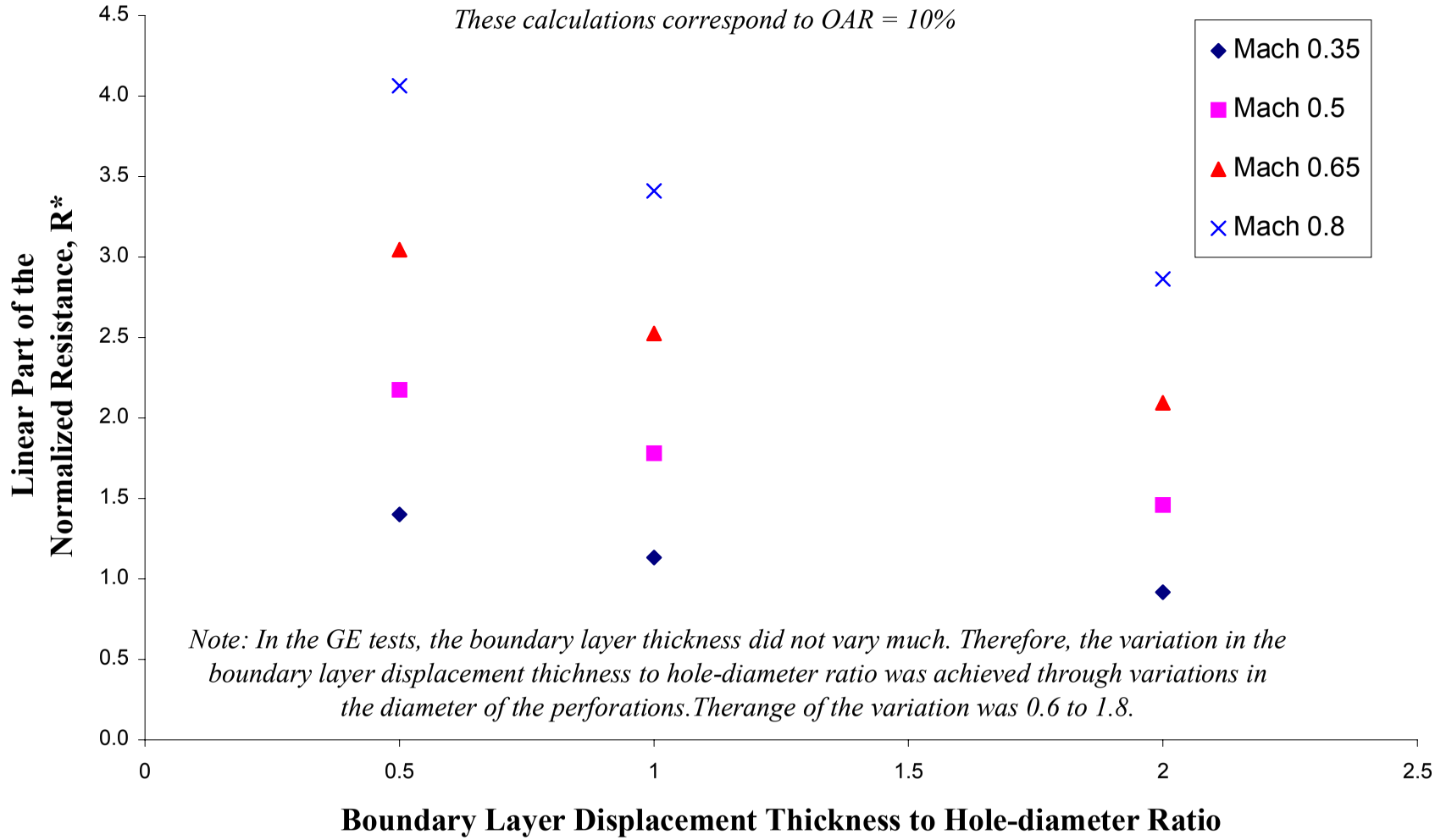

Figure 38
Comparison of the current GE Correlation with that of Rice / Heidelberg[2]

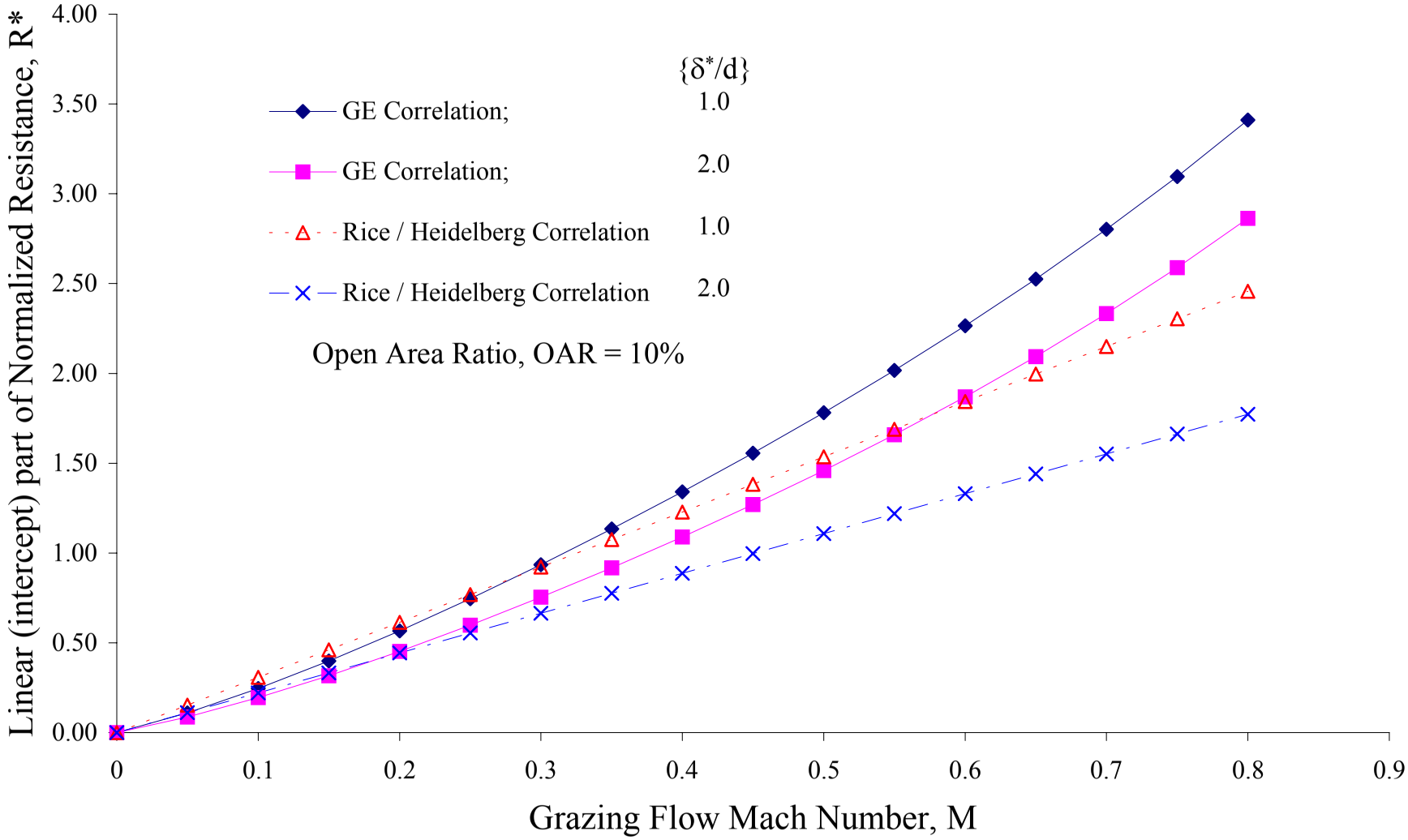

Figure 39
Flow Resistance Data Measured on a "Wiremesh-on-Perforate" type
Linear Face Sheet Material.

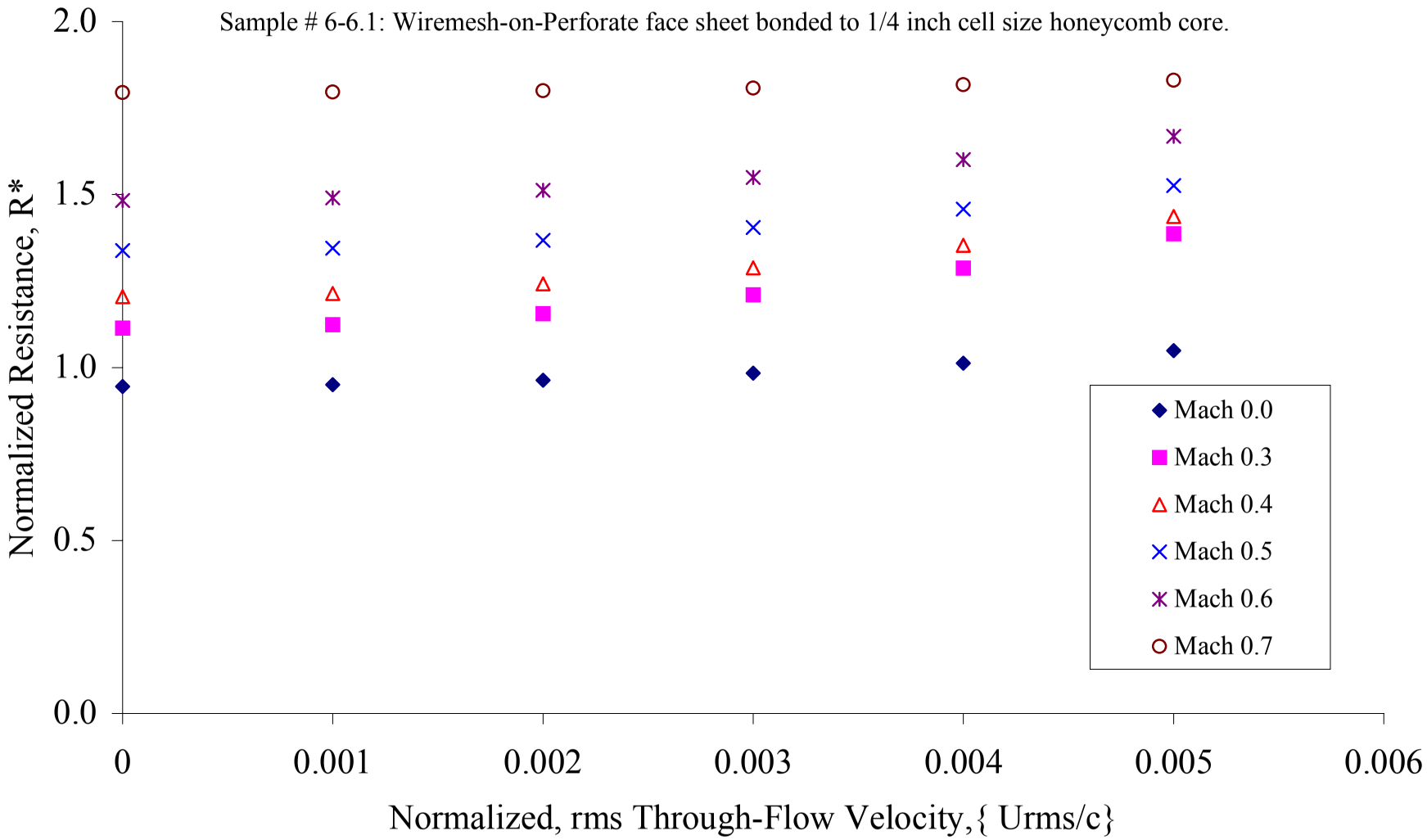

Figure 40
Flow Resistance Data Measured on a "Wiremesh-on-Perforate" type Linear Face Sheet Material.

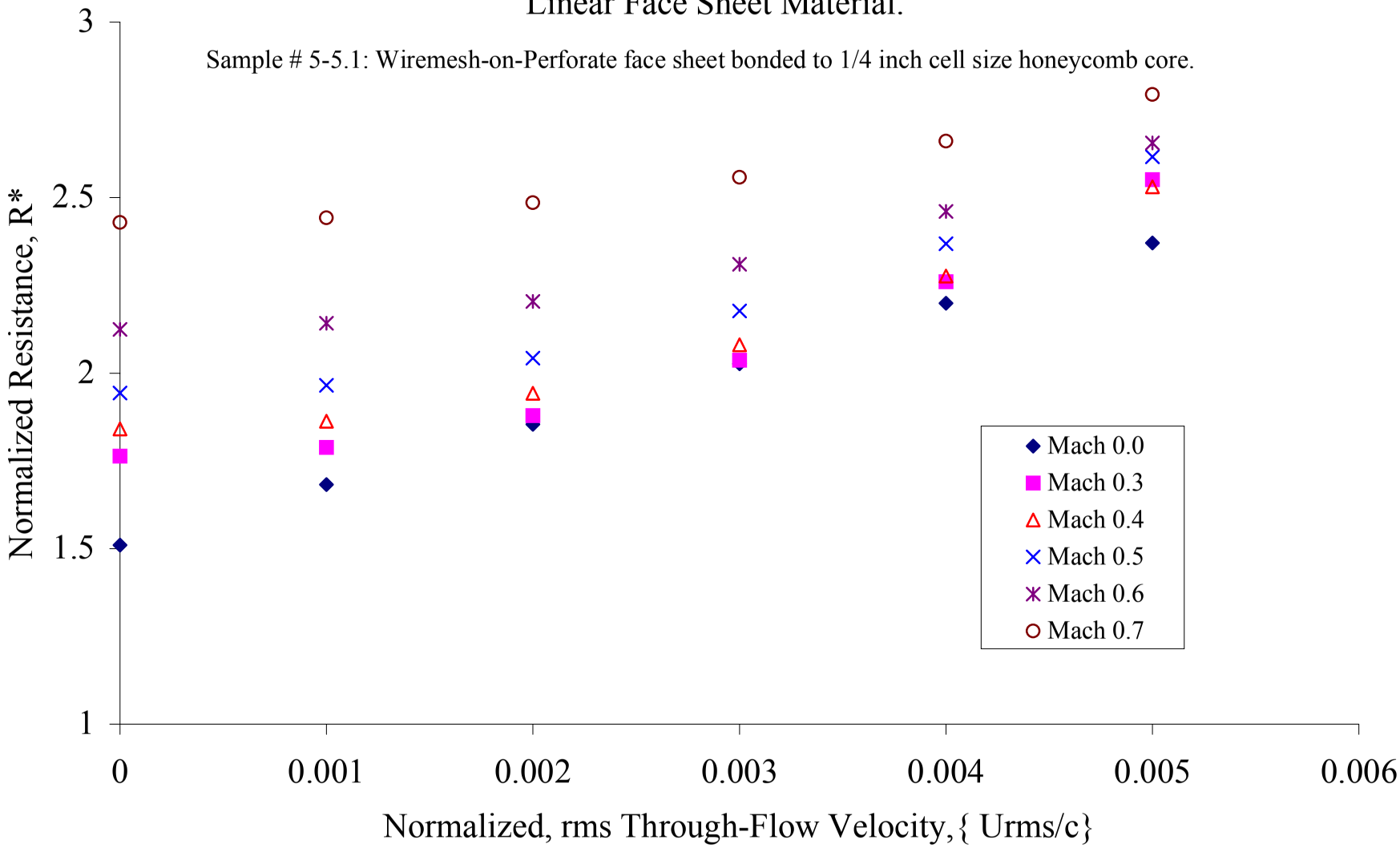

Figure 41
Flow Resistance Data Measured on a "Wiremesh-on-Perforate" type
Linear Face Sheet Material.

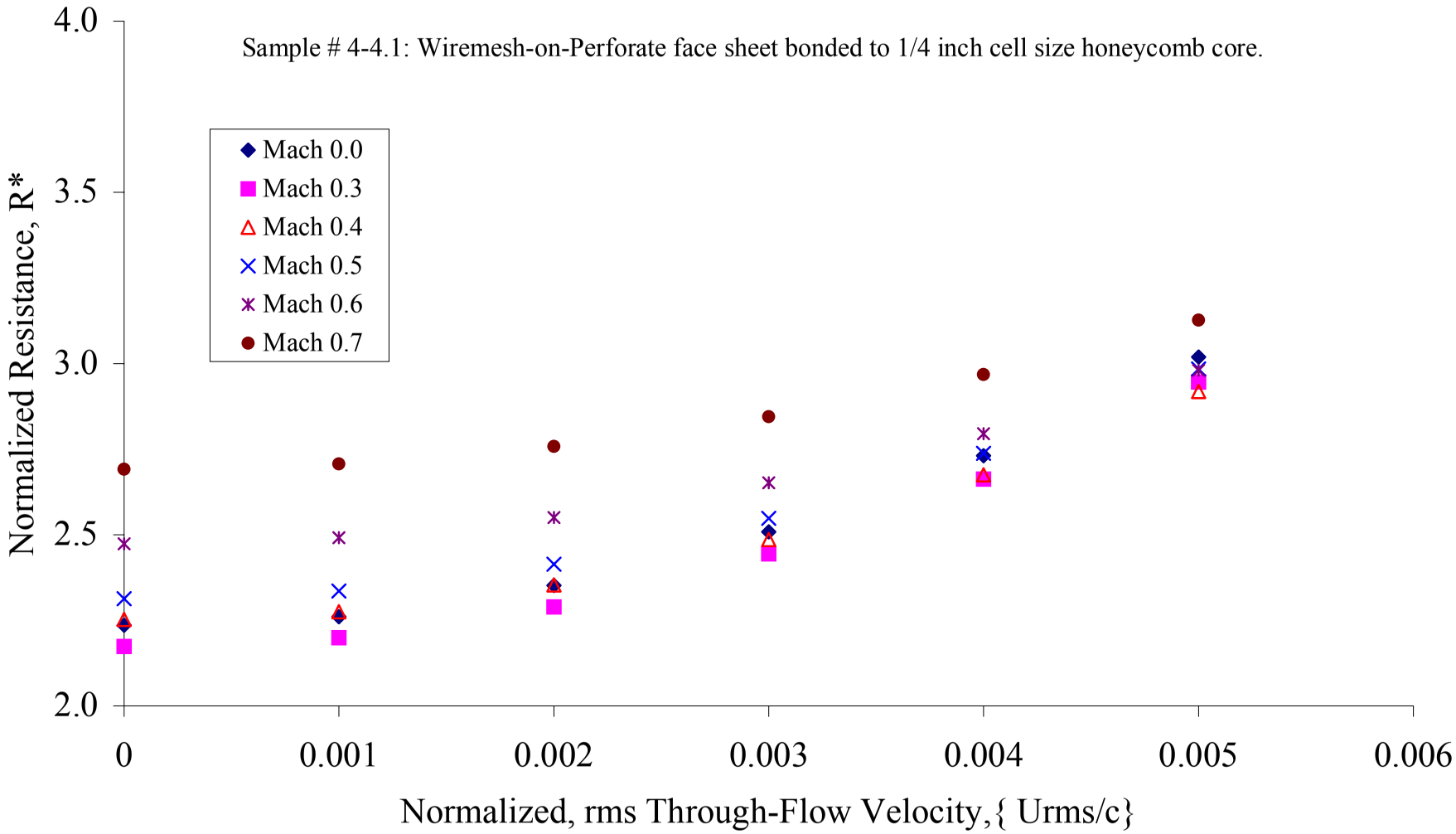

Figure 42
Flow Resistance Data Measured on a "Wiremesh Only" type Linear Face Sheet Material.

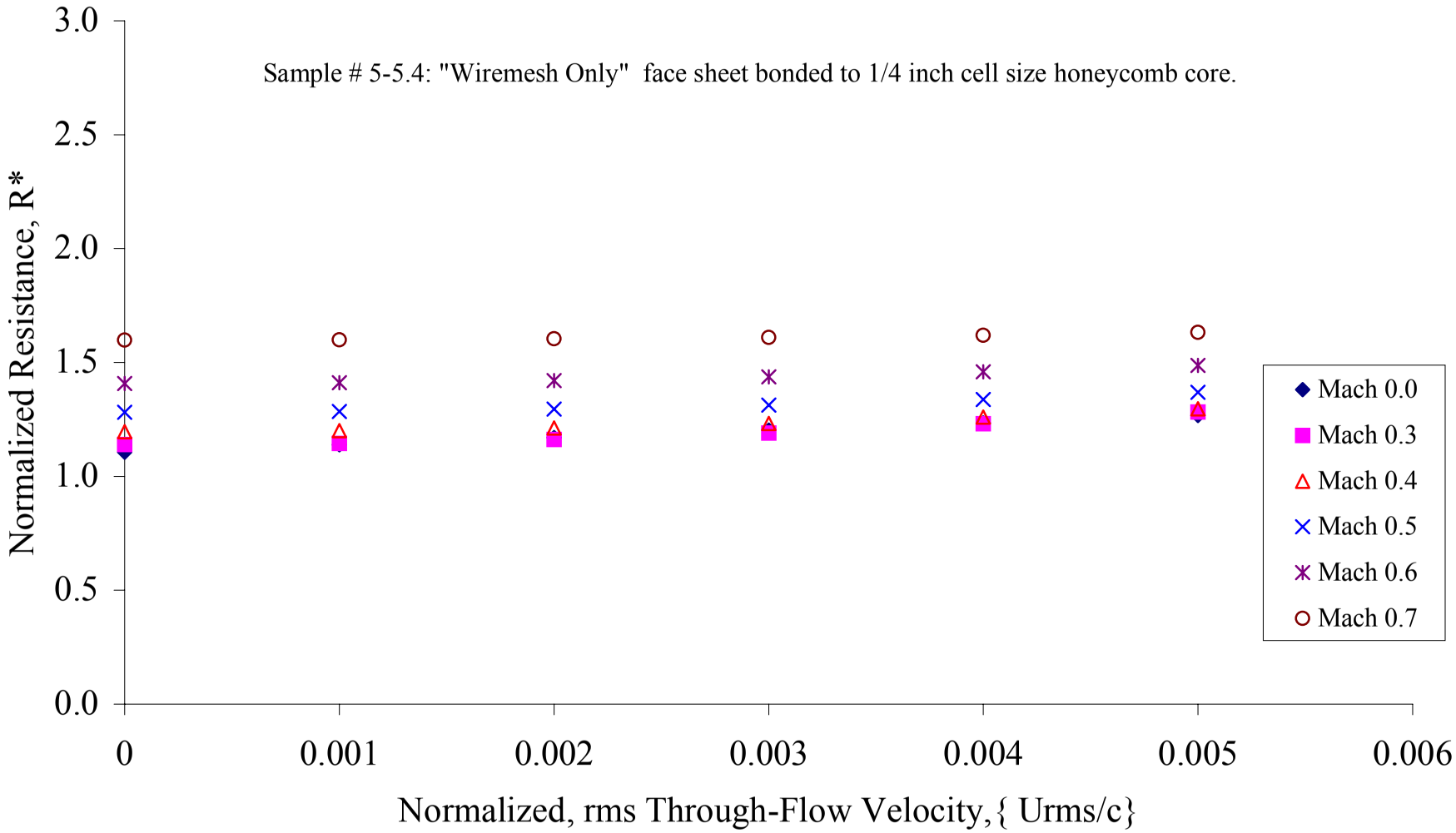

Figure 43
Flow Resistance Data Measured on a "Wiremesh Only"
type Linear Face Sheet Material.

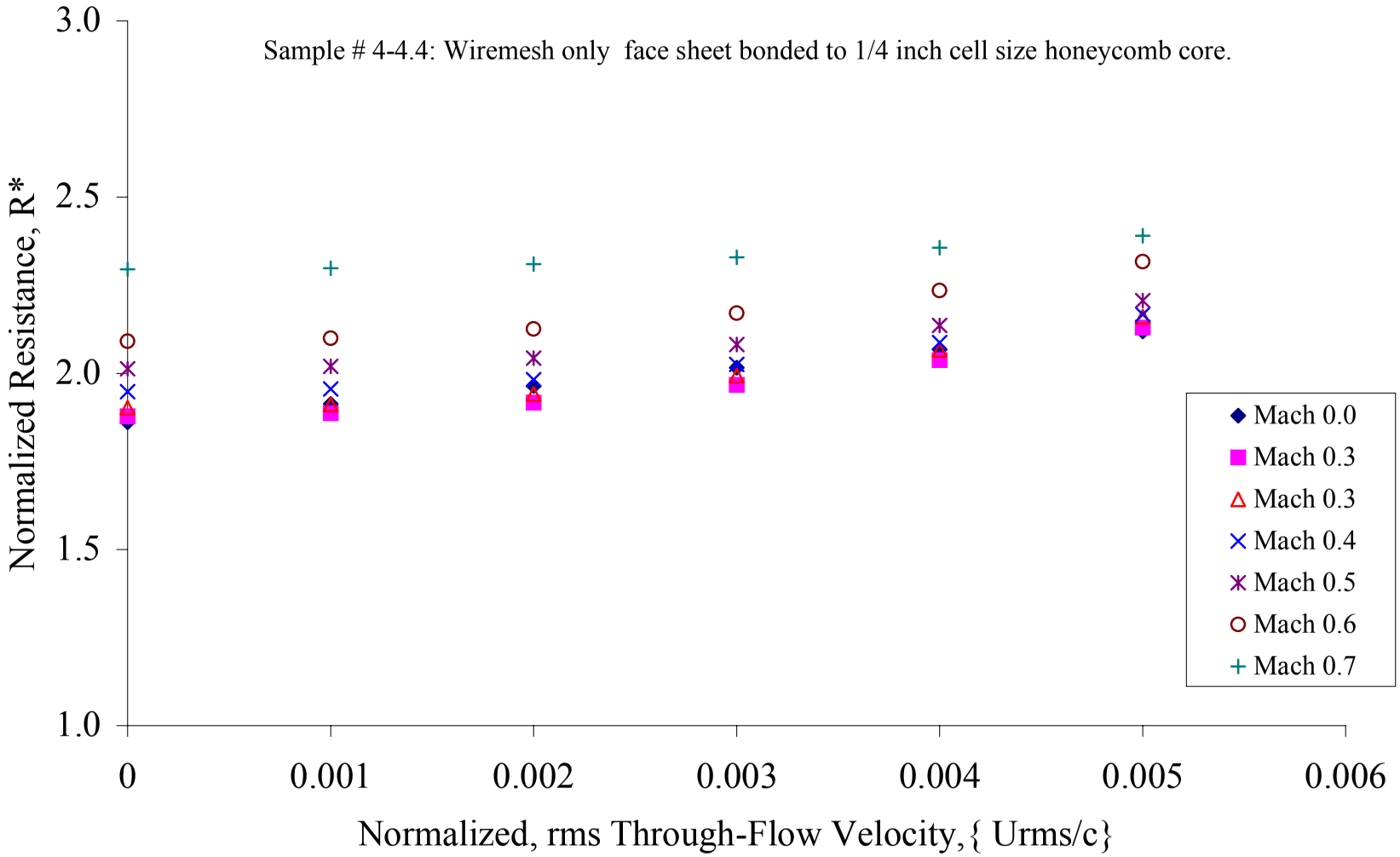

Figure 44
The Effects of Grazing Flow on the Normalized Resistance of Wiremesh Type Linear Face Sheet Materials.

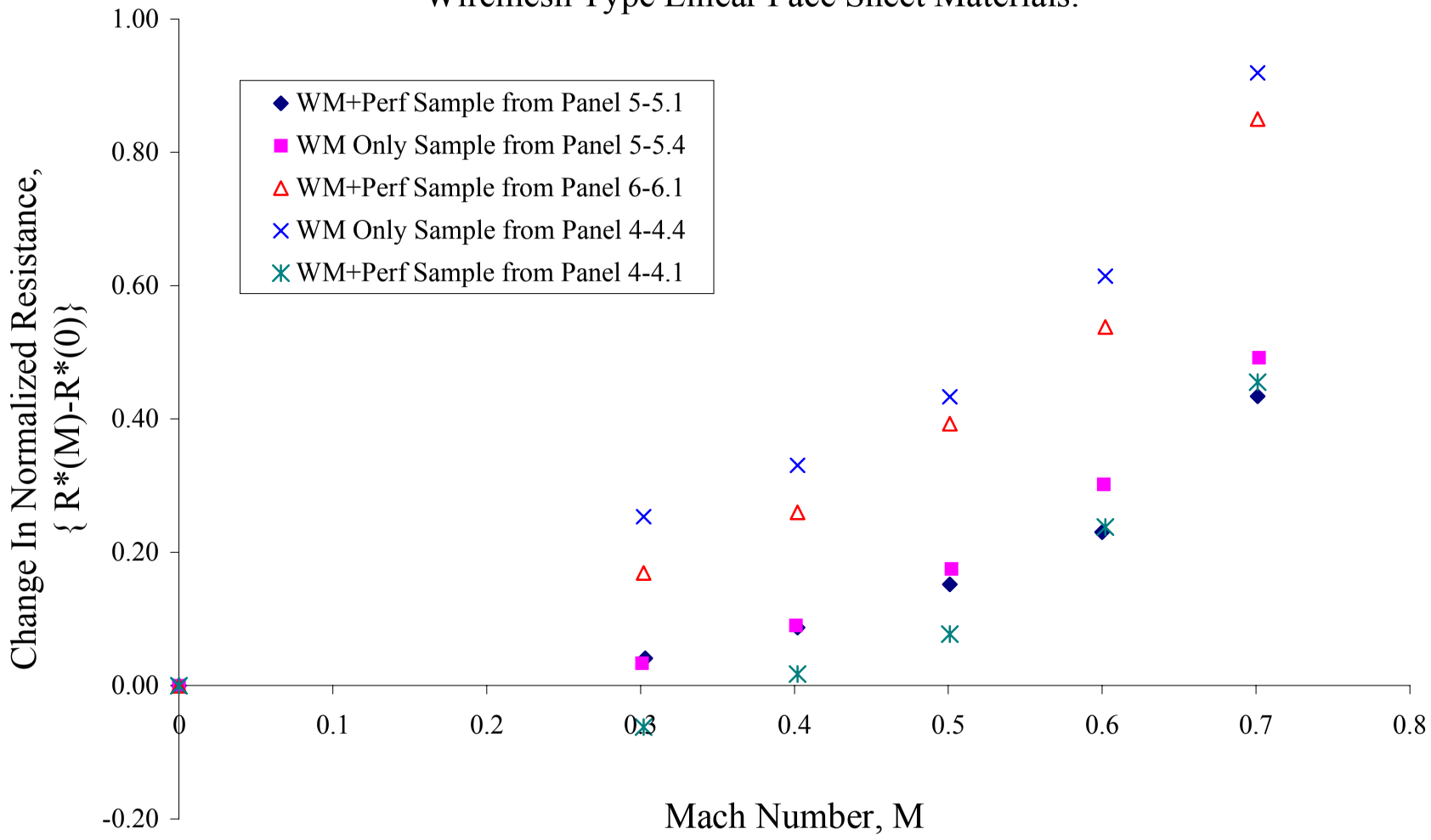

NASA Contract NAS3-98004 Task Order 3

Semi-empirical Acoustic Impedance Model Worked Performed by B. F. Goodrich

by

Jia Yu, H. W. Kwan, and Eugene Chien
B. F. Goodrich Aerospace
Aerostructures Group
Chula Vista, California.

BFGoodrich Semi-empirical Acoustic Impedance Model

General Impedance Model

The impedance model used for perforate plates is derived from BFGA/AG empirical data and is well-established in open literature.[1,2,3] The basic equation can be expressed as follows:

$$Z/\rho c = R + jX$$

$$= R_o + R_{of} + S_r V_p + R_{cm}(V_{cm}) + j[X_m + S_m V_p + X_{em}(V_{cm}) - \cot(kh)] \quad \text{.....(1)}$$

where,

Z/ρc is a complex number representing normalized impedance
R is the normalized acoustic resistance
i is √**-1** (imaginary number)
X is the normalized acoustic reactance
ρ is the air density and ***c*** is the speed of sound
ρ***c*** is the characteristic impedance (unit: cgs- Rayl)
R_o is the frequency independent linear acoustic resistance
R_{of} is the frequency dependent linear acoustic resistance
S is the non-liner DC flow resistance slope
S_r is the non-linear acoustic resistance slope
V_p is the root-mean-square particle velocity over the entire frequency range in cm/sec
V_{cm} is the Mach number
$R_{cm}(V_{cm})$ is the acoustic resistance induced by grazing flow.
X_m is the mass reactance (including end correction)
S_m is the non-linear mass reactance slope
$X_{em}(V_{cm})$ is the non-linear mass reactance
X_c is the cavity reactance
k is the wave number per cm
d is the perforate plate hole diameter in inch
cot(kh) is the backing cavity reactance, h is cavity depth

Perforate Plate Impedance Model Parameters

Detailed parameters for perforate plate liners are described below:

$$Z_{of}/\rho c = (R_o + R_{of}) + i(X_m) = i\omega(t + \varepsilon d)/(c\sigma)]/F(k_s r) \quad \text{.....(2)}$$

where,

$$F(k_s r) = 1-\{2J_1 (k_s r) / [k_s rJ_0 (k_s r)]\} \quad (3)$$

$$k_s^2 = -i \omega\rho / \mu \quad (4)$$

$$S_r = \frac{1.0}{\rho c}\left(\frac{\rho}{2C_d^2}\frac{1-\sigma^2}{\sigma^2}\right) \quad (5)$$

For perforate plates at t/d≤1

$$S_r = \frac{1.336541}{\rho c}\left(\frac{\rho}{2C_d^2}\frac{1-\sigma^2}{\sigma^2}\right) \quad (6)$$

$$S_m = -.0.000631\frac{k}{\sigma^2} \quad (7)$$

$$C_d = 0.80695\sqrt{\sigma^{0.1} / e^{-0.5072(\frac{t}{d})}} \quad (8)$$

$$\varepsilon d = \frac{0.85kd(1-0.7\sqrt{\sigma})}{1+305(V_{cm})^3} \quad (9)$$

$$R_{cm} = \frac{V_{cm}}{\sigma(2+1.256\frac{\delta^*}{d})} \quad (10)$$

where,

t is the perforate plate thickness in inches
f is the acoustic frequency in Hz
σ is the perforate plate open area ratio
c is the in-duct speed of sound in cm/sec
ω is the angular velocity cm/sec (ω=*kc*)
μ is the coefficient of viscosity in gm/cm-sec
ε ***d*** *is* the effective Mass end correction
$\boldsymbol{K_s}$ is the wave-number of the viscous Stokes wave
r is the perforate plate hole radius
C_d is the discharge coefficient
δ* is displacement boundary layer thickness in inch

TESTING AND VALIDATION

Acoustic Testing

In this part of the study, various laboratory tests were conducted to evaluate liner acoustic properties and to validate advanced treatment impedance models discussed previously. These laboratory tests included DC flow resistance measurements, normal incidence impedance measurements, DC flow and impedance measurements in the presence of grazing flow, and in-duct liner attenuation as well as modal measurements. In this paper, the DC flow resistance measurement data and normal incidence impedance test results are discussed.

The DC flow resistance measurements were conducted at airflow rates of 30, 60, 105, 150, and 200 cm/sec. All the data were normalized to reference ambient conditions (70 °F and 29.92" Hg). The first order least squares curve fit was used to generate required data including intercept, slope, R(105), and NLF. The R(105) is DC flow resistance data at 105 cm/sec and the NLF, which is referred as non-linear factor, is the ratio of resistance data at 200 cm/sec to data at 20 cm/sec (R(200)/R(20)).

A 3-cm diameter 8 Hz bandwidth sound impedance measurement system was used to perform liner normal incidence impedance measurements.

A two-microphone technique and random noise signal are used in all normal incidence impedance measurements. Figure 1 shows impedance measurement set-up for single degree of freedom liner measurement. The Left-hand side is a sketch and the right-hand side is a photo.

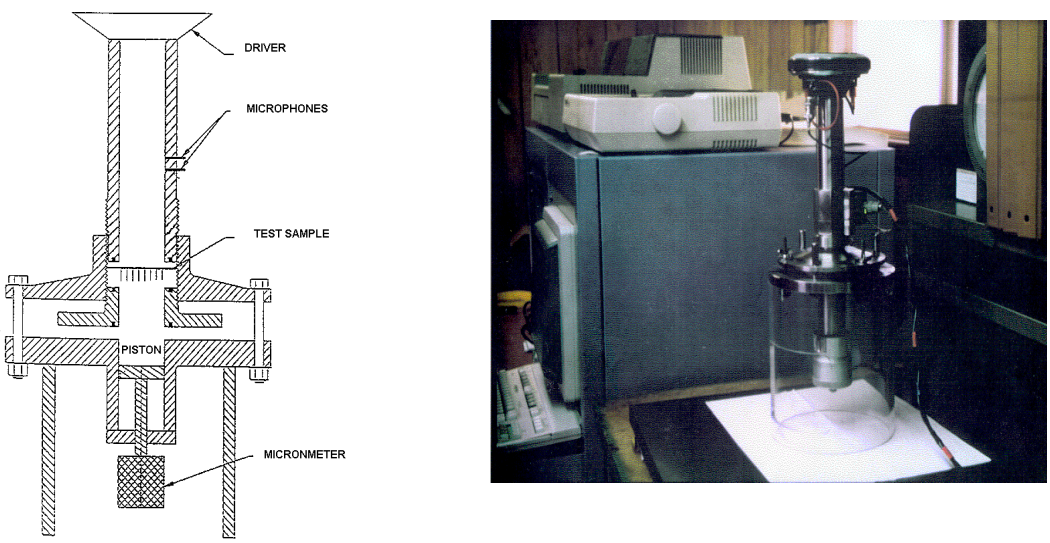

Figure 1 Impedance measurement set-up for single degree of freedom liner measurement. (Left-hand side is a sketch and right-hand side is a photo)

Validation of Semi-empirical Model

Validation of the advanced treatment impedance models without grazing flow present was accomplished through the use of DC flow and normal incidence acoustic impedance

measurements. The study indicates that the theoretical impedance model described previously can precisely predict acoustic impedance for perforate plate acoustic treatment. The success of the semi-empirical model is based on several key items:

1. Effective POA and effective hole diameter values obtained from DC flow resistance data are used as input parameters for impedance calculations.
2. An exact solution is used to solve Crandall's Equation.
3. Non-linear behavior is applied to both resistance and reactance data. The non-linear slope constants are determined empirically.
4. The perforate plate thickness to hole diameter ratio must be less than one ($t/d \leq 1$) for both full- and sub-scale liners to maintain a predictable discharge coefficient.
5. DC flow resistance data is used as an input parameter to calculate linear liner impedance.

Effective POA and Hole Diameter

Using the DC flow resistance data that averages entry side and exit side data as well as the plate thickness and average hole spacing (center to center) measurements, one can easily calculate effective POA and effective hole diameter for an unbonded perforated skin. The same approach is not suitable for bonded acoustic panels because accurate DC flow measurements can only be performed from the unbonded perforated plate surface. A modified measurement technique derived from Rohr's empirical data base was used to determine the effective POA and hole diameter on bonded panels.

The basic equation used for effective POA and hole diameter calculation can be derived from Pousielle approximate model.

$$R(V) = R(0) + S \cdot V = 32\,\mu\, t/(\sigma\, d^2) + S \cdot V \quad \text{.....} (11)$$

where S is the slope of the velocity-dependent term and V is the DC-flow velocity. The relationship between open area ratio, σ, and average hole diameter, d, can be determined by the perforate hole pattern. It can be expressed as

$$\sigma = \pi \frac{(d/2)^2}{S_p^2} \quad \text{.....} (12)$$

where S_p is the hole spacing (center to center) and can be defined by using an average measurement value. Use of a measured DC flow resistance value, plate thickness, and average hole spacing, one can easily calculate effective POA and hole diameter from Equations (11) and (12).

Test Matrix:

Table1 is matrix of proposed acoustic treatment panels with perforated face sheets for impedance measurements under grazing flow conditions.

Table 1

No.	Candidates	Initial Open Area Ratio (POA)*	Availability	Hole Diameter ¥ ***d*** (inch)	Plate thickness ***t*** (inch)	Core Depth (GE/NASA) ***h*** (inch)
1	Base liner	8.7	Yes	.039	.025	1.5/1.5
2	Min **POA**	6.4	Yes	.039	.025	1.5/1.5
3	Max **POA**	15	Yes	.039	.025	1.5/1.5
4	Min ***d***	13.2	yes	.039	.025	1.5/1.5
5	Max ***d***	13.0	yes	.093	.032	1.5/1.5
6	Min ***t***	7.3	Yes	0.05	.02	1.5/1.5
7	Max ***t***	7.3	Yes	0.05	.04	1.5/1.5
8	Min ***h***	8.7	Yes	.039	.025	0.75/3
9	Max ***h***	8.7	Yes	.039	.025	0.75/3
10	Special 1	10.5	Yes	.039	.028	1.5/1.5
11	Special 2	8.7	Yes	.050	.045	1.5/1.5
12	Composite	8.3	Yes	0.062	0.028	1.5/1.5
13	PU film	18/34	Yes	.062/0.005	.015/.032	1.5/1.5
14	GE (pin-mandrel)	9%	Yes	0.062	0.030	1.5 / 1.5
15	MRAS (pin-less)	9%	Yes	0.062	0.030	1.5 / 1.5

*Due to the tooling availability, the POA may be varied.
Also note that there is 7% blockage caused by the sheet reticulation process for bonding to the honeycomb.

¥ For all perforated sheets, $d/t \geq 1$ is required for punched aluminum perforate plate.
All the parameters as well as DC flow Resistance will be conducted before and after bonding NASA Panel 2”x 15.852” (frame required - see Figure 2); BFG/GEAE panel: 5.5”x 24” (see Figure 1).
Configuration 8 and 9 are the same; 9 was chosen to use.

DC Flow Resistance Data:

DC flow resistance data and geometrical definitions for 12 BFGA perforate samples are contained in the Excel file DC-resis-data.xls.[1]

Normal Incidence Impedance Data

Normal incidence impedance data (measured and predicted) for 12 BFGA perforate samples and 1 PU film sample are contained in the Excel file NM-Imp-data.xls.[1] The data include two core depths. One is 1.5 inch (sample R801 to R813) and the other is 0.75 inch (Samples R901 to R913).

Flow Duct Insertion Loss Data

Flow duct insertion loss data for 12 BFGA perforate samples, 1 PU film sample, 3 DynaRohr samples, and 3 GEAE composite samples are contained in the Excel file insertion-loss-data.xls.[1] The definitions of DynaRohr samples (#16, 17, & 18) are listed in the file DC-rersis-data.xls second sheet. The sample # 19 is provided by GEAE and the POA is unknown.

Grazing Flow Impedance

Three sets of flow duct insertion loss data were used to indirectly assess the perforate liner impedance mode with the grazing flow. DynaRohr panel #17 was selected as a reference panel to estimate in-duct modal distribution at various grazing flow Mach numbers. Based on estimated modal distribution. The measurement data for perforate panels #1 and #3 were used to compare with the prediction result at the Mach number 0.3 and 0.5. It shows reasonable agreement between prediction and measurement on the test sample #1 (8.2 POA) except. However, at the frequency with peak attenuation, the prediction is under estimate at 0.3 M number and slight over calculated at 0.5 M. The data points at 5000 Hz are ignored because the cavity reactance –cotan(kh) term is near the unstable condition. For the test sample #3, it is over predicted at peak frequency for 0.3 M. However, it is well under predicted at peak frequency region (1250 to 2000 Hz) for 0.5 M. The under prediction can be contributed to the high aerodynamic noise generated by the grazing flow. In general, the results indicate that the semi-empirical model seems working reasonable to handle grazing flow conditions but further refinement is definitely required. All the test data are included in the reference [1].

Reference

Data files generated in this study are archived on a CDROM entitled "Perforated Sheet Study Data - 2001." Individual files include "att-data.xls", "DC-resis-data.xls", "Dyna17-att.xls", "impedance data.doc", "NM-imp-data.xls" and "Perf1&3-att.xls."

NASA Contract NAS3-98004 Task Order 3

Acoustic Treatment Design Technology

The Procedure for Computing and Normalizing DC Flow Resistance Data

By

Asif A. Syed
Aero Technology Laboratories
GE Aircraft Engines
1 Neumann Way
Cincinnati, OH 45215

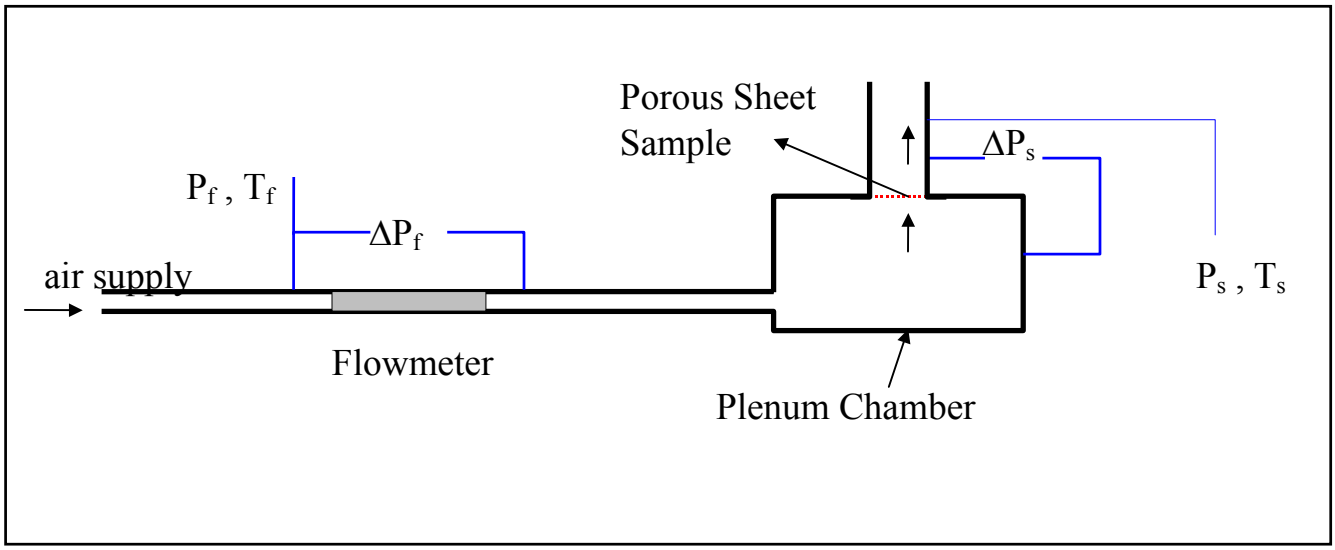

<u>Schematic Diagram of a typical apparatus for the measurement of DC Flow Resistance of porous materials.</u>

P_0 = 14.695 psia (29.92 In. of Hg. At 39° F) ; reference pressure
T_0 = 530° R (70° F) ; the reference temperature

<u>The above values of the reference Temperature and Pressure are to be used for normalizing all DC flow resistance data.</u>

The Meriam Flow Meter gives a volume flow rate, CFM (cubic feet per minute), corresponding to the pressure drop, as follows

$$CFM = B \times (\Delta P_f) + C \times (\Delta P_f)^2 \qquad \ldots\ldots\ldots\ldots \qquad (1)$$

where the constants B and C are obtained from the calibration chart of the flow meter.

V_{fo} = Volume flow rate (SCFM) based on Flowmeter calibration and measured ΔP_f - corresponds to the reference pressure and temperature, P_0 & T_0 .

$$V_{fo} = SCFM = CFM \times \{(P_f / P_0)(T_0 / T_f)^{0.75}\} \qquad \ldots\ldots\ldots \qquad (2)$$

V_f = Actual volume flow rate (ACFM) at Temperature T_f and Pressure P_f measured at the inlet to the Flowmeter

$$V_f = CFM \times (T_0 / T_f)^{0.75} \qquad \ldots\ldots\ldots\ldots \qquad (3)$$

m = mass flow rate = $\{\rho_f V_f\} = \rho_f \{CFM \times (T_0 / T_f)^{0.75}\}$ ….. (4)

U_s = Flow Velocity, into the test sample corresponding to Pressure P_s and Temperature T_s (°R)

$= \{m/(A\rho_s)\} = \{\rho_f/(A\rho_s)\} \{CFM \times (T_0 / T_f)^{0.75}\}$

$U_s = \{CFM/A\} \{(P_f / P_s)) (T_s / T_f) (T_0 / T_f)^{0.75}\}$ ……(5)

where A is the area of the test samples.

U_{s0} = Flow Velocity into the test sample corresponding to Pressure P_0 and Temperature T_0 (°R) at the test sample
$= (U_s)(\rho_s/\rho_0)(\mu_0/\mu_s)$ …. *[based on the equality of Reynolds number]*

$U_{s0} = \{CFM/A\} \{(P_f / P_s)(T_s / T_f)(T_0 / T_f)^{0.75}\} \{(P_s / P_0)(T_0 / T_s)^{1.75}\}$

$U_{s0} = \{CFM/A\} (P_f / P_0)(T_0 / T_f)^{2.5}$ …….…..... (5)

R_s = The DC Flow Resistance = $\Delta P_s / U_s$
$= \Delta P_s / [\{CFM/A\} \{(P_f / P_s)(T_s / T_f)(T_0 / T_f)^{0.75}\}]$

$= [\Delta P_s / \{CFM/A\}] \{(P_s / P_f)(T_f / T_0)^{0.75}\}$ …….....…. (6)

$R_{s0} = R_s (\mu_0 / \mu_s) = [\Delta P_s / \{CFM/A\}] (P_s / P_f)$ ….....…. (7)

Note that in equations (5), (6) & (7), it is assumed that $T_s = T_f$.

The rationale behind the normalization of the measured DC flow data of equations (5) and (7) to a reference temperature and pressure, is based on the principle of dynamical similarity. This was explained in detail in a technical paper by Motsinger, Syed and Manley [1].

DC flow data (R_{s0} & U_{s0}) are expressed in c.g.s units. The Volume Flow rate, CFM, as measured by a Meriam flow meter is expressed in cubic feet per minute. This has to be converted into cubic centimeter per second. The area, **A**, is input as square inches. It has to be converted into square centimeters. Finally, the pressure drop, ΔP_s, across he sample is measured in inches of water at 4°C. This has to be converted into Dynes/(sq.cm.). Therefore the above equations with the conversion factors are as follows

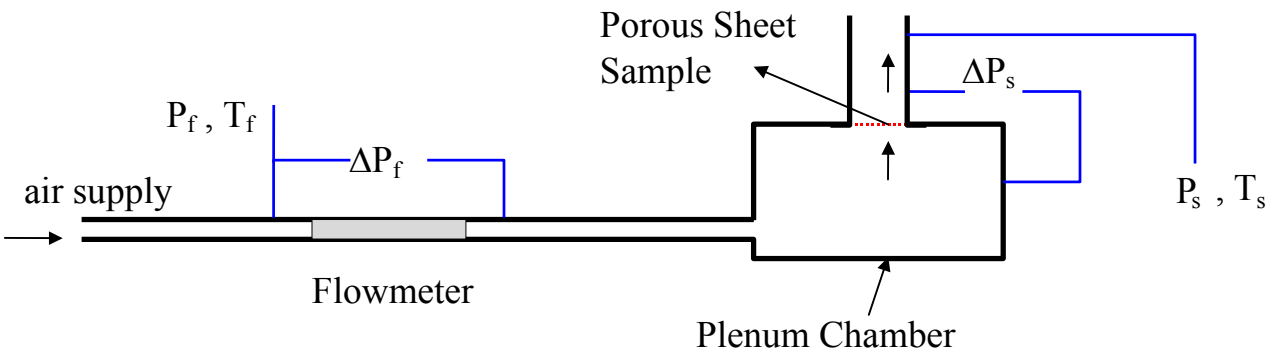

$CFM = B \times (\Delta P_f) + C \times (\Delta P_f)^2$	…….	flow rate (Cubic Feet per Minute)
$U_{s0} = 73.151 \{CFM/A\} (P_f / P_0)(T_0 / T_f)^{2.5}$	……	assumes $T_s = T_f$
$R_{s0} = 34.0504 [\Delta P_s/\{CFM/A\}] (P_s / P_f)$	……	assumes $T_s = T_f$

Note:- The temperatures T_f and T_0 must be expressed in degrees R.

P_0 = 14.695 psia (29.92 In. of Hg. At 39° F) ; reference pressure
T_0 = 530° R (70° F) ; the reference temperature
A = area of the sample (square inches) is known

Measured Data → | ← **Computed Data**

P_s	ΔP_s	P_f	ΔP_f	T_f	**CFM**	**(CFM/A)**	ΔP_s**/(CFM/A)**	U_{s0}	R_{s0}
psia	inches H_2O	psia	inches H_2O	°R	Feet^3/ min			cm/s	cgs Rayl

A number of measurements are made. The data are then used to obtain, by linear regression, a correlation of the form

$$R_{s0} = a + b\, U_{s0} \qquad \ldots\ldots\ldots\ldots \qquad (8)$$

where a and b are constants (determined by linear regression).

For Metallic Perforated sheet materials [2 & 3], the **effective porosity** is determined, by an iterative process, as follows:

$C_d = 0.80695 \sqrt{\{\sigma^{0.1} / \exp(-.5072t/d)\}}$ ……. (9)

$b = \{\rho_0/(2\, C_d^2)\}\ \{(1-\sigma^2)/\sigma^2\}$ …….. (10)

where t is the thickness, d is the hole diameter of the perforated sheet, σ is the effective porosity (a fraction <1.0), ρ_0 is the density of air at the reference values of temperature and pressure, and C_d is the discharge coefficient for the perforated sheet material. *Note that ρ_0 = 0.0012 (gm/cc) for use in (10).*

If the spacing of the hole pattern is known, then an estimate of the hole diameter can also be obtained as follows:

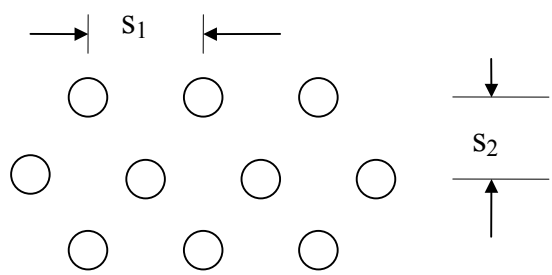

The porosity of the hole pattern is given by

$\sigma = \pi d^2 / (4\, s_1 s_2)$

Therefore, the effective diameter of the hole pattern is given by

$d = \sqrt{[(4\, s_1 s_2\, \sigma)/\pi]}$ ……. (11)

It is also assumed that the thickness, t, of the face sheet, after all processes, is known.

Equations (9) and (10) can be solved using an iterative approach, to obtain the effective porosity and hole diameter. The following iterative process is used to compute the values of σ and d.

1. Assume $C_d = 0.76$, and $t/d = 0.3$ (say)
2. Compute σ from equation (10) and d from equation (11). Compute new value of (t/d) .
3. Compute new value of C_d from equation (9)

4. Repeat step 2. Compare new value of σ with its previous value. If the difference is insignificant (<1%), then stop the iteration. Otherwise repeat steps and 3 and 2.

The process map for the iterative computations described above is shown below. An example of this method is illustrated in FIGURE 1.

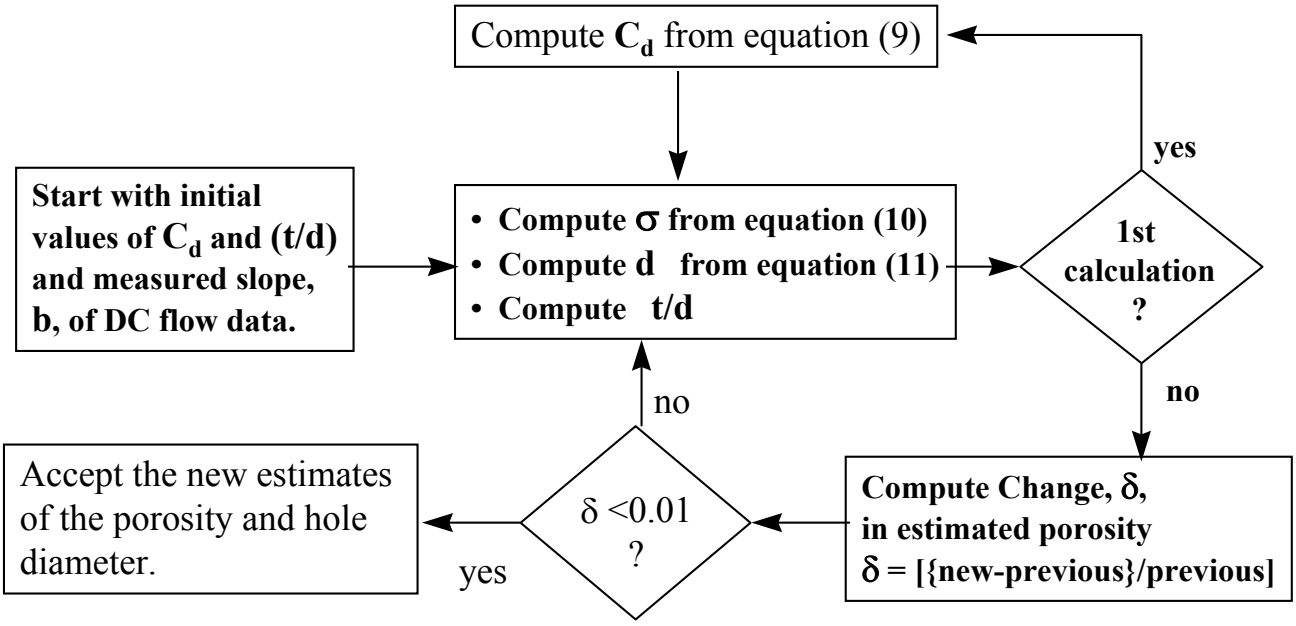

REFERENCES

1. E. Motsinger, A. A. Syed, and M. B. Manley, "The Measurement of the Steady Flow Resistance of Porous Materials," AIAA-83-0779, 8th Aeroacoustics Conference in Atlanta Geogia, April 19983.
2. Jia Yu, H. W. Kwan (Rohr Inc.) and R. E. Kraft (GEAE) -- NASA Contract NAS3-26617 Task Order 25 Final Report: "Acoustic Treatment Design Scaling Methods, Volume 2 - Advanced Treatment Impedance Models for High Frequency Ranges." Submitted in 1998.
3. Jia Yu, H. W. Kwan and J. King, "Microperforate Liner Acoustic Properties Evaluation," presentation during Orifice Impedance Model Workshop held at Chula Vista, California, on 24 February 1998.

REPORT DOCUMENTATION PAGE

Form Approved
OMB No. 0704-0188

Public reporting burden for this collection of information is estimated to average 1 hour per response, including the time for reviewing instructions, searching existing data sources, gathering and maintaining the data needed, and completing and reviewing the collection of information. Send comments regarding this burden estimate or any other aspect of this collection of information, including suggestions for reducing this burden, to Washington Headquarters Services, Directorate for Information Operations and Reports, 1215 Jefferson Davis Highway, Suite 1204, Arlington, VA 22202-4302, and to the Office of Management and Budget, Paperwork Reduction Project (0704-0188), Washington, DC 20503.

1. AGENCY USE ONLY (*Leave blank*)

2. REPORT DATE
July 2002

3. REPORT TYPE AND DATES COVERED
Contractor Report

4. TITLE AND SUBTITLE
The Steady Flow Resistance of Perforated Sheet Materials in High Speed Grazing Flows

5. FUNDING NUMBERS
NAS3-98004

781-30-14-01

6. AUTHOR(S)
Asif A. Syed, Jia Yu, H. W. Kwan, and E. Chien

7. PERFORMING ORGANIZATION NAME(S) AND ADDRESS(ES)
GE Aircraft Engines, Cincinnati, Ohio 45215-1988

B.F. Goodrich Aerospace, Chula Vista, CA 91910-2098

8. PERFORMING ORGANIZATION REPORT NUMBER

9. SPONSORING/MONITORING AGENCY NAME(S) AND ADDRESS(ES)
National Aeronautics and Space Administration
Langley Research Center
Hampton, VA 23681-2199

10. SPONSORING/MONITORING AGENCY REPORT NUMBER
NASA/CR-2002-211749

11. SUPPLEMENTARY NOTES
Langley Technical Monitor: Michael G. Jones

12a. DISTRIBUTION/AVAILABILITY STATEMENT
Unclassified-Unlimited
Subject Category 71 Distribution: Nonstandard
Availability: NASA CASI (301) 621-0390

12b. DISTRIBUTION CODE

13. ABSTRACT (*Maximum 200 words*)
A study was conducted to determine the effects of high speed grazing air flow on the acoustic resistance of perforated sheet materials used in the construction of acoustically absorptive liners placed in commercial aircraft engine nacelles. Since DC flow resistance of porous sheet materials is known to be a major component of the acoustic resistance of sound suppression liners, the DC flow resistance of a set of perforated face-sheets and linear "wiremesh" face-sheets was measured in a flow duct apparatus (up to Mach 0.8). Samples were fabricated to cover typical variations in perforated face-sheet parameters, such as hole diameter, porosity and sheet thickness, as well as those due to different manufacturing processes. The DC flow resistance data from perforated sheets were found to correlate strongly with the grazing flow Mach number and the face-sheet porosity. The data also show correlation against the boundary layer displacement thickness to hole-diameter ratio. The increase in resistance with grazing flow for punched aluminum sheets is in good agreement with published results up to Mach 0.4, but is significantly larger than expected above Mach 0.4. Finally, the tests demonstrated that there is a significant increase in the resistance of linear “wiremesh” type face-sheet materials.

14. SUBJECT TERMS
DC Flow Resistance, Acoustic Impedance, Perforated Face-sheet, Wiremesh Liner Grazing Flow

15. NUMBER OF PAGES
103

16. PRICE CODE

17. SECURITY CLASSIFICATION OF REPORT
Unclassified

18. SECURITY CLASSIFICATION OF THIS PAGE
Unclassified

19. SECURITY CLASSIFICATION OF ABSTRACT
Unclassified

20. LIMITATION OF ABSTRACT
UL